

A PASSIVE WIRELESS PLATFORM FOR  
CHEMICAL-BIOLOGICAL SENSORS

Dissertation

Submitted to

The School of Engineering of the  
UNIVERSITY OF DAYTON

In Partial Fulfillment of the Requirements for  
The Degree of  
Doctor of Philosophy in Electrical Engineering

By

Mark Alan Patterson

Dayton, Ohio

December, 2012



A PASSIVE WIRELESS PLATFORM FOR  
CHEMICAL-BIOLOGICAL SENSORS

Name: Patterson, Mark Alan

APPROVED BY:

---

Guru Subramanyam, Ph.D.  
Advisory Committee Chairman  
Chair & Professor  
Department of Electrical &  
Computer Engineering

---

Partha Banerjee, Ph.D.  
Committee Member  
Professor  
Department of Electrical &  
Computer Engineering &  
Electro-Optics

---

Malcolm Daniels, Ph.D.  
Committee Member  
Associate Professor  
Department of Electrical &  
Computer Engineering

---

James Grote, Ph.D.  
Committee Member  
Principal Electronics Research  
Engineer  
Air Force Research Laboratory

---

John G. Weber, Ph.D.  
Associate Dean  
School of Engineering

---

Tony E. Saliba, Ph.D.  
Dean, School of Engineering  
& Wilke Distinguished Professor

## ABSTRACT

### A PASSIVE WIRELESS PLATFORM FOR CHEMICAL-BIOLOGICAL SENSORS

Name: Patterson, Mark Alan  
University of Dayton

Advisor: Dr. Guru Subramanyam

This research presents several different platforms for detecting chemical or biological agents without the use of probes or wires and without the use of a battery. These platforms all use an interrogator to transmit power through either radio or low frequency electromagnetic waves to a sensor device. The sensor device has a functionalized surface which aids in selectivity to the analyte of interest. The sensor device sends back a portion of the power through radio frequency waves with altered frequency, amplitude and phase. The characteristics of the received signal contain the information about the analyte of interest. The platforms were tested with several volatile organic compounds, gasoline, sulfuric acid, hydraulic fluid, and chlorine. The results were statistically significant.

Dedicated to Mira and Christian

## ACKNOWLEDGMENTS

My special thanks to all of the people at the University of Dayton who have helped me get this far. I especially want to thank Dr. Guru Subramanyam, my advisor, for taking me alongside years ago and sponsoring me for several years while I was working at UD. I also want to thank my two previous bosses, Scott Segalewitz and Larrell Walters, for encouraging me to continue my education. I also want to thank Karolyn Hansen for teaching me all that I know about biological sensing. There are also numerous professors that I have enjoyed working with over the years that helped me achieve my dreams.

My special thanks to all of the people at the Air Force Research Laboratory who have helped me get this far. I especially want to thank Doug Rabe for giving me a job and the time off to finish this dissertation. I also want to thank Jim Gillespie and Kevin Leedy for giving me access to the Sensors Directorate cleanroom.

Lastly, I want to thank my family for putting up with me all these years while I finished up my education.

## TABLE OF CONTENTS

ABSTRACT.....	iii
DEDICATION.....	iv
ACKNOWLEDGMENTS.....	v
LIST OF ILLUSTRATIONS.....	ix
LIST OF TABLES.....	xiv
LIST OF SYMBOLS/ABBREVIATIONS.....	xv
CHAPTER I. INTRODUCTION.....	1
1.1 Motivation .....	2
1.2 Significance .....	5
1.3 Objective .....	6
1.4 Organization.....	6
CHAPTER II. BACKGROUND.....	7
2.1 Amperometric Chemical-Biological Sensors .....	7
2.2 Conductometric Chemical-Biological Sensors .....	9
2.3 Optical Chemical-Biological Sensors .....	11
2.4 Calorimetric Chemical-Biological Sensors .....	14
2.5 Piezoelectric Chemical-Biological Sensors .....	15
2.6 Other Chemical-Biological Sensors .....	21
CHAPTER III. PLATFORM CONSIDERATIONS.....	23
3.1 Why Wireless? .....	23

3.2	Why Passive?	23
3.3	System Level Design	24
3.3.1	Antenna Analysis	25
3.3.2	Resonant Energy / Inductive Power Transfer	27
3.3.3	Antenna Rectifier Circuit	28
3.3.4	Oscillator Designs	29
3.3.5	Relaxation Oscillator Design	32
3.4	Functionalized Surfaces	33
CHAPTER IV. PLATFORMS		36
4.1	IDSense	36
4.1.1	IDSense Antenna Design	37
4.1.2	IDSense Rectifier Design	39
4.1.3	IDSense Relaxation Oscillator Design	40
4.1.4	IDSense Interrogator Design	41
4.2	Passive RF	44
4.3	Bio-Bridge	46
4.3.1	DNA Research	46
4.3.2	DNA Charge Transduction Background	47
4.3.3	Physical Construction	48
4.3.4	Biological Part	51
4.3.5	Construction	53
4.3.6	Sensing Mechanism	53
4.3.7	Vapor Testing	54
4.3.8	Electro-Magnetic Device Testing	54
4.3.9	Applications	55
4.4	Other RF Designs	56
4.4.1	RF Antenna Designs	61
4.4.2	Complete Sensor Design	63
4.4.3	IDC Based RF Design	64
CHAPTER V. RESULTS		67
5.1	IDSense Testing Results	67
5.1.1	IDSense Test Setup	67
5.1.2	IDSense Platform Baseline Characterization	67
5.1.3	Wet Chemical Testing	79
5.1.4	Vapor Testing	83
5.1.5	Compound Testing	84

5.2	Passive RF Testing Results.....	86
5.2.1	Passive RF Test Setup.....	86
5.2.2	Passive RF Platform Baseline Characterization.....	86
5.2.3	Passive RF Chemical Testing.....	91
5.3	Previous Chemical Testing Results.....	94
CHAPTER VI. CONCLUSION.....		98
6.1	Platform Comparisons.....	98
6.1.1	Sensitivity.....	98
6.1.2	Selectivity.....	99
6.1.3	Stability.....	99
6.1.4	Reproducibility.....	100
6.1.5	Dual Sensitivity.....	100
6.1.6	Minimal Volume.....	100
6.1.7	Useful Range.....	101
6.1.8	Accuracy.....	101
6.1.9	Linearity.....	101
6.1.10	Noise.....	102
6.1.11	Size.....	102
6.1.12	Bio-Compatibility.....	102
6.1.13	Sterilizability.....	103
6.1.14	Cost.....	103
6.1.15	Response Time.....	104
6.2	Summary.....	104
6.3	Future Research.....	104
BIBLIOGRAPHY.....		106

## LIST OF ILLUSTRATIONS

1. Block diagram of a passive wireless sensor platform .....	24
2. Self-oscillating passive wireless sensor model.....	25
3. Received power vs. distance for a pair of matched coils.....	27
4. Antenna rectifier circuit model.....	28
5. Parametric amplifier design board with passive components.....	30
6. CPW parametric amplifier layout.....	31
7. Circuit diagram of relaxation oscillator with inductive feed.....	32
8. Resonant energy transfer board set.....	37
9. Swept frequency S21 plot of resonant energy transfer.....	38
10. Induced DC voltage vs. transmitted power for the 40 MHz energy transfer system.....	39
11. Full wave bridge DC voltage power transfer.....	40
12. Schematic of inductive fed relaxation oscillator.....	40
13. Final IDSense board layout .....	41
14. Received interrogator signal with reference.....	42
15. Final IDSense interrogator board.....	43
16. IDC based CPW antenna wireless sensor.....	44

17. Close-up of IDC structure.....	45
18. Passive RF interrogator board.....	45
19. CPW Bio-Bridge platform showing close-up section (right).....	48
20. Test coupon for SEM bridging gap analysis.....	49
21. Results of SEM images of test coupon.....	50
22. A close-up view of a SEM image.....	50
23. Measured gap vs. drawn gap for four developer combinations.....	51
24. Plasmid pBR322 and its cut sites.....	52
25. Model of a RF varactor shunt switch with a single series inductor..	56
26. Swept frequency reflected power (S11) for a varactor shunt switch with a single series inductor at the low resonant frequency point....	57
27. Swept frequency reflected power (S11) for a varactor shunt switch with a single series inductor at the middle resonant frequency point	57
28. Swept frequency reflected power (S11) for a varactor shunt switch with a single series inductor at the high resonant frequency point...	57
29. Model of a RF varactor shunt switch with a series inductor and capacitor.....	58
30. Swept frequency reflected power (S11) for a varactor shunt switch with a series inductor and capacitor at the low resonant frequency point.....	58
31. Swept frequency reflected power (S11) for a varactor shunt switch with a series inductor and capacitor at the middle resonant frequency point.....	59

32. Swept frequency reflected power (S11) for a varactor shunt switch with a series inductor and capacitor at the high resonant frequency point.....	59
33. Twin varactor shunt switch with transmission line simulation at 0.2 pF and 0.6 pF respectively.....	60
34. Coplanar waveguide loop antenna with balun.....	61
35. 900 MHz loopstick antenna.....	62
36. Complete sensor design 1.....	63
37. Complete sensor design 2.....	64
38. Single CPW antenna IDC based sensor.....	65
39. Interrogator for single CPW antenna IDC based sensor.....	65
40. Swept frequency reflected power (S11) measurements of single CPW antenna IDC based sensor.....	66
41. DC spectral response of IDSense passive wireless board.....	68
42. AC spectral response of IDSense passive wireless board.....	69
43. Output frequency spectral response of IDSense passive wireless board.....	70
44. The curve fit of resonant output frequency vs. input frequency.....	70
45. Placement correlation test results within a set.....	72
46. Pearson set correlation between two placement sets.....	72
47. Relationship between the mean frequency of the samples and transmitted voltage.....	73
48. IDSense statistical results comparing transmitted voltage and mean frequency.....	74

49. Relationship between the output voltage and transmitted voltage....	75
50. Correlation relationship between the output voltage, capacitor voltage, and the transmitted voltage.....	76
51. Model results between the capacitor voltage and the transmitted voltage.....	77
52. Model results between the output voltage and transmitted voltage .	78
53. Evaporation testing of isopropanol on a bare board.....	79
54. Evaporation testing of isopropanol on a silk coated board.....	80
55. Evaporation testing of isopropanol on a Nafion coated board.....	81
56. Evaporation testing of ethanol on a bare board.....	81
57. Evaporation testing of ethanol on a silk coated board.....	82
58. Evaporation testing of ethanol on a Nafion coated board.....	83
59. Statistical results of compound testing.....	86
60. Swept frequency reflected power (S11) response for the passive wireless interrogator antennas.....	87
61. Swept frequency forward power (S21) and reflected power (S11) response with and without a wireless sensor on the interrogator antennas for the Passive RF wireless sensor.....	88
62. Swept frequency reflected power (S11) response with different calibration structures on the interrogator antennas for the Passive RF wireless sensor.....	89
63. Swept frequency forward power (S21) response with different calibration structures on the interrogator antennas for the Passive RF wireless sensor.....	90

64. Swept frequency forward power (S21) measurements of the evaporation of ethanol on a bare Passive RF wireless IDC board ....	91
65. Swept frequency reflected power (S11) measurements of the evaporation of ethanol on a bare Passive RF wireless IDC board ....	92
66. Swept frequency forward power (S21) measurements of the evaporation of isopropanol on a bare Passive RF wireless IDC board.....	93
67. Swept frequency reflected power (S11) measurements of the evaporation of isopropanol on a bare Passive RF wireless IDC board.....	94
68. Swept frequency forward power (S21) measurements of the evaporation of water on the resonant test structure coated with silk.....	95
69. Swept frequency forward power (S21) measurements of the evaporation of water on the resonant test structure coated with Nafion.....	96
70. Swept frequency forward power (S21) measurements of the evaporation of ethanol on the resonant test structure coated with silk.....	96
71. Swept frequency forward power (S21) measurements of the evaporation of isopropanol on the resonant test structure coated with silk.....	97

## LIST OF TABLES

1. Antenna selection matrix.....	26
2. Statistics of mean of samples.....	71
3. Vapor testing with water and ethanol on various boards.....	83
4. Results of silk chemical testing.....	85
5. Results of Nafion chemical testing.....	85

## LIST OF SYMBOLS/ABBREVIATIONS

AC	Alternating Current
ANOVA	Analysis of Variance
BAW	Bulk Acoustic Wave
BST	Barium Strontium Titanate
Chem-Bio	Chemical-Biological
CO	Carbon Monoxide
CPW	Co-Planar Waveguide
D/A	Digital to Analog
DC	Direct Current
DNA	Deoxyribonucleic Acid
EIRP	Effective Isotropically Radiated Power
FET	Field Effect Transistor
HC	Hydrocarbon
HPSSW	Horizontally Polarized Surface Shear Wave

IDC	Inter-Digitated Capacitor
IDT	Inter-Digitated Transducer
LAN	Local Area Network
LC	Inductance and Capacitance in Series
LCD	Liquid Crystal Display
MEMS	MicroElectroMechanical Systems
PCR	Polymerase Chain Reaction
PDMS	Polydimethylsiloxane
QCM	Quartz Crystal Microbalance
RF	Radio-Frequency
RFID	Radio-Frequency Identification
SAM	Self-Assembling Monolayer
SAW	Surface Acoustic Wave
SEM	Scanning Electron Microscope
SH	Shear Horizontal
SMA	Sub-Miniature version A
SPR	Surface Plasmon Resonance
TELISA	Thermometric Enzyme-Linked Immuno-Sorbent Assay
VCO	Voltage Controlled Oscillator
VOC	Volatile Organic Compound

## CHAPTER I

### INTRODUCTION

#### **Research Areas:**

This research involves two main realms of science: Electromagnetic Communication and Chemical-Biological Sensing. Historically these two realms of science are almost never seen together. This is mainly because Electrical Engineers do not generally understand Biology and Biologists do not generally understand Electromagnetics. This crossing is a fertile research area with minimal past publications. The recent advances in Electronics are able to complement the recent advances in Biology to introduce new devices. This research presents some new devices.

#### **Passive Wireless Chem-Bio Sensors:**

Chemical-Biological (Chem-Bio) sensors are analytical devices which convert a chemical or biological response into an electrical signal. Chemical sensors traditionally consist of only a transducer. A transducer converts a recognition event into a measureable signal. A biological sensor requires a bio-receptor in addition to the transducer. A bio-receptor is a biomolecule that recognizes the target analyte. An analyte is a parameter of interest such as glucose. The electrical signal from the transducer is used to determine the concentration of analyte or other parameters of

biological interest. In a biological sensor, these parameters could be caused by enzymes in a biologically responsive material, whole cell metabolism, ligand binding, or an antibody-antigen reaction.

There is a vast array of Chem-Bio sensors available in both industry and academia. These sensors come in many different designs, even for the same analyte. However, there are two things in common with most of these sensors; they require power and they require expensive machines in a laboratory environment. The current momentum in Chem-Bio sensors is to make these sensors cheap, portable, simple, and quick. In order to get these Chem-Bio sensors out in the field, a portable sensing platform will need to be created. There are several commercial sensors out there such as Surface Acoustic Wave (SAW) sensors which are portable; however they have their limitations as well. Several of the other sensor techniques generate an electrical signal from the transducer which is often low and superimposed upon a relatively high amount of noise. A wireless Chem-Bio sensor platform could provide a way to miniaturize sensors and decrease their cost. If the sensor device could be passive (no batteries), the cost and size could be even less. Recent progress in Radio Frequency Identification (RFID's), capacitive/inductive power transfer, functionalized polymers, and nanotechnology has made this sensor platform possible.

## 1.1 Motivation

Chem-Bio sensors represent a rapidly expanding field with an estimated 60% annual growth rate [1]. The major reason for this growth is the health care industry, homeland security, the food industry, the military and environmental monitoring.

Sensors in the health care industry are currently a \$1 billion/year market [1]. The problem is that only 0.1% of the industry is using modern Chem-Bio sensors [1]. Most of the sensor techniques used currently are slow and cumbersome in addition to being antiquated. There is an increasing demand for inexpensive and reliable sensors for doctor's offices, emergency rooms, and operating rooms. It would be much more convenient to do tests at the office instead of sending them to the lab for assays. For example, 6% of the world is diabetic and would benefit greatly from the availability of a simple, rapid, accurate, glucose monitor [1]. Currently most of the sensors used in the health care industry are amperometric, potentiometric, or colorimetric paper enzyme strips.

Home land security has been a recent thrust in sensor development. It is desirable to install real time monitoring and alarm systems at potential terrorist sites to detect specific analytes such as ricin, nerve gas, explosives, or biological agents. The food industry can also benefit greatly from new Chem-Bio sensors. Several new sensors have been created in recent years to detect bad fish, e-coli, lead and mercury poisoning, heavy metals, bitterness in beer, toxic chemicals in foods, and more. The military requires rapid analysis of a situation for successful operations. The presence of a chemical or biological warfare agent needs to be detected as fast as possible to limit exposure to our troops. OSHA has mandated more environmental monitoring every year. Common environmental monitoring analytes are biological oxygen demand, atmospheric acidity, pH, detergents, herbicides, and fertilizer concentrations in drainage and river water. Monitoring systems can be installed at sites of potential pollution to limit the spread of pollutants.

The potential for biosensor technology is huge and the potential impact is far reaching. Nature offers a variety of molecules with abilities to recognize chemical and biological substances, from pheromones to environmental odors [2]. These molecules can be utilized for military as well as civilian applications by designing them to specifically bind to chemicals such as those used in explosives, biological agents, or environmental pollutants providing the possibility for a quick, highly specific and inexpensive detection system of these compounds [2]. Research and development in the Chem-Bio sensor field combines Chemistry, Biology, Physics, Material Science, Electrical Engineering, and Computer Science. While there are methods which yield detection limits in the parts-per-billion regime in principle, lack of specificity and irregularities due to interferences are problems yet to be solved. A new fabrication process and sensor design needs to be developed which solves these deficiencies, and also results in inexpensive, compact, and reliable sensors.

For this dissertation, a chemical-biological sensor platform was built for several different analytes of interest. This platform drew from several different groups of knowledge. These groups of knowledge included: antennas, energy transfer, resonant circuits, interdigitated capacitors, thin films, wireless technologies, and functional surfaces. This dissertation contributes two passive wireless sensor platforms and a biological sensor platform that were the basis for three patent applications and several publications.

## 1.2 Significance

Currently, most methods of sensing chemical/biological agents are restricted to assays in a laboratory environment. The devices used are prohibitively expensive and relatively large. The studies in this dissertation research/develop mobile methods to expand Chem-Bio sensor use as well as improve upon sensor sensitivity and selectivity. A successful chemical-biological sensor must possess at least some of the following beneficial features:

1. Be highly sensitive to the analyte of interest.
2. Be highly specific to the analyte of interest.
3. Be stable under normal storage conditions for a good lifetime.
4. Show good reproducibility over a large number of samples.
5. Be independent of environmental factors (temperature, ph, flow, etc).
6. Work with minimal chemical interaction.
7. Have a useful range that covers the needed detection levels.
8. Be accurate over the useable range of the device.
9. Be linear over the useable range of the device.
10. Be free from noise effects.
11. Be small and portable.
12. Be biocompatible with its working environment.
13. Be sterilizable.
14. Be inexpensive.
15. Have a good response time.

### 1.3 Objective

The objective of this dissertation is to develop a chemical-biological sensor platform consisting of a passive wireless sensor device and an interrogator device to measure the sensor response. The sensor platform will then be characterized with different functional surfaces to identify one or more of the following chemicals of interest; volatile organic compounds (VOCs), hydrocarbons (fuels), battery acid, hydraulic fluid, and chlorine.

Prior experimentation has shown that using a biopolymer as the dielectric layer in a resonant test structure can sense chemicals. Sensing is achieved by monitoring the resonant frequency shifts of the device. This resonant frequency change occurs because of a change in the effective permittivity of the polymer layer which affects the capacitance of the sensor. This research builds on the chemical testing performed on polymer coated resonant test structures by Erica Jones for a Master's thesis at the University of Dayton. Erica tested both silk and nafion polymers with ethanol, isopropanol, and water to determine the sensitivity of the dielectric polymers to chemicals. Her research showed substantial changes in resonant frequency for water, however small changes in resonant frequency for ethanol and isopropanol. Some of her results are included at the end of the results chapter.

### 1.4 Organization

This dissertation is organized into four distinct sections; chemical-biological sensor background research, platform considerations and building blocks, the platforms themselves, and the statistical results of platform characteristic testing.

## CHAPTER II

### BACKGROUND

There are several approaches to building a Chem-Bio sensor platform. Several of the types of Chem-Bio sensors are determined by the transducer which converts the analyte signal to an electronic signal. Some major types of Chem-Bio sensors are Amperometric, Conductometric, Optical, Calorimetric, and Piezoelectric. There are also several newer lesser known types of Chem-Bio sensors. Several of the analytes currently detected by these types of sensors could also be detected by the new sensor platform. These types of sensors are reviewed because the chemicals, materials, and polymers used in these sensors are analyte specific and could be used as part of the new sensor platform.

#### 2.1 Amperometric Chemical-Biological Sensors

Amperometric Chem-Bio sensors measure the movement of electrons (current) produced during the oxidation or reduction of a product or reactant usually at a constant applied potential between two electrodes [3]. There are potentiometric Chem-Bio sensors as well which measure the rate of potential change of a substrate. However, they are rarely used except in pH monitoring [3]. Amperometric Chem-Bio sensors generally have response times, dynamic ranges and sensitivities similar to the potentiometric biosensors. Potentiometric biosensors make use of ion-selective electrodes in order to transduce the

biological reaction into an electrical signal. In the simplest terms this consists of an immobilized enzyme membrane surrounding the probe from a pH, where the catalyzed reaction generates or absorbs hydrogen ions.

Electrochemical immunosensors are a form of amperometric and potentiometric Chem-Bio sensor. They are based on conventional antibody-based enzyme immunoassays. An electrical signal is generated through the catalysis of substrates by an enzyme conjugated to an antibody.

Amperometric Chem-Bio sensors have recently been constructed for salmonella [4], E. coli [5], hydrogen gas [6], ethanol [7], methanol, N-propanol, formaldehyde, N-butanol [8], for enzymatic and non-enzymatic detection of glucose [7, 9, 10], silicate [11], carbohydrates [12], hydrogen peroxide [12], and peroxide [13].

Some advantages of amperometric Chem-Bio sensors are that they are linearly dependent on a nalyte concentration, exhibit good sensitivity and selectivity, and are stable. The main disadvantage of this type of sensor is that it is unsuitable for clinical detection methods because it requires complicated chemical procedures and the detection sensitivity is restricted [7]. The main limitation of amperometric Chem-Bio sensors is the signal to noise ratio of the measurement [7, 14]. Some other disadvantages are their response times are between 10 and 50 seconds, the signal is linear only from 1-10% concentration, and they only have a 0.01  $\mu\text{A/ppm}$  sensitivity at best [6].

Amperometric glucose sensors have been developed for concentrations as small as 2  $\mu\text{M}$  to as high as 11 mM. The issue with this is that the normal level of human blood glucose, from hypoglycemia to hyperglycemia is from 1.3-22 mM [14, 15].

Development in amperometric sensors is mainly about coating the electrodes with different materials such as gold [7], platinum [6], nickel [9], carbon nanoparticles [9], copper oxide nanorods [12], and lead [14]. There are some other developments in enzyme immobilization in polymer layers [8].

## 2.2 Conductometric Chemical-Biological Sensors

Conductometric chemical-biological sensors measure the changes in the conductance of the chemical-biological component arising between a pair of electrodes [3]. Monitoring solution conductance was originally applied as a method of determining reaction rates. The technique involves the measurement of changes in conductance due to the migration of ions. Many enzyme linked reactions result in a change in total ion concentration and this would imply that they are suitable for conductometric biosensors. Conductometric is sort of an advanced form of amperometric. There are many different levels of conductometric sensors. Whereas amperometric usually implies a DC applied potential across the electrodes, conductometric involves an AC applied potential across the electrodes. This can be in the form of a slow square wave or a high frequency sine wave. By using an AC excitation instead of a DC excitation, the real and imaginary components of impedance can be determined. Another form of conductometric is the capacitive tests. Many Chem-Bio sensors work on the change of the dielectric constant (capacitance) of the material. There are constant capacitance tests and capacitive-voltage tests. The most advanced form of conductometric sensing is called impedance spectroscopy. This involves a swept frequency AC sine wave applied to the electrodes. Instead of a single frequency point, multiple frequency points can be used in parallel to determine the reaction rate, analyte, etc. Usually resonant frequencies are observed with

impedance spectroscopy. This method is similar in analysis to spectroscopic imaging which is able to determine percentage of individual elements in matter.

There are several conductometric sensors already in use. There are four main types of structures used for the sensors and then some other lesser known structures. These structures are: Interdigitated capacitors, charge based capacitive structures, chemiresistors, and field effect devices.

The interdigitated capacitor is the most prevalent design. Interdigitated capacitors have been used for the detection of biological warfare agents (bacillus anthracis spores [16], CO gas [17], organic gases (acetone, ethanol, toluene, and methanol) [18], humidity [19], dangerous marine biotoxins (contaminated acid) in mussels [20], volatile inorganic (ammonia) and organic (dimethylamine) amines [21], water, toluene vapor [22], atrazine [23], on-line cell adhesion and cytotoxicity [24], toxicological of chemicals [25], and viruses such as herpes simplex [25].

Charge based capacitance sensors have been used for the monitoring of protein-metal interactions [26], detecting humidity and ethanol vapor [27], trace-level detection of chemical warfare agents [28], and explosives [28].

Chemiresistor sensors have been used for gas sensors (N<sub>2</sub>, Ar, O<sub>2</sub>) [29], and light alkanes such as methane [30].

Field effect capacitive devices have been developed for multi-parameter detection of charged macromolecules [31], and volatile organic compounds (VOCs) [32].

Other devices such as nano/mesostructures have been used for hydrogen sensing [33], detecting amino acids such as glycine, aspartic acid, lysine, and phenylalanine [34], measuring tensile or compressive strain because of organic solvent vapors [35], predicting estrus onset in cattle [36], detecting toxic chemicals, combustible or corrosive gases, blood agents [37], and chloride sensors [38].

Conductometric Chem-Bio sensors have several advantages compared to conventional Chem-Bio sensors. The ability to examine phase in addition to magnitude adds another dimension to the decision making logic. These sensors have good sensitivity, selectivity, longevity [17], rapid response and recovery times, good reproducibility, linearity, stability [19], can be used in real time monitoring [21], are rugged, lightweight, and low cost [37]. Capacitance detection, dominated by dielectric effects, is less sensitive to charge effects and, thus, offers increased signal-to-noise ratio, improved sensor recovery, and larger dynamic range [28].

### 2.3 Optical Chemical-Biological Sensors

Optical chemical-biological sensors are based on the measurement of light absorbed or emitted as a consequence of a chemical or biological reaction [3]. In this type of sensor, light waves are usually guided by means of optical fibers or lens to suitable detectors [3]. There are two main areas of development in optical biosensors. These involve determining changes in light absorption between the reactants and products of a reaction, or measuring the light output by a luminescent process. The former usually involves the widely established colorimetric test strips. These are disposable single-use cellulose pads impregnated with an enzyme and reagents. The most common use of this technology is for whole-blood monitoring in diabetes control [1].

There are several different technologies used to acquire optical data for use as a Chem-Bio sensor. Some of these technologies are: Surface Plasmon Resonance (SPR), Raman Scattering, Fluorescence, Quantum Dots, Optical Waveguides, Visual Imaging, and Infrared Imaging.

SPR is one of the most sensitive label-free detection methods there is and has been applied in a wide range of chemical and biological sensing. SPR exploits the change in refractive index of a bioaffinity coating on a gold film when binding takes place. When light undergoes total internal reflection within a prism, a certain amount of energy propagates a small distance beyond the optical interface into the surrounding medium, forming an evanescent field. If a thin layer of metal is coated onto the surface, this energy can be absorbed by the free electrons at the metal surface and give rise to surface plasmon resonance. The angle of incidence at which this energy absorption occurs is critically dependent on the refractive index of the external medium. If a binding partner, such as an antibody, is immobilized on the surface of the prism, the angle at which surface plasmon resonance occurs can be used to monitor rate and extent of the biological interaction in real time. Normally, antibodies or receptors for detection of food-borne pathogens or toxins are immobilized in a biolayer attached to a sensing surface. When binding takes place, it alters the angle of light reflected off the medium, resulting in a signal. Currently, this system has been applied to the on-line monitoring of a target analyte in a complex mixture by using a specific interaction between antigens and antibodies [39]. Recent research has been on the characterization of the glass slides used in SPR [40], parylene thin films as a linker layer [39], TNT detection [41], and sensitivity enhancement [40]. This system has been used for detection of whole cells of *E. coli*

O157:H7, salmonella, and listeria at variable concentrations [42]. It also showed strong signals with small toxin molecules, such as staphylococcal or botulinum [43].

Raman spectroscopy is a useful tool for analysis because of its excellent chemical group identification capability; however its limitation is low sensitivity. Surface enhanced Raman scattering has been shown to observe DNA hybridization. Current research has been conducted with polyimide nanoimprint lithography to enhance the effectiveness of surface enhanced Raman spectroscopy [44].

In Fluorescence energy transfer, a spectrofluorometer or an epifluorescence microscope is used to measure the emission of fluorescence when a fluorescent-labeled antibody is used. One disadvantage of fluorescence is that the sensitivity of these methods are in the range of  $10^4$ – $10^7$  bacterial cells, and the assays take about 3–4 hours to complete [5].

Recent developments in fluorescence have involved quantum dots. Semiconductor CdSe quantum dots (QDs) have been surface-functionalized with aromatic ligands for the sensitive and selective detection of aromatic hydrocarbons (HCs) [45]. SnO<sub>2</sub> quantum dots have been used to detect show high selectivity to CO in the presence of methane [46].

In order to couple light closer to the source, optical waveguides have been used. The advantage of fiber-optic sensors is that they are disposable, minimally invasive, and can provide in vivo monitoring of various analytes for several weeks [47]. Fiber optics with a long period grating coated with a functional material exhibit sensitivity to the aromatic compounds toluene and benzene, while being relatively insensitive to the

aliphatic hydrocarbon hexane [48]. Optical fibers have also been used for the real-time detection of biological agents (such as bacterial cells, toxins, or spores) in the air, soil, or environment [42]. The fiber-optic biosensor operates by covalently linking a specific antibody to the fiber-optic cable, binding a target antigen to the antibody, and then detecting the antigen-antibody complex by means of a secondary antibody conjugated to molecules that can be stimulated to emit fluorescent light which is measured by a laser detector. Current antibody-coupled fiber-optic biosensors have been developed for the detection of botulinum toxin, staphylococcal enterotoxin, E. coli O157:H7, listeria, and salmonella [42].

Information can be gathered from looking at visual light on the sensor. Some methods involve a change in transparency. Xerogels have properties like optical transparency that enable them to act as a chemical sensor [49]. Infrared light gives additional advantages due to the reduction of water interference in the signal [50].

#### 2.4 Calorimetric Chemical-Biological Sensors

Calorimetric chemical-biological sensors are based on the measurement of heat absorbed or emitted as a consequence of a chemical or biological reaction. Many enzyme catalyzed reactions are exothermic, generating heat which may be used as a basis for measuring the rate of reaction and, hence, the analyte concentration. This represents the most generally applicable type of biosensor. The temperature changes are usually determined by means of thermistors at the entrance and exit of small packed bed columns containing immobilized enzymes within a constant temperature environment. All chemical reactions are accompanied by the adsorption or evolution of heat. Microcalorimetry has been demonstrated for the differential calorimetric determination of

glucose concentrations [4, 5, 42]. In Thermometric Enzyme-Linked ImmunoSorbent Assay (TELISA), the difference in steady-state output voltage of the enzyme-modified sensor compared to the unmodified sensor after addition of 2–100 millimoles glucose was related to the catalytically induced temperature change and thus to the glucose concentration.

## 2.5 Piezoelectric Chemical-Biological Sensors

Piezoelectric chemical-biological sensors operate on the principal of generation of electric dipoles on subjecting an anisotropic natural crystal to mechanical stress with a mass or mass change [3]. Piezo-electric crystals (e.g. quartz) vibrate under the influence of an electric field. The frequency of this oscillation depends on their thickness and cut, each crystal having a characteristic resonant frequency. This resonant frequency changes as molecules adsorb or desorb from the surface of the crystal. In the case of a bio-sensor, an antibody is immobilized on the sensor surface, and when the antibody-antigen reaction takes place, an increase in mass results, forming the basis for an immunoassay [4, 5, 42, 51].

Biosensors based on microcantilevers have become a promising tool for directly detecting biomolecular interactions with great accuracy. Microcantilevers translate molecular recognition of biomolecules into nanomechanical motion that is commonly coupled to an optical or piezo-resistive read-out detector system. The sensor response is mechanical bending due to absorption of molecules. Biosensors based on cantilevers are a good example of how nanotechnology and biotechnology can go together. High-throughput platforms using arrays of cantilevers have been developed for simultaneous measurement and read-out of hundreds of samples. As a result, many interesting

applications have been performed and the first sensor platforms are being commercialized [52]. The sensor signal is the relative variation of the microcantilever resonant frequency which depends on both the viscosity and the density of the fluid surrounding the microcantilever. Most micro-cantilevers are made of silicon on insulator, silicalite [53], or aluminum nitride on metal [54]. Microcantilevers are used both with and without sensitive coatings [55]. A sensitive coating used is Diamond films [54]. Micro-cantilevers are unique in that they can be used as both sensors and actuators [54]. The downside is that laser-based optical vibrometers have to be used to measure the resonant properties [53]. The advantages of micro-cantilevers are that they are portable, compact, modular, and have good physical properties with regard to response time, sensitivity, selectivity, and stability [55]. Micro-cantilevers have been built as chemical sensors to detect the presence of ethanol vapors [53], to detect the nerve agent dimethyl methyl phosphonate in parts-per-billion concentrations even in binary and ternary mixtures [56], to detect binary gas mixtures such as He/N<sub>2</sub> and CO<sub>2</sub>/N<sub>2</sub> [55], and to measure the adsorption of very minute quantities of biochemicals [53]. In gaseous environment, polymer-coated microcantilevers are used as electronic nose for characterization of vapors, resulting in cantilever bending due to polymer swelling upon exposure. Medical applications involve fast characterization of exhaled patient's breath samples for detection of diseases, based on the presence of certain volatile organic chemicals in breath [57].

The Quartz Crystal Microbalance (QCM) is a variation of the piezoelectric system which consists of a thin quartz disc with implanted electrodes. Any interaction with the surface can result in a change in signal, thus making the detection of binding an

inherently nonspecific method [4, 5, 42, 51]. The resonant frequency can be changed by the addition of a thin mass layer on the electrode of the QCM. The change in frequency is proportional to the deposited mass. The frequency change can be determined by monitoring the QCM at any odd harmonic, e.g., first, third, or fifth, etc. The frequency change, the area of the electrode over which the mass is spread, and the material properties of the quartz enable the mass change to be calculated. This could be accurate enough to measure picogram changes of mass or measure mass changes as small as a fraction of a monolayer. Dissipation is often measured for further analysis. This sensitivity to mass is the reason that the QCM is widely used as a microbalance. QCMs are often coated with a film or liquid to detect a specific analyte. Some coatings are; porphyrins [58], polyaniline, emeraldine [59], 1-butyl-3-methylimidazolium chloride, 1-butyl-3-methylimidazolium hexafluorophosphate, 1-dedocyl-3-methylimidazolium bis(trifluoromethylsulfonyl)imide, silicone oil [60], poly(styrene-co-chloromethyl styrene), and morpholine [61]. Quartz Crystal Microbalances have been constructed to detect salmonella and listeria [4, 5, 42, 51], thiols of varying structures bearing amine, acid or aromatic functionalities, 2,4-dinitrotrifluoromethoxybenzene, methylethylketone, toluene, dichloromethane [62], low-concentrated vapors of explosive compounds [63], aliphatic alcohols such as ethanol, methanol, 2-propanol and 1-propanol vapors [59], toluene [60], and HCl gas in air [61]. Some of advantages of QCM are; the ability to process the results in real time [51], the results are linear [59], good reproducibility and reversibility [59], and high qualitative recognition success rates [60].

Piezoelectric materials provide the required coupling between electrical signals and mechanical motion to generate surface acoustic waves. Crystalline piezoelectric

materials, such as quartz, lithium niobate, and lithium tantalate, exhibit low attenuation and dispersion, and are therefore ideal for acoustic propagation. Surface acoustic waves in such a material are generated through a localized electric field at the surface that is created by applying voltage to an array of metal electrodes or fingers. This electrode array is known as an interdigital transducer (IDT). The IDT can also be used to detect surface waves, producing electrical output and hence an overall response. Surface-acoustic-wave (SAW) devices have led to a versatile technology for analog signal processing in the frequency range  $10^7$ – $10^9$  Hz. The much slower propagation velocity of acoustic waves as compared to electromagnetic waves permits time delays in SAW devices, as compared to electrical delay lines, that are crucial for signal processing applications. Notable devices include band-pass filters, resonators, oscillators, pulse compression filters, fast Fourier transform processors, and more recently chemical and biological sensors. Consumer application areas include mobile phones, television and satellite receivers, keyless entry systems (garage doors, cars, and so forth), and wireless applications. Commercial applications include fiber-optic communication, oscillators, local-area networks (LANs), test equipment, and chemical and biological detection systems, with military applications in radar, sonar, and advanced communications. There are several types of surface acoustic waves; there are Love waves, a wave propagating along a layer on a surface, Stoneley waves, a wave propagating along an interface between two solids, and Bleustein-Gulyaev-Shimizu waves, transverse guided waves on solids. Love waves are shear-horizontal (SH) waves that have displacement only in a direction perpendicular to the plane of propagation [64, 65, 66, 67, 68]. Surface acoustic wave (SAW) devices based on horizontally polarized surface shear waves (HPSSW)

enable label-free, sensitive and cost-effective detection of biomolecules in real time. Binding reactions on the sensor surface are detected by determining changes in surface wave velocity caused mainly by the uptake of mass or viscosity changes in the sensing layer [69]. Most SAW devices are made of lithium niobate or lithium tantalate with gold transducers [69]. There are numerous coatings that have been used on SAW devices in order for them to detect specific analytes. Some common coatings are AlN [4, 70-78], aminodextran (AMD) [69], poly(2-chloro-p-xylylene) [69], poly-4-vinylphenol (P4VP), poly-vinylacetate (PVAc), poly-N-vinylpyrrolidone (PNVP), polyethyleneglycol (PEG), polystyrene (PS), polystyrene-co-maleic anhydride (PSMA), and polysulfone (PSu) [79], modified diamond nanoparticles [80], triethanolamine [81], poly(p-diethynylbenzene) (PDEB) and sodium polysulfonesulfonate (NaSPF) [82], polyisobutylene (PIB), polyepichlorohydrin (PECH), polydimethylsiloxane (PDMS), polybutadiene (PBD) and polyisoprene (PIP) [82]. Surface Acoustic Wave (SAW) platforms have been built mainly as electronic noses to detect many different analytes [79]. The SAW can differentiate between apple varieties, ripe and unripe pineapple, and even an off-flavor in sugar [83]. It is used to detect chemical warfare agent simulants [84], explosives [81], and also chemical warfare agents dimethylmethylphosphonate (DMMP), acetonitrile (CH<sub>3</sub>CN), dichloromethane (CH<sub>2</sub>Cl<sub>2</sub>) and dichloropentane (DCP) [82]. In addition it can detect other nitro-aromatic compounds, nerve-agent stimulants, toxic gases, dinitrotoluene (DNT), dimethylmethylphosphonate (DMMP), ammonia (NH<sub>3</sub>) and relative humidity (RH) [80]. Some organics such as ammonia, propanone, hexane, acetic acid, toluene, methanol, tetrachloromethane, chloroform, ethanol and dichloromethane have also been detected [85]. In the medical field, SAW's have been

used to detect H<sub>2</sub>S in the exhaled breath [81], and gluconic acid in aqueous solutions [86]. One metal ion, Cu<sup>2+</sup> has also been detected [86]. There are several advantages to SAW devices. They are one of the few sensor systems that can be hand-held [87]. When used in an array, they provide the possibility of classification with principal component analysis (PCA) [82, 88]. They can provide an easy, low cost, and fast label free detection method for molecules with biological relevance [4, 70-78]. They are much more sensitive than QCM crystal sensors for glucose [86]. The sensor system can also provide on-line measurement of chemical and biochemical processes, to supplement for human sensory experiments and for detection of microorganism contamination [83]. The sensors also have high sensitivity to the target compounds, good repeatability and low detection limit at sub-ppm levels, even at room temperature [80]. The biggest disadvantage that mass-sensitive Chem-Bio sensors such as quartz crystal microbalances (QCM) or SAW devices have is a slow dynamic response [89].

Bulk Acoustic Wave (BAW) sensors are similar to SAW sensors with regards to impedance, bandwidth, charge, stability, resolution, resonance conditions, and sensitivity. Current BAW sensors are made of aluminum nitride or PbZrTiO<sub>3</sub> (PZT) whereas SAW sensors are made of LiTaO<sub>3</sub> or LiNbO<sub>3</sub>. BAW devices do have several advantages over SAW devices. In frequencies between 1 and 10 GHz they exhibit a high power handling capability, a small volume, a low cost, a low temperature drift, and a reasonable coupling coefficient. The biggest advantage that BAW devices have over other technologies such as ceramic or SAW filters is the possibility of being fabricated above integrated circuits, since their materials and thermal budget are compatible with a post-processing approach. One disadvantage of thin film BAW resonators is that the longitudinal wave mode is

adversely affected when used for sensing in liquid phase environment, because the liquid absorbs most of the acoustic energy [90]. BAW biochemical sensors have been constructed to detect genetically modified organisms or mass difference on a biochemical prepared surface.

## 2.6 Other Chemical-Biological Sensors

There are several other forms of Chem-Bio sensors which cannot be easily classified in one of the previous categories. Some of these sensors are MEMS, microfluidics, capacitive, field-effect devices, and many others. Some lesser known Chem-Bio sensors are; micro/nano structures, nano crystals, thin/thick films, nano rods/wires, nano particles, nanocomposite, chips, wireless systems, and self-assembled monolayers.

Microelectromechanical Sensors (MEMS) come in all sorts of designs. They benefit greatly from advances made in the semiconductor industry with regard to low-cost manufacturing processes. Polymer based MEMS capacitors have been constructed which exhibit a fast change when subjected to a chemical stimulus. One special device the PCR microchip has a serpentine microchannel of varying width for "regional velocity control." Some of the advantages that MEMS devices have are: greater independence from packaging shape constraints due to decreased device size, repeatable manufacturing processes as well as economic advantages can follow from batch fabrication schemes such as those used in integrated circuit processing. Their main disadvantage is that the design with the greatest utility is based on a hybrid approach, where mechanical processing and electronic processing are separated until a final packaging step [91-95].

Field effect devices are used extensively in the semiconductor industry and are capable of detecting changes in ion concentration when the gate is exposed to a solution that contains ions. Therefore pH and ions can be measured with a FET. There are several commercially available FET pH sensors available. Many field effect devices have been built and are used as Chem-Bio sensors. Most of the new FET designs involve carbon nanotubes or polymer channels. FETs with a polymer coating layer have been employed to avoid nonspecific binding and sense CO<sub>2</sub> gas in air at ambient temperature. Some advantages of FETs are: low-cost, low-complexity, highly sensitive, wireless, small size, low power consumption, highly selective, direct electrical detection of charged macromolecules, label free detection, and a small detectable signal. The biggest disadvantage of carbon nanotube (CNT) FET's is due to the CNTs themselves. Because of their small diameter, very little current can flow through them which results in a very low AC level and therefore a poor accuracy of scattering parameters. This is especially evident at high frequencies [96-103].

## CHAPTER III

### PLATFORM CONSIDERATIONS

A passive wireless platform consists of several different elements forming one large system. This chapter explains the different elements and the design methodology.

#### 3.1 Why Wireless?

While there are some disadvantages to wireless sensors, there are many advantages. It is not only the cost of the wires that makes wired sensors expensive but rather the connectors and the enclosure around the wires in some cases (conduit). Connectors are both expensive and bulky. If the wire for the sensor is housed in conduit it is very costly to install or relocate the sensor. Some of the biggest advantages to a wireless sensor system are flexibility and mobility which lead to low installation costs.

#### 3.2 Why Passive?

A wireless system needs power in order to be able to communicate. This leaves only two options; a battery or a temporary power storage device (capacitor). Batteries have limited shelf-life, tend to fail, can be large and heavy, and do not have infinite shelf life. Replacing batteries leads to repeated maintenance costs. They can be a hazardous material for handling and disposal purposes. While some batteries can be recharged, there is not always a sufficient light source. A passive wireless system uses an energy storage device such as a capacitor to capture power and rebroadcast it or works through

reflection principles only and is truly passive. Capacitors are very reliable and have no/low maintenance over their entire life. This would enable battery-less sensors to be placed in hard to service areas.

### 3.3 System Level Design

A passive wireless sensor system would consist of two distinct parts. One part is the wireless sensor itself and the other part would be the transceiver used to interrogate the sensor.

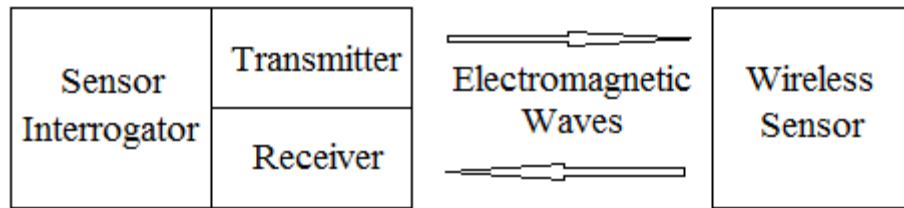


Figure 1. Block diagram of a passive wireless sensor platform.

The first challenge of a passive wireless sensor platform is to couple energy to the wireless sensor. There are several approaches to coupling energy to the sensor. The two most probable methods would be inductive and RF. The method of providing power to the wireless sensor sets the sensor platform apart from other designs. Figure 2 shows two ways of sending power to the wireless sensor. The first method is through RF waves, the second method is through low frequency electromagnetic waves.

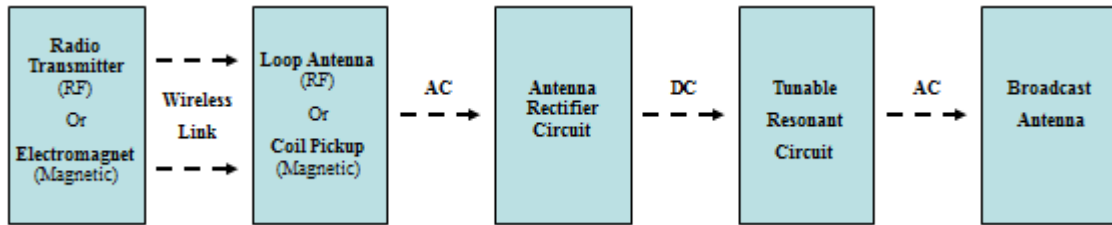


Figure 2. Self-oscillating passive wireless sensor model.

In both adaptations of this design, AC current is induced in the wireless sensor and converted to DC power. This DC power is used to power a tunable resonant circuit which creates AC again at a different frequency and re-broadcasts the information back to the interrogator unit.

### 3.3.1 Antenna Analysis

An analysis was performed to determine which type of antenna should be chosen for this type of a platform. The following matrix was used to select the optimum antenna for the sensor. The factors in Table 1 used for consideration were size, gain, bandwidth, and adaptability. From the results of this matrix, it appears that there are several choices that would be plausible for an RF passive wireless sensor platform. The choice of the type of antenna would drive the shape and size of the wireless sensor design. The loop stick antenna would make a great choice for the sensor platform because of its wide bandwidth and small size. Some of the other antenna types such as the patch antenna or log periodic antenna would also make great choices because they would make the wireless sensor flat. If the small loop or small dipole were chosen, a balun would also be required in the design. Most of the other designs are prohibitively large unless you are transmitting at a very high frequency. The seven designs in yellow are roughly equivalent. The antenna type chosen for the wireless sensor will also drive which type of antenna is chosen for the interrogator unit.

Name	Size	Size Pts	Gain	Gain Pts	Bandwidth	BW Pts	Adaptability Pts	Total
Short dipole	0.05	5	1.76	1	0.1:1	1	4	11
Short loop	0.09	4	1.8	1	0.1:1	1	4	10
Half wave dipole	0.125	4	2.15	1	0.1:1	1	4	10
Metal strip dipole	0.225	3	2.15	1	0.1:1	1	4	9
Ribbon dipole	0.225	3	2.15	1	0.1:1	1	4	9
Folded dipole	0.225	3	4.8	2	8:01	5	4	14
Microstrip patch	0.25	3	8.04	4	0.03:1	1	5	13
Yagi	0.375	2	9.2	4	0.1:1	1	3	10
Spiral	0.375	2	6.25	3	8:01	5	3	13
Log periodic	0.375	2	7.5	3	10:01	5	4	14
Bow tie	0.375	2	2.15	1	0.9:1	3	4	10
Toothed log periodic	0.375	2	7.5	3	10:01	5	4	14
Trapezoidal log periodic	0.375	2	7.5	3	10:01	5	4	14
Quarter wave dipole	0.04	5	5.14	3	0.1:1	1	2	11
Vee dipole	0.31	2	2.63	2	0.03:1	1	4	9
Long line	2	1	8.51	4	2:01	4	2	11
Capacitive plate monopole	0.04	5	3.6	2	0.04:1	1	1	9
Loop stick antenna	0.05	5	15	5	5.5:1	5	1	16
J pole antenna	0.15	3	2.15	1	1.7:1	4	4	12
Large loop antenna	0.125	4	3.09	2	1.5:1	4	4	14

Table 1. Antenna selection matrix.

### 3.3.2 Resonant Energy / Inductive Power Transfer

Another way of transmitting power to the wireless sensor is to use low frequency electromagnetic waves instead of radio frequency waves. The advantage to this method is power transfer, the disadvantage is range. The key to conducting the maximum amount of energy is resonant energy transfer between the two antennas or coils in this case. By using matched coils, you ensure the same frequency response for both the transmitter and the receiver. The following figure shows the test results of received power versus range for a pair of matched coils that were constructed from copper patterns on pcb boards. The transmitter was outputting 0 dBm at 40 MHz. The peak power transfer of approximately -3 dBm was received at a distance of 1.5 cm. As distance increases, the received power decreases.

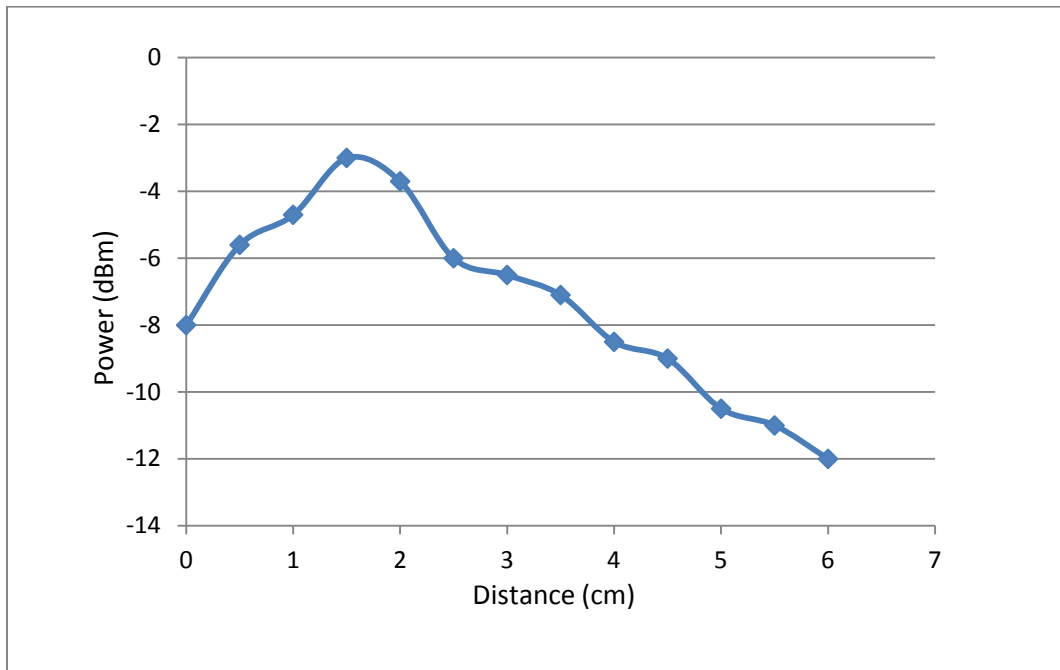


Figure 3. Received power vs. distance for a pair of matched coils.

Inductive designs rely on near field radiation effects or magnetic coupling to transfer a relatively high amount of power to the wireless sensor. They are similar to a transformer and are able to couple far more power to the sensor than an RF source.

### 3.3.3 Antenna Rectifier Circuit

The antenna rectifier circuit consists of either a single diode or a full wave bridge rectifier. RF energy is absorbed through an antenna and converted from AC to DC through diodes and is then stored in a capacitor for use by the load. The antenna rectifier circuit was designed, modeled, and constructed in 2008 with the assistance of Jiadong Wang [104]. Figure 4 shows the model used for analysis of the antenna rectifier circuit.

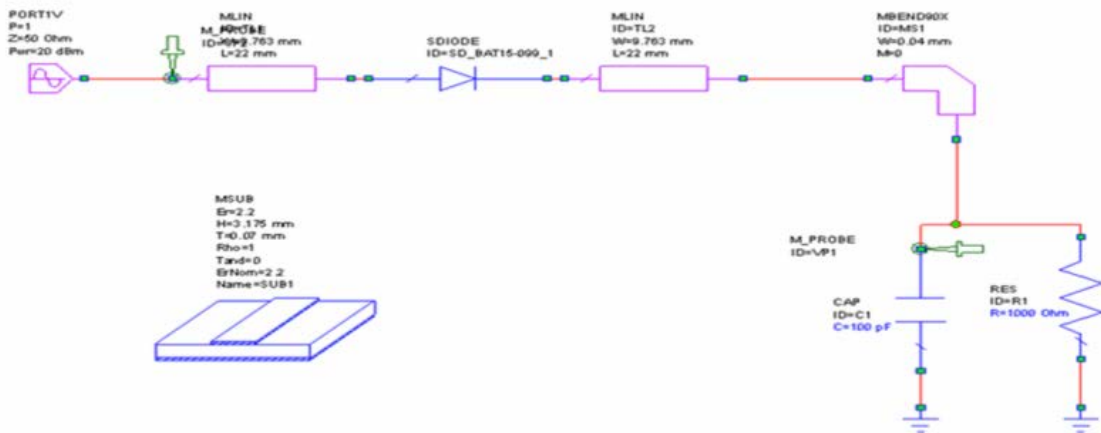


Figure 4. Antenna rectifier circuit model.

The constructed version of the antenna rectifier required approximately 10 mW of power to be received by the antenna to successfully forward bias the diode and charge the load capacitor. This means that the transmitted power had to be much higher than 10 mW. Actual tests were performed using 1 Watt of power to charge the capacitor at distances of up to 1 meter using a frequency of 2.4 GHz. Improving the range of the wireless sensor system would depend mainly on antenna gain and transmitter power. The

antenna gain on the sensor will be fairly limited because most antennas with higher gain ( $>10$ ) are also fairly large. The antenna on the transmitter is more wide open and depends primarily on what is available on the market, how large you would like it to be, and the frequency and polarization of the sensor. The transmitter power also depends on what is available on the market for the frequency of interest. Recently some power harvesting modules have shown up on the market that functionally perform the same as the antenna rectifier. Powercast now has a wireless product available that can receive  $\mu\text{W}$  or  $\text{mW}$  power levels from their  $3\text{W}$  EIRP transmitter and convert that power to DC at distances up to 10 meters [105]. The power harvesting module is fairly small, however it still needs a standard  $50\ \Omega$  antenna which can be rather large.

#### 3.3.4 Oscillator Designs

Several different oscillator designs were considered for use on the wireless board in order to transfer back the information. The intent was to use the fewest components necessary so that the wireless sensor itself could be small and inexpensive. A sort of direct FM circuit was originally desired. The VCO chips studied required a regulated voltage source and a much higher voltage and power than the interrogator source could supply at the time. Some of the common oscillator configurations such as the Hartley, Colpitts, and Clapp required extensive circuitry as well. The crystal and FET crystal oscillators were not selected because of their narrow tuning range. The FET feedback oscillators (common gate, common drain, and common source) were considered but not implemented. The parametric amplifier was designed, built and tested but the feedback signal could never be found and so that design was abandoned. Figure 5 shows the parametric amplifier design board used for experimental testing.

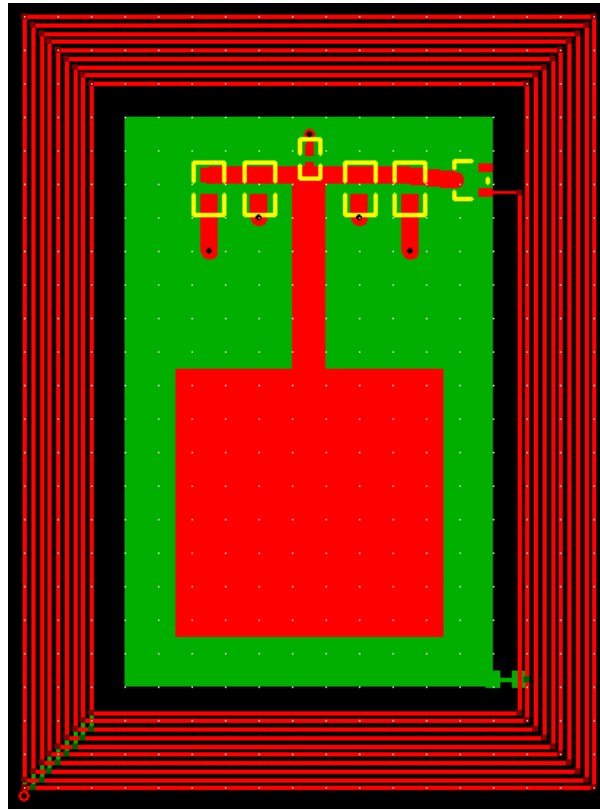


Figure 5. Parametric amplifier design board with passive components.

This design used an inductive power transfer loop antenna, a single diode, and five variable hybrid components on a circuit board with a patch antenna to retransmit. The patch was designed to transmit back the signal at 10 GHz. This design was similar to some found on proximity cards, but without using a chip and instead using passive components. The parametric amplifier works similar to a parallel LC tank circuit. When the input diode is forward biased, energy is stored in the capacitor. When the input diode becomes reverse biased, the capacitor discharges through the inductor causing a magnetic field to form around the inductor. The energy is now stored in the magnetic field around the inductor. When the current through the conductor ceases, the magnetic field

collapses, causing a current flow through the capacitor in the reverse direction. The voltage across the capacitor is in the reverse direction. When the current ceases, the process repeats in the opposite direction. The resonant frequency of the oscillation is equal to  $1/2\sqrt{LC}$ . The resonant tank circuit does not get re-energized until the input diode is forward biased again and then becomes reverse biased. This energy provided by an RF wave is called a pump. Some of the resonant energy gets transmitted out the antenna to the interrogator. The following figure shows a CPW parametric amplifier with a much smaller form factor.

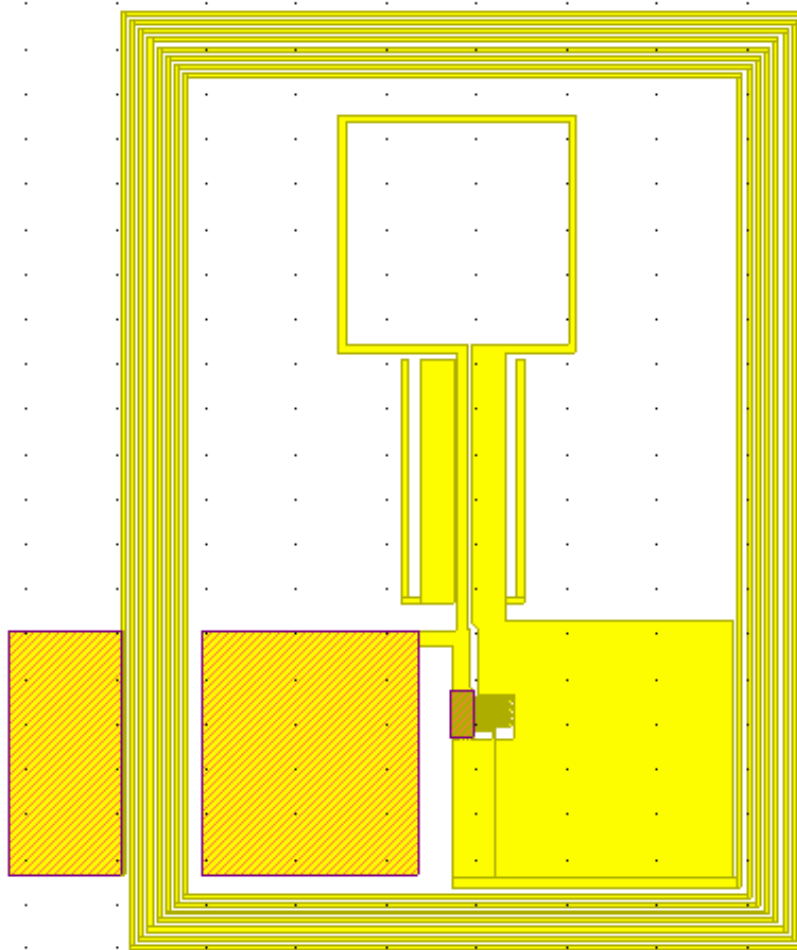


Figure 6. CPW parametric amplifier layout.

The capacitor and inductor are part of the metal layer and the only component required is the diode. The CPW loop antenna has matching baluns installed. The capacitor is an inter-digitated capacitor and can be changed by merely modifying the polymer coating on top of the wafer. This polymer changes its impedance characteristics when subjected to an analyte of interest and thus causes the resonant frequency to change.

The design that was ultimately chosen was a relaxation oscillator.

### 3.3.5 Relaxation Oscillator Design

The relaxation oscillator can run on a varying voltage source, has very few components, is very small, and can have a wide tuning range simply by changing the charge capacitance circuit. The unijunction transistor (UJT) implementation of the relaxation oscillator using the 2N6027 programmable UJT was specifically chosen.

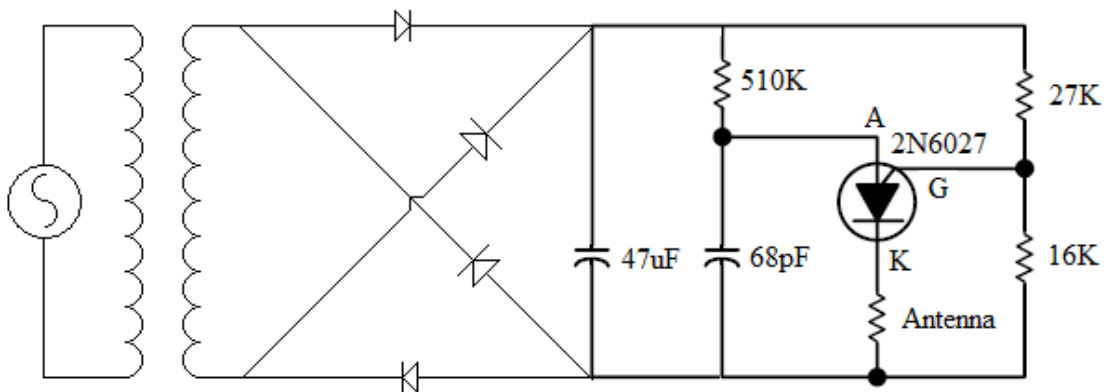


Figure 7. Circuit diagram of relaxation oscillator with inductive feed.

The circuit works by charging the capacitor attached to the anode of the unijunction transistor to a threshold value set by the bias resistor pair. The input resistor limits the charge time, but it is also there to limit valley current to cutoff the unijunction

transistor during the discharge segment of operation. When the voltage on the capacitor gets slightly above the value of the bias resistor pair on the gate of the UJT, the transistor turns on and discharges the capacitive energy through the cathode. Since the input charge resistor limits the amount of current that can flow once the capacitor discharges, the UJT shuts off and the cycle starts over again. The UJT needs a minimum amount of current to flow through it to stay on. This is known as valley current. If the current drops below the valley current threshold, the UJT turns off.

The programmable UJT is not a UJT at all, but a four layer PNP device that can be arranged to act like a UJT. The programmable UJT is called programmable because the bias voltage can be chosen at will.

### 3.4 Functionalized Surfaces

Functionalized surfaces is about the ability to pattern a surface at very small (sub-100 nm) length-scales, and to control the chemical and physical properties of surfaces at this level. This can be done to alter wetting or adhesion characteristics, improve nanoparticle dispersion in matrices, enhance catalytic properties of the surface, or to order an interfacial region. Lithographic techniques do not inherently allow control over the surface chemistry. There are several chemical techniques that can build (pseudo-) 3D structures. A new area is the creation of specific surface sites on nanoparticles for selective molecular attachment.

For this research a functionalized surface will specifically mean: a substrate with standard bulk material properties that has had its surface modified either chemically or physically so that it is sensitive and selective to an analyte of interest. The surface chemistry of the sensors will be modified to enhance chemical bond formation. Different

thiols will be bonded to the gold surface to attach to proteins, DNA, and other biological matter.

In order to only affect the surface chemistry in a few areas a soft-lithographic technique can be used. Structures can be fabricated and replicated using elastomeric stamps, molds, and conformable photomasks. It is called "soft" because it uses elastomeric materials, most notably PDMS. Soft lithography is generally used to construct features measured on the  $\mu\text{m}$  to  $\text{nm}$  scale. Some advantages are lower cost than traditional photolithography in mass production, it is well-suited for applications in biotechnology, it is well-suited for applications involving large or non-planar (non-flat) surfaces, there are more pattern-transferring methods than traditional lithography techniques, and it does not need a photo-reactive surface to create a nanostructure.

Another way to affect the surface chemistry is through Self-assembled monolayers. Self-Assembled Monolayers (SAMs) are widely used in a variety of emerging applications for surface modification of metals and oxides. SAM growth results in a pronounced increase of the surface conductivity of organic materials, which can be very large for SAMs with a strong electron-withdrawing ability. For example, the conductivity induced by perfluorinated alkyl silanes in organic molecular crystals approaches  $10^{-5}\text{S}$  per square, two orders of magnitude greater than the maximum conductivity typically achieved in organic field-effect transistors (OFETs). The observed large electronic effect opens new opportunities for nanoscale surface functionalization of organic semiconductors with molecular self-assembly. In particular, SAM-induced conductivity shows sensitivity to different molecular species present in the environment, which makes this system very attractive for chemical sensing applications.

Another method similar to self-assembling monolayers is self-organization. The principle of self-organization, which allows very economical use of resources, is also exploited in the production of functionalized surfaces required in molecular electronics, sensor applications, catalysis and photovoltaic components. The idea of the manufacturing process is that molecular components are brought into contact with a substrate material, and then “magically” find their preferred positions in the desired molecular network. The starting components are selected to display specific structural and chemical features intended for the envisaged application.

Any of these methods can be used to alter the surface chemistry of the IDC or gap surface. Another method using polymers creates a surface modification that allows for the creation of chemical specific surfaces. These can be thin, thick, bio, or doped polymer films. This is one of the methods being used in this research.

## CHAPTER IV

### PLATFORMS

Several different platforms were built and tested for this research. The first platform is an inductive fed relaxation oscillator sensor system about the size of a credit card. The second platform is a coplanar waveguide patch antenna system with an interdigitated capacitor that is about the size of a paperclip. The third platform is a coplanar waveguide probed biological sensor about the size of a grain of sand. There were several other RF platforms that were designed that are presented and simulated. Some of them were actually constructed and tested, but not all. They are all presented below.

#### 4.1 IDSense

IDSense is a platform about the size of a credit card. It consists of spiral loop transmit/receive antennas, a full wave bridge rectifier and a relaxation oscillator. The charge capacitor in the relaxation oscillator consists of a surface mount capacitor in parallel with an Inter-Digitated Capacitor (IDC). The IDC is coated with either a silk biopolymer or nafion film for chemical/biological testing. The impedance characteristics of the polymer film change when subjected to an analyte of interest. This in turn causes the charge time for the capacitor pair to vary, affecting the resonant frequency of the relaxation oscillator.

#### 4.1.1 IDSense Antenna Design

An 18 loop copper planar coil was designed using a 0.015” wide trace with 0.01” separation between traces. The 0.01” separation was because of the current industry limits for PCB manufacturing. The 0.015” width was to maximize the number of loops in a certain given area of the board. The outer most edges of the coil measured 1.7” x 2.4.” The wireless sensor board and the transmitting board had almost identical antennas.

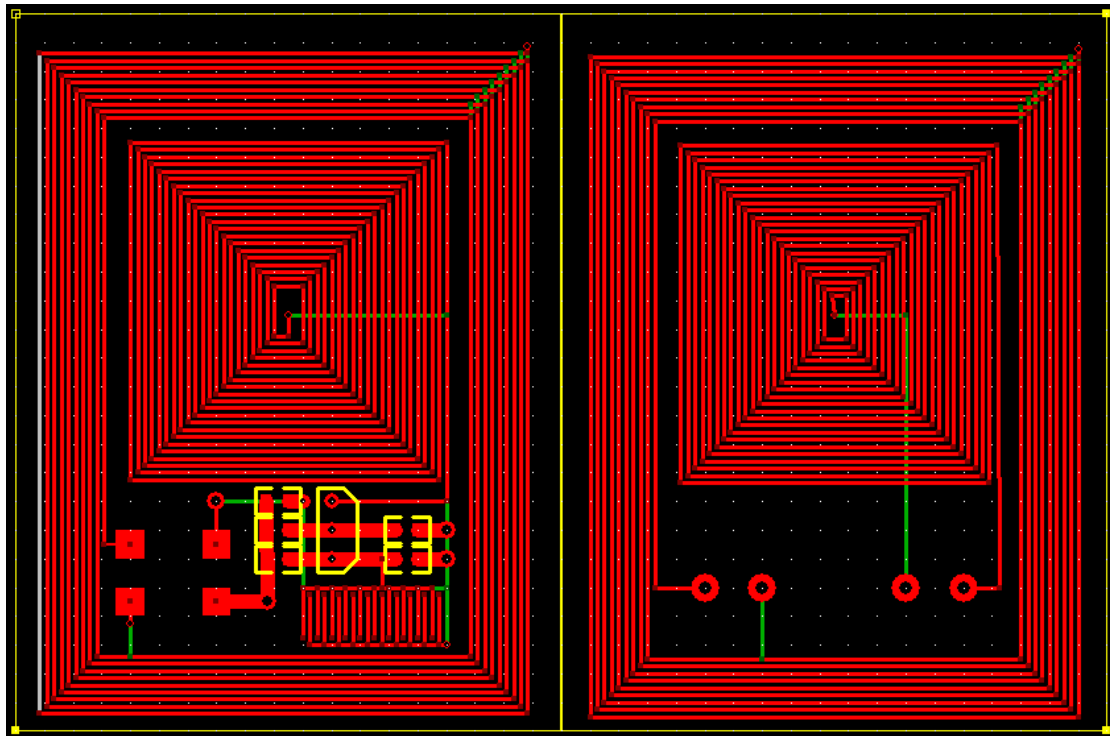


Figure 8. Resonant energy transfer board set.

Figure 8 shows the PCB layout of the two boards. The outer loop on the right board is the interrogator transmitting antenna. The outer loop on the left board is the wireless sensor receiving antenna. The inner loop on the left board is the wireless transmitting antenna. The inner loop on the right board is the interrogator receiving antenna. The antennas on the relaxation device use magnetic coupling to power up the wireless sensor and to transfer information back to the interrogator.

An analysis of the frequency response of the matched coil set was performed with a network analyzer. Figure 9 shows that the band of frequencies between 30 - 40 MHz and around 100 MHz provided a good flat response for the transmitter/receiver pair. The low frequencies also provided a good response. This means that minimal loss will occur across the pair of antennas at these frequencies.

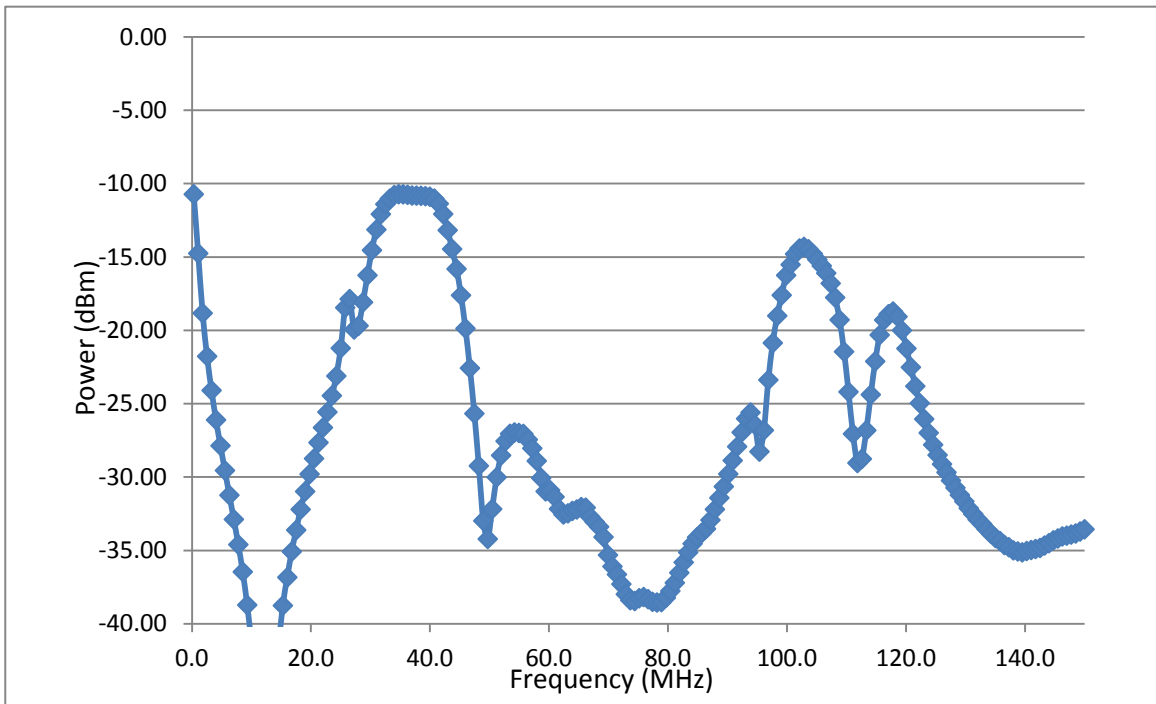


Figure 9. Swept frequency S21 plot of resonant energy transfer.

The spectral response was tested all the way out to 3 GHz but didn't yield any greater responses. Because the inner set of antennas use a very low frequency in the 10 kHz range, their low frequency behavior is very similar to the outer antennas and thus their spectral response is not shown. The crosstalk behavior from the outer antenna loops to the inner loops was also tested to find an optimal interrogation frequency for sending power with minimal interference on the receiver.

#### 4.1.2 IDSense Rectifier Design

The rectification method used in the wireless receiver board was slightly different. The first design utilized a single diode for simplicity and worked similar to a half wave bridge rectifier. This was found to limit the amount of power transferred to the board and the subsequent DC voltage created across the holding capacitor. Figure 10 shows the DC voltage induced on the wireless board with a single diode rectifier circuit.

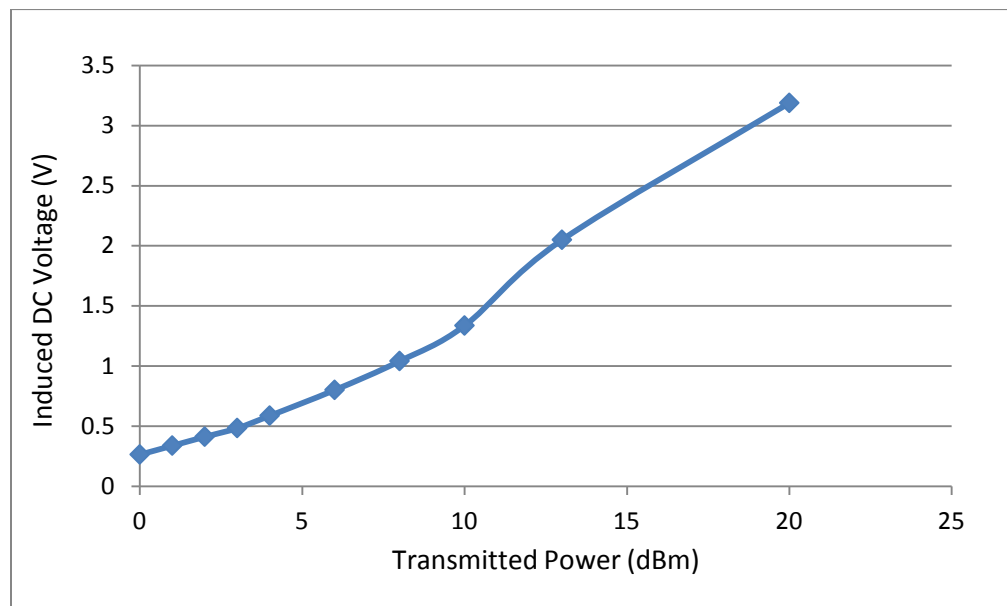


Figure 10. Induced DC voltage vs. transmitted power for the 40 MHz energy transfer system.

This design was replaced with a full wave bridge rectifier which had much better power characteristics. Figure 11 shows the DC voltage induced on the wireless board with a full wave bridge rectifier.

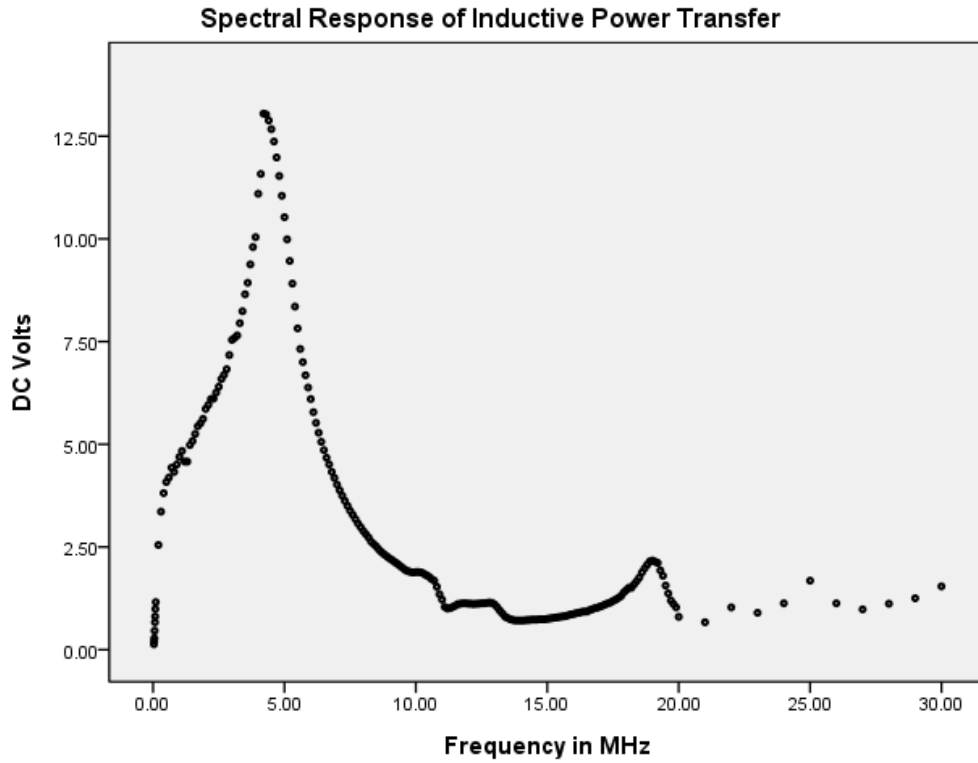


Figure 11. Full wave bridge DC voltage power transfer.

#### 4.1.3 IDSense Relaxation Oscillator Design

The IDSense platform used the standard unijunction transistor implementation of the relaxation oscillator with the 2N6027 programmable UJT.

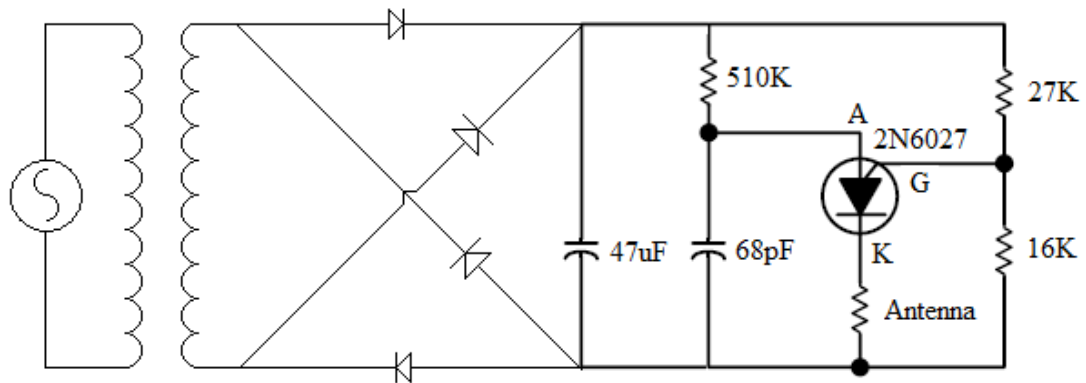


Figure 12. Schematic of inductive fed relaxation oscillator.

The only difference is that an interdigitated capacitor was placed in parallel with the 68 pF charge capacitor. The IDC had a nominal capacitance of about 20 pF when bare or coated with Silk. When the IDC was coated with Nafion, the nominal capacitance was closer to 74 nF. Figure 12 shows the schematic of the inductive fed relaxation oscillator setup used for the IDSense platform.

The final layout of the components changed slightly with the third revision of the IDSense board. The soldered components were moved to the left to keep the IDC area more accessible.

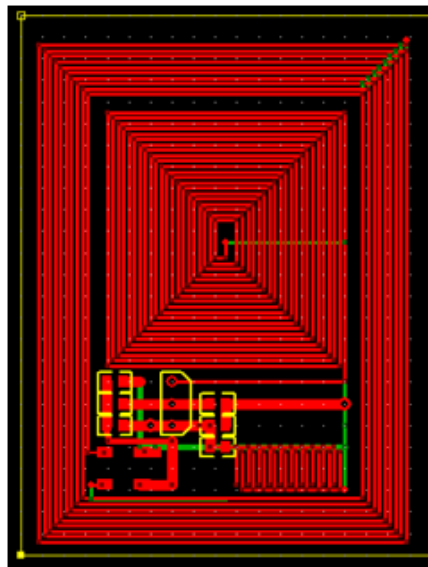


Figure 13. Final IDSense board layout.

#### 4.1.4 IDSense Interrogator Design

The Interrogator must be able to transmit power to the IDSense board and also receive and decode the return signal to obtain the intelligence. Several different types of waves were tested with a function generator to see which type of waves could be tolerated on the inductive fed passive wireless sensor front end. The sine wave was of course the best, however the triangle and square waves worked, but with less power

transfer. This would be because of higher order harmonics being suppressed by the inductive coil transmission properties (S21). The transmitting piece of the interrogator could be either a voltage controlled oscillator, or a fixed oscillator. If a square wave was used, the output of a microcontroller on a n interrupt loop would also work. The impedance of the transmitter coil is very low and requires an amplifier to buffer the output. The receiving side is actually easier to work with. The received signal contains feedback from the transmitter in addition to the pulse from the relaxation oscillator output. However the received pulse is sufficiently large enough to separate from the carrier feedback that a simple comparator could be used. The timing between pulses would determine the information from the sensor. Figure 14 shows the voltage on the charge capacitor on the bottom for a reference and the received signal on the top.

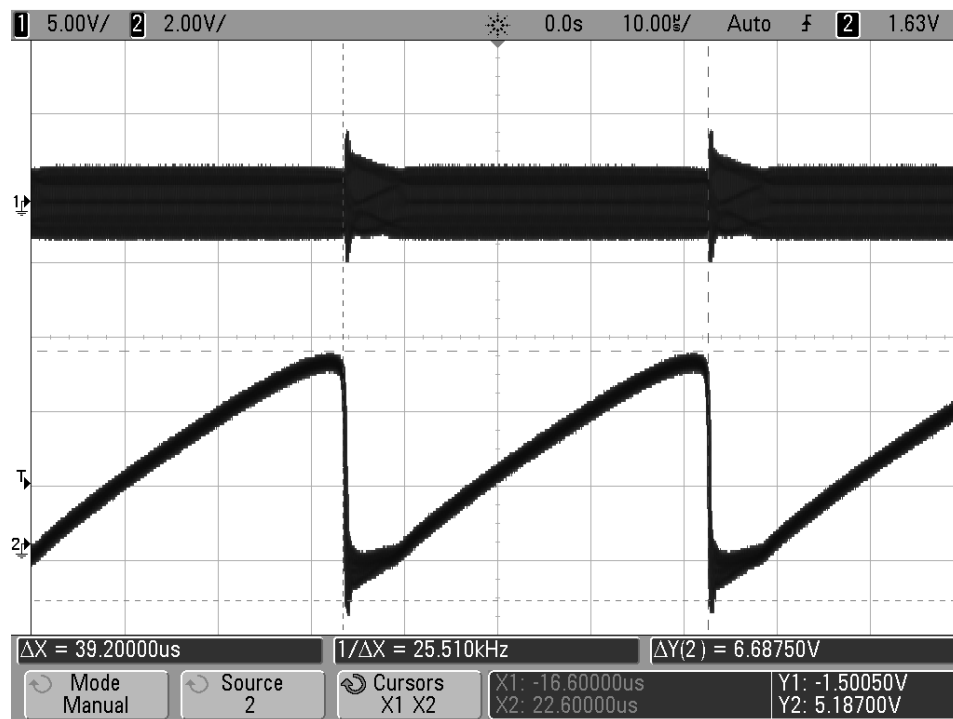


Figure 14. Received interrogator signal with reference.

The most plausible way to design the interrogator seems to be with an embedded microcontroller. The microcontroller would use an interrupt output to create the transmitting signal, which after being fed through a buffer amplifier would power the transmitting antenna. The received signal would come in and could either be sampled with an analog input or sent straight to a comparator. The comparator reference could even be made dynamic with a D/A output from the microcontroller. This system would be able to account for differences in received signal strength due to misalignment or distance changes. The microcontroller could be placed on the same board as the Transmit/Receive antenna pair or could be a separate board connected to the other board. The microcontroller board even with an LCD display would be much smaller than the Transmit/Receive antenna pair board. This whole system could be handheld and about the size of a cell phone. The interrogator design didn't change with the other revisions of the IDSense board. The final interrogator antenna design is shown in Figure 15.

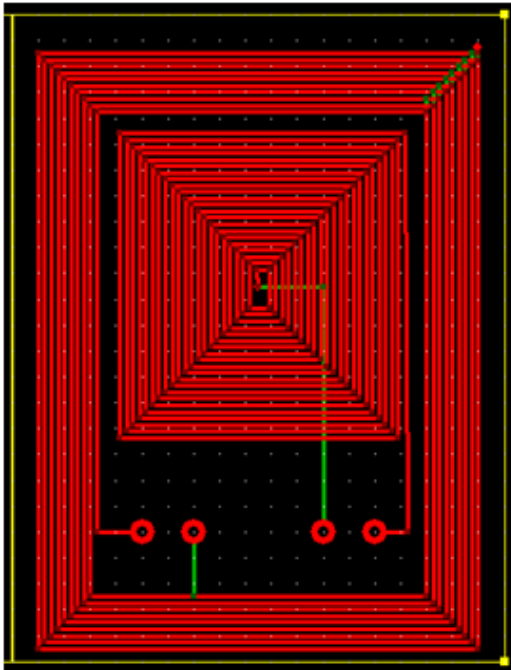


Figure 15. Final IDSense interrogator board.

## 4.2 Passive RF

The following sensor is composed of a pair of CPW patch antennas separated by an inter-digitated capacitor (IDC). The design is symmetrical and allows power to arrive in any of the antennas and flow out the other antenna or be reflected back. The IDC could be coated with a polymer or other functionalized surface so that it only changes its properties when the chemical of interest is present. When the IDC value changes, the amount of power reflected (S11) and transmitted (S21) will change and be easily detected on a network analyzer. The special part of this design is that it is all on one layer. This design could be printed onto a non-conductive surface and functionalized rather easily. There are no hybrid components to add and the design could be submerged in a liquid.

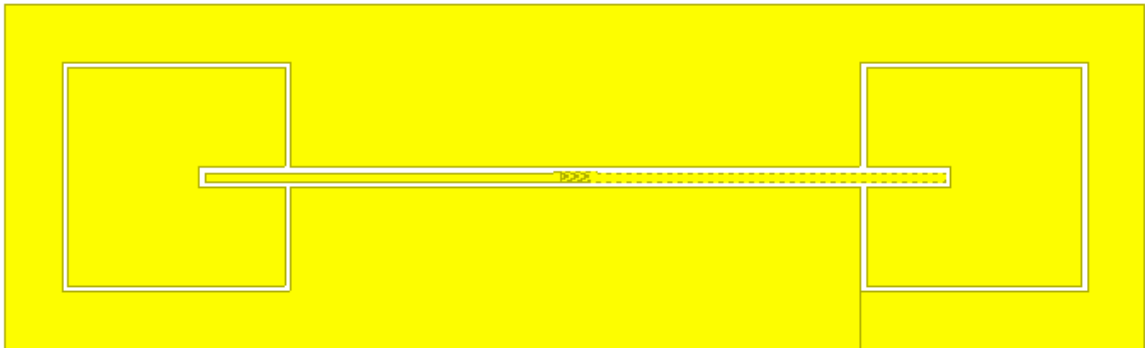


Figure 16. IDC based CPW antenna wireless sensor.

The following figure is a close-up of the inter-digitated capacitor.

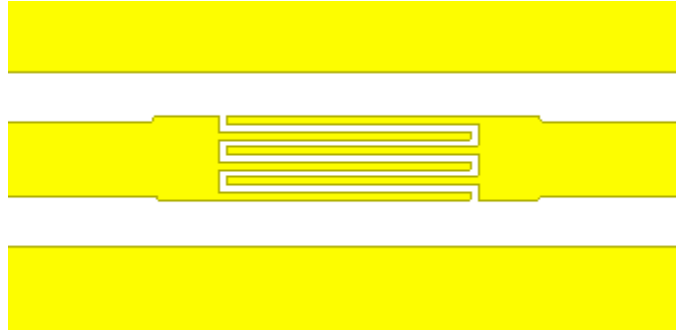


Figure 17. Close-up of IDC structure.

The next figure is the interrogator board that is used to couple signals to/from the passive RF board. The left and right end CPW feed lines will have SMA-CPW adapters soldered on so that a generic network analyzer can be used to interrogate the passive RF board.

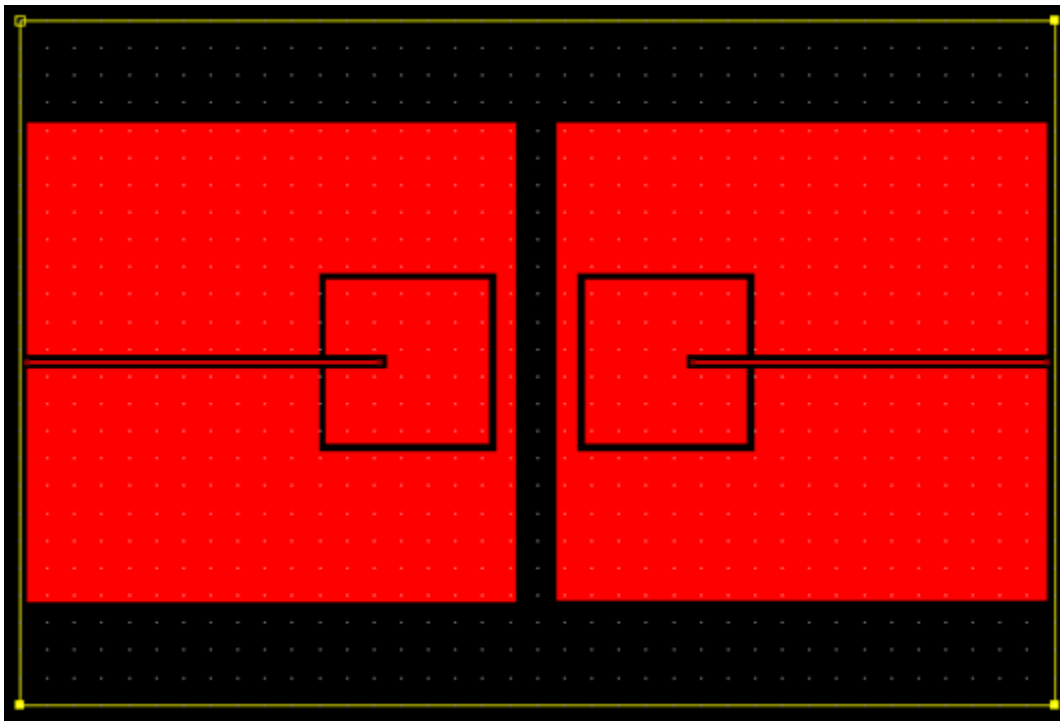


Figure 18. Passive RF interrogator board.

The S parameters from the network analyzer will be used to determine the analyte concentration and identification. This will have to be done with a computer program after extensive characterization and analysis.

### 4.3 Bio-Bridge

While the two previous designs were more oriented towards chemical sensors, this following design is primarily for volatile organic compound (VOC) sensing or possibly even single molecule detection. This design is called Bio-Bridge and it utilizes DNA as a molecular ‘wire’ to create an organic circuit. The Bio-Bridge sensor design places the DNA in a true wire orientation: current enters one end of the DNA, passes through the ‘wire’ and out the other end of the DNA. The Bio-Bridge sensor device is functionalized with DNA of known length and base pair sequence in order to accomplish the VOC sensing. Sensitivity of DNA sequence to selected VOCs incorporates a bio-sensing capability into the circuit design.

#### 4.3.1 DNA Research

VOC detection using DNA as the sensing molecule is an emerging research area. Current research on DNA as a molecular wire and for VOC sensing utilizes DNA that has been immobilized via adsorption or chemical tethering to a sensor or electrode surface [106, 107]. DNA has been proposed for use as a molecular wire for a least 10 years but no studies to-date have examined the actual transport of electrical current through DNA strands tethered at both ends to form a linear circuit. This is the first instance of using strands of DNA truly as a molecular wire to create an oriented hybrid organic circuit.

#### 4.3.2 DNA Charge Transduction Background

Charge transduction through DNA has been a topic of much research in the last decade due to the advent of using DNA for molecular computing. The Barton research group at the California Institute of Technology has published prolifically on many aspects of charge transport through DNA and their recent review evaluated a large body of research on the mechanism of DNA charge transport [108]. Essentially, charge transport through double-stranded DNA is dependent on the structure, or pi stacking, of the DNA base pairs and the integrity of the pi stack. Charge can take two paths to travel through DNA: linearly through the bases arrayed in each of the complementary strands (intrastrand) or laterally across the hydrogen bonded complementary base pairs (interstrand). Regardless of the path, charge travels through the base pair stack, not along the sugar-phosphate backbone on the outside of the DNA helix. The effect of length on the DNA strand has been considered problematic in the development of DNA molecular wires. Slinker et al. used DNA of two different lengths (100 versus 17 DNA base pairs) to elegantly demonstrate that regardless of length, the rate of charge transfer through DNA was the same; in addition, this is the first published report using 100 base pair DNA of known sequence to examine charge transfer [109]. Synthesis of long DNA strands (> 50 base pairs) is known to be problematic therefore most of the research has been conducted using 20-40 base pairs. Charge transduction through DNA exposed to selected volatile organic compounds (VOC's; e.g. ethanol, toluene) is altered due to transient VOC adsorption. Positioning the known sequence and length DNA across the gap completes the electrical circuit and allows measurement of DNA charge transport (as current, I) in response to exposure to selected volatile organic compounds.

### 4.3.3 Physical Construction

Bio-Bridge is a micro-sized sensor with a nano-sized gap in which the DNA bridge is formed. Since nano-meter sized probes don't currently exist, the Bio-Bridge structure uses a Co-Planar Waveguide (CPW) probe pattern of ground-signal-ground in which to make contact with the sensor. However the size of the DNA is in the order of nanometers while the CPW probes have a pitch of approximately 100 micrometers. In order to get down to the small size of DNA, the CPW trace goes through a necking-down (size reduction) step to get down to a 5 micrometer intermediate size. Then there is another necking-down step that occurs in the very center of the CPW structure from the intermediate size to a final diameter of only 300 nanometers.

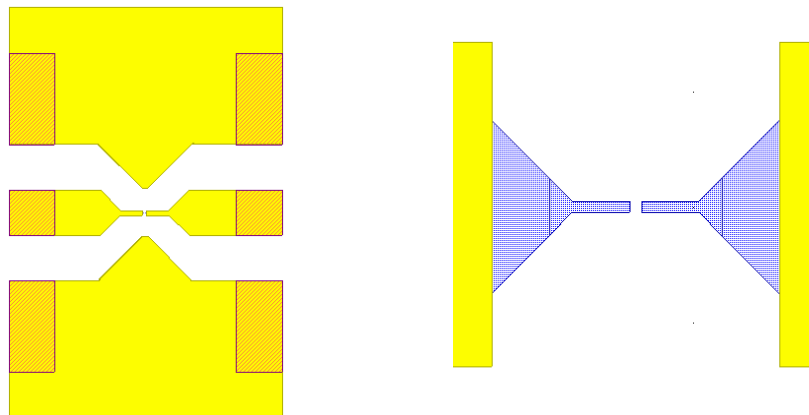


Figure 19. CPW Bio-Bridge platform showing close-up section (right).

Because the dimensions of the bridge are so small, standard lithography techniques could not be used. A special electron beam lithography system made by JEOL available at AFRL was used to achieve the nano-sized patterns on the metal layer. The gap between one signal line on one side and the other was varied across a range of 60 to 200 nanometers in order to find out which gap distance provided the optimum

connectively as well as selectivity. The devices are fabricated with a range of gap distances so we can explore the signal transduction as a function of DNA length as well as sequence. DNA of known sequence and length will be used to ‘bridge’ the gap and create a closed circuit. The optimum design would allow a single strand of DNA to be connected to both sides of the sensor and sort of be stretched across the gap. All CPW structures and reduction steps are symmetrical. The Bio-Bridge structure is constructed on silicon with single layer Ti-Au electrodes using standard electron beam deposition techniques.

A test coupon was constructed to test the JEOL capability and to have an accurate gap between the center electrodes. This test coupon is shown in Figure 20.

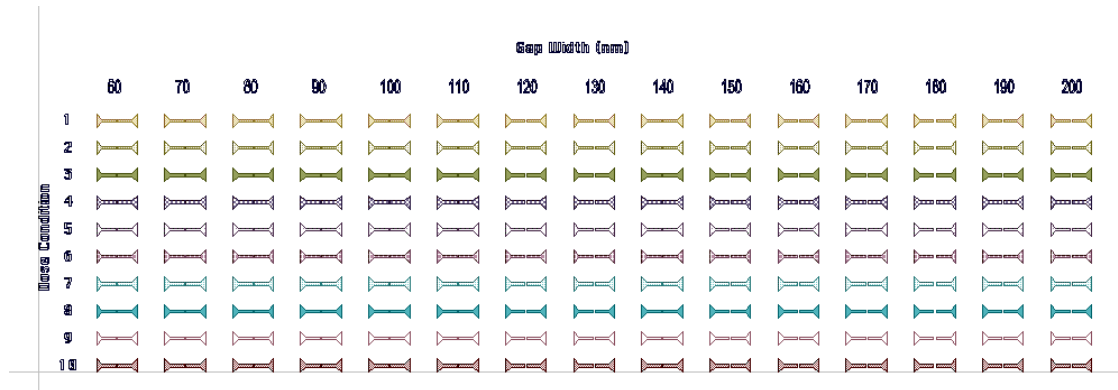


Figure 20. Test coupon for SEM bridging gap analysis.

During construction of the first wafer it was discovered that over etching of the photo resist was occurring and the gap was becoming non-existent or too small. When this happened, the gap disappeared, shorted out, or had miniature stringers across the gap which also made it short out.

Figure 21 shows some of the results of the test coupon after fabrication for several different recipes. A Scanning Electron Microscope was used to take the images.

Drawn Gap (nm)	100	110	120	130	140	150	160	170	180	190	200
Sample A											
Actual Gap							42	58	75	75	98
Sample B											
Actual Gap								20	31	29	
Sample C											
Actual Gap								80	95	112	
Sample D											
Actual Gap									51	68	

Figure 21. Results of SEM images of test coupon.

The next figure shows a blown up image of the gap showing the tapering, over-etching, and resulting bridge gap.

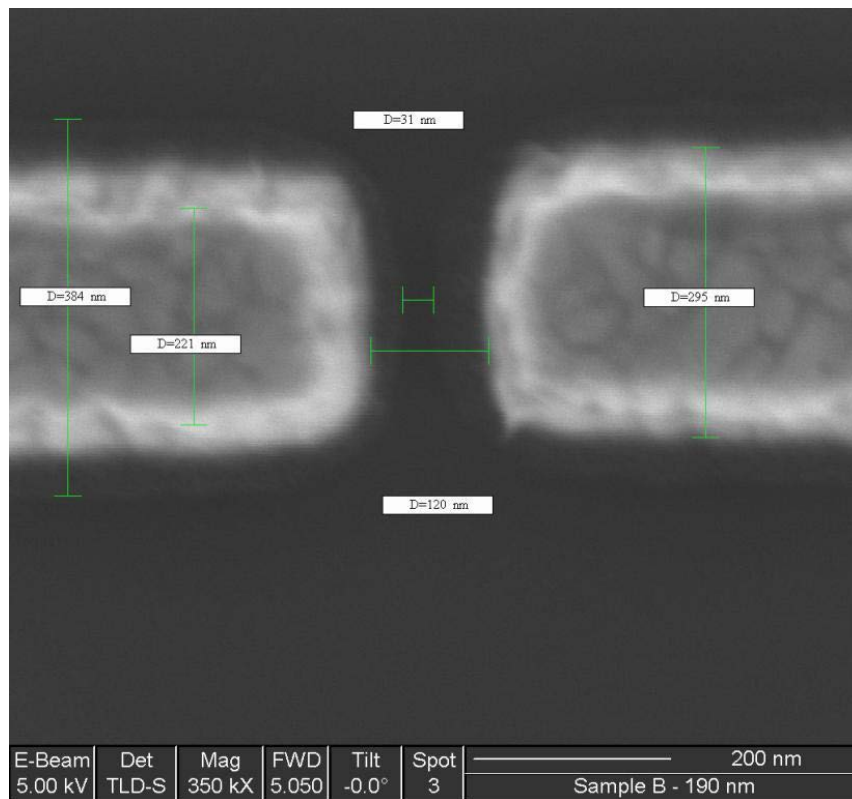


Figure 22. A close-up view of a SEM image.

The measured gap versus drawn gap was compared to try and determine which of the four recipes created the best resultant gap structure. The developer process D was determined to make the most linear result after the process was complete. Figure 23 shows the result of four different developer combinations and their linearity results in addition to slope and offset.

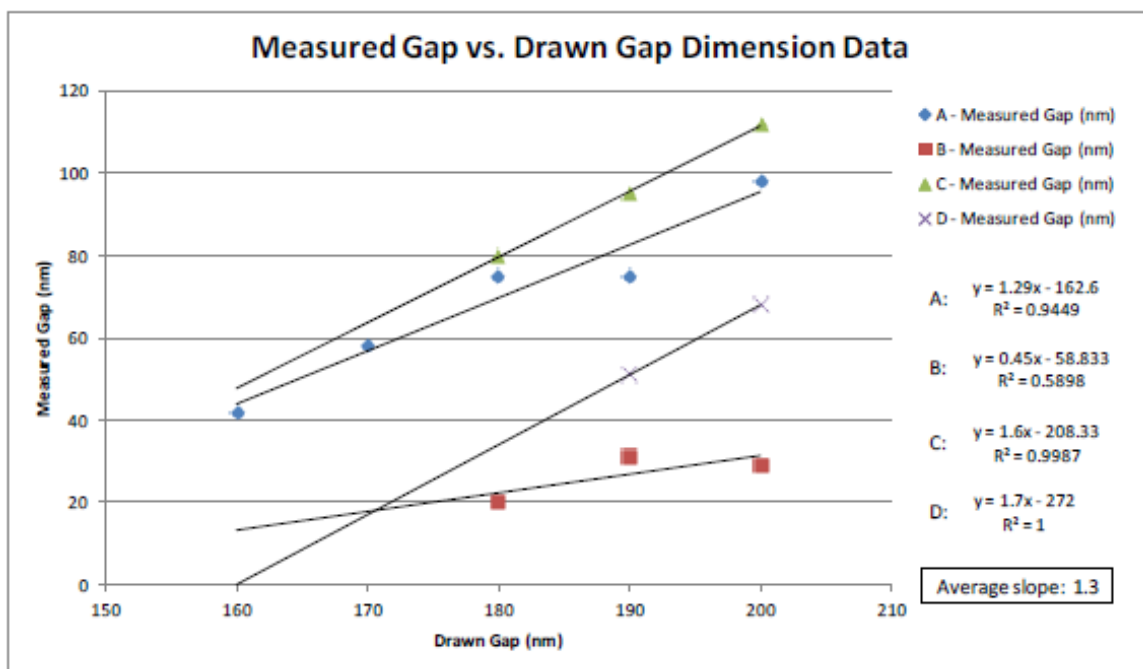


Figure 23. Measured gap vs. drawn gap for four developer combinations.

#### 4.3.4 Biological Part

A ready source of known length and known sequence DNA exists in the form of a bacterial plasmid DNA. Plasmids are pieces of circular DNA that can be transferred/exchanged between bacterial cells and have been used for many years to introduce genes into bacteria (they are called vectors). The Bio-Bridge sensor uses a common molecular biology vector, plasmid pBR322, which is a circular DNA molecule of known length (4361 base pairs) and known sequence.

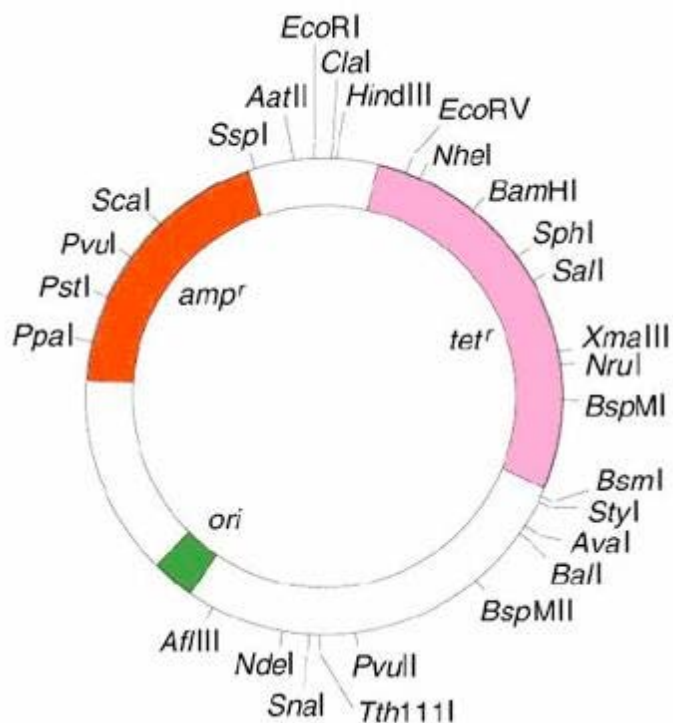


Figure 24. Plasmid pBR322 and its cut sites [110].

Plasmids have known enzymatic cut sites where genes can be inserted into the plasmid DNA. Plasmid pBR322 has multiple restriction enzyme cut sites (designated on image). Variable length DNA can be generated by choosing the appropriate cut sites to yield a specific length. When digested with a particular enzyme the plasmid DNA is cut into fragments of known length and sequence. The DNA fragment pattern allows us to closely match the DNA strand length for a given gap distance (range 50-250 nanometers). For reference: 100 nm length DNA is approximately 300 base pairs of double stranded DNA. Cut DNA of known length in the range of 50-250 nm (150-750 base pairs) is tethered to bridge a nanoscale gap of known distance. Use of plasmid DNA as the molecular wire gives us a range of DNA length options currently unavailable via DNA synthetic techniques and therefore widens the capability for generating longer fragments of DNA (150-750 base pairs) for exploring DNA charge transport.

#### 4.3.5 Construction

After the metallization sequence of making the Bio-Bridge sensor is complete, the DNA biomolecules need to be deposited on the mechanical structure. This next sequence requires nanoliter volumes of reagents and biomolecules to be deposited on opposing sides of the gap in an ordered fashion to form a closed hybrid organic circuit. First, short thiolated DNA linker molecules with 'sticky' ends will be deposited on opposing sides of the gap. Second, DNA will be prepared by enzymatic digestion of pBR322 plasmid DNA at specific cut sites to yield fragments of defined/known length with complementary 'sticky' ends. Finally, the DNA fragments of selected length will be ligated to the thiol-tethered linkers to complete assembly of the organic Bio-Bridge circuit. This is how the DNA strands are formed into a molecular wire. After construction, Scanning Electron Microscope (SEM) imaging is used to inspect the bridge.

#### 4.3.6 Sensing Mechanism

The specific sequence of DNA base pairs can be used for sensing of volatile organic compounds (VOCs). VOC detection using DNA as the sensing molecule is an emerging research area which combines the structure and orientation of DNA as a molecular wire with VOC biosensing capability (DNA sequence-specific sensitivity and selectivity). White et al. (2008; via fluorescent tags) and Lu et al. (2010; using graphene sheets) incorporated short single stranded DNA lengths (< 24 bases) of varying sequence to discriminate between selected VOCs. It is anticipated that certain DNA sequences will have some selective affinity for specific VOCs. The specificity will be a function of the DNA sequence and the affinity of a given VOC for the sequence. DNA sequences can be varied to determine affinity and selectivity of the DNA for individual VOCs.

#### 4.3.7 Vapor Testing

In order to determine the response of the assembled DNA/Bio-Bridge device to VOCs, the assembled devices will be exposed to selected VOCs via a vapor generation system. The different solvent vapors change the electrical current flow due to the interaction of the solvent with the DNA of known sequence. Devices will be subjected to repetitive increasing/decreasing VOC exposures to determine concentration response and regeneration of the devices. Selected VOCs interact with known DNA sequences with some specificity and the interaction results in a change (+/-) in electrical current through the DNA/Bio-Bridge circuit. Electrical response of the Bio-Bridge device will be determined using an electronic probe station before and after VOC exposure to assess the change in current through the DNA strands due to VOC binding.

#### 4.3.8 Electro-Magnetic Device Testing

The electrical response of the bio-bridge sensor device will be tested with an electronic probe station and a network analyzer. The network analyzer allows many more parameters than just current to be measured and it also allows us to vary the frequency of the interrogating signal. The network analyzer is connected to the CPW probes on the electronic probe station and is able to measure the nano-watt power levels across the bridge and calculate the impedance of the DNA strand. The Bio-Bridge design is impedance matched for minimal reflective power loss to work properly with the network analyzer. There is a CPW probe effectively touching each side of the strand of DNA. Testing will first be conducted to determine the baseline characteristics of the metal layer by itself prior to biological construction. Then, the viability of the fabricated Bio-Bridge sensor devices will be tested. The Bio-Bridge sensor device will be tested

under standard ambient conditions and then be subjected to VOCs. Variations in signal can be used to analyze DNA sequence or the number of DNA strands across the gap. The assembled Bio-Bridge sensor will be exposed to selected VOCs to determine sensitivity of the Bio-Bridge and specificity of the DNA for individual VOCs. The differential signal between non-VOC-exposed and VOC-exposed Bio-Bridge devices is the desired metric to demonstrate if VOC binding changes the current across the DNA organic circuit. Current ( $I$ ,  $\mu\text{Amps}$ ) will also be plotted as a function of time with periodic VOC exposure (on-off) intervals. Repeated exposure of Bio-Bridge devices to VOCs will allow determination of regeneration capability and/or degradation of sensors. The Bio-Bridge sensor device will be tested for each selected DNA fragment sequence and length. Statistical analysis will be conducted using standard techniques with the Prism statistical software package.

#### 4.3.9 Applications

The Bio-Bridge sensor device can be fabricated in a multi-device array to allow for discrimination of complex volatile mixtures. The fabrication and DNA functionalization protocols are elegantly simple and inexpensive and could be produced in an array format as an affordable sensor.

#### 4.4 Other RF Designs

There were several other RF platforms that were designed and some of them were even built. Not all designs were inductive based. There were several concepts that were designed based on RF signals only and the change in amplitude and phase for select frequencies. One concept involves an antenna, a varactor shunt switch, and a series inductor so that the series resonance would cause the combined impedance to pass through a local minimum at a design frequency. Following in figure 25 is a schematic of how the inductor would fit into the circuit model for the varactor shunt switch.

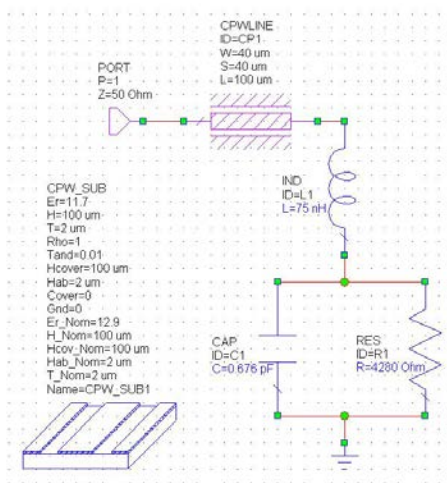


Figure 25. Model of a RF varactor shunt switch with a single series inductor.

Figures 26-28 shows the S11 parameters for the normal range of the varactor shunt switch with a fixed inductor in series. As the capacitance of the varactor shunt switch changes, the resonant frequency of the device moves from approximately 700 MHz to 1300 MHz. As capacitance decreases, the resonant frequency of the device increases. Amplitude also varies with a change in capacitance. The peak dip appears around 980 MHz. Another concept involves a series capacitor in addition to the series inductor to shift the frequency up around 10 GHz.

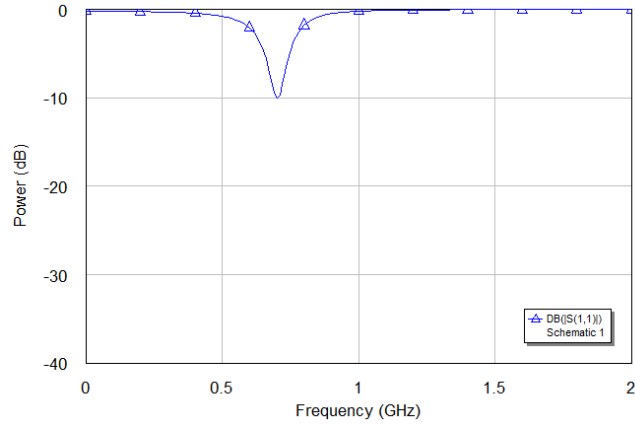


Figure 26. Swept frequency reflected power (S11) for a varactor shunt switch with a single series inductor at the low resonant frequency point.

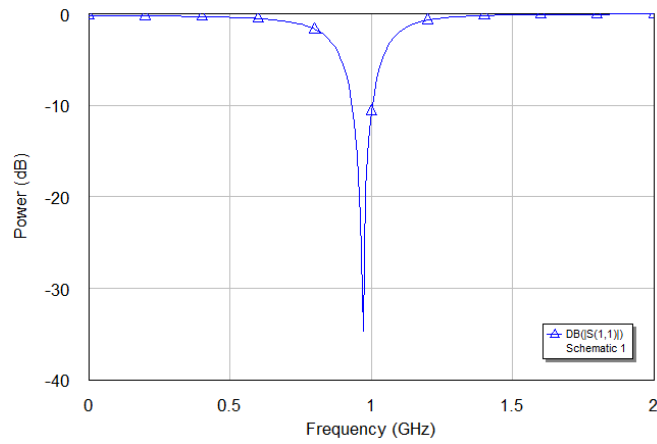


Figure 27. Swept frequency reflected power (S11) for a varactor shunt switch with a single series inductor at the middle resonant frequency point.

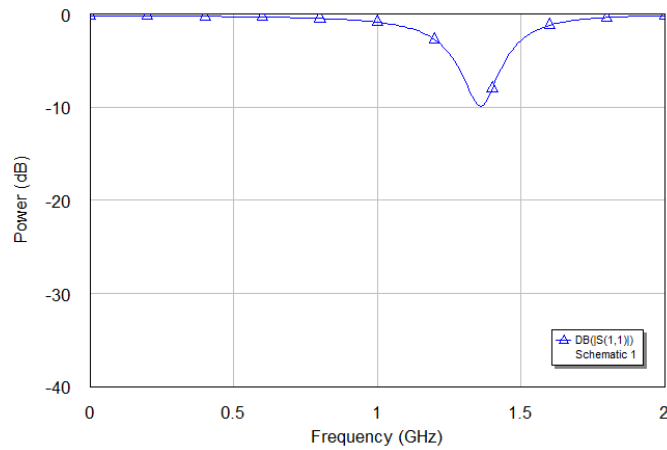


Figure 28. Swept frequency reflected power (S11) for a varactor shunt switch with a single series inductor at the high resonant frequency point.

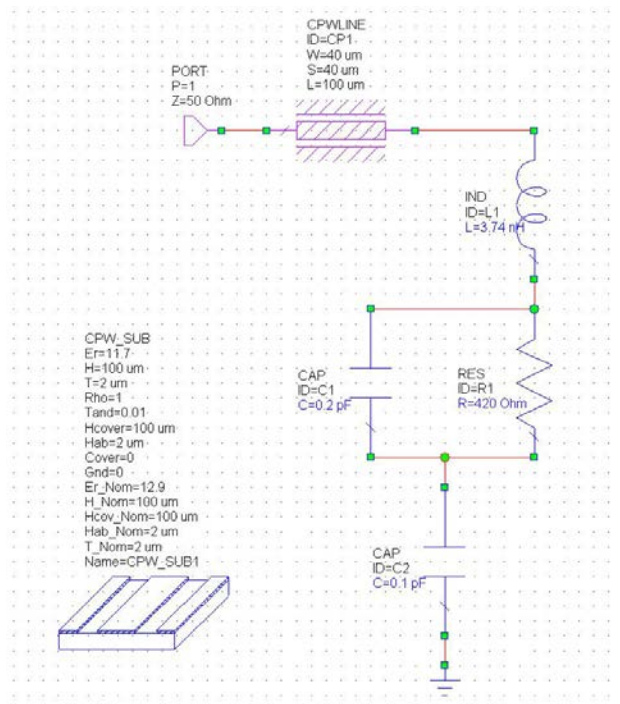


Figure 29. Model of a RF varactor shunt switch with a series inductor and capacitor.

Following are S11 parameters for the normal range of the varactor shunt switch with an inductor and capacitor in series.

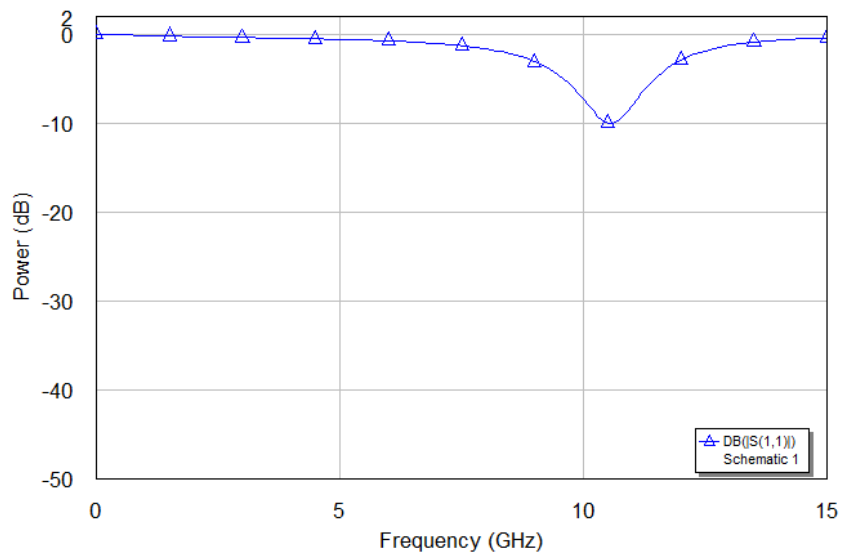


Figure 30. Swept frequency reflected power (S11) for a varactor shunt switch with a series inductor and capacitor at the low resonant frequency point.

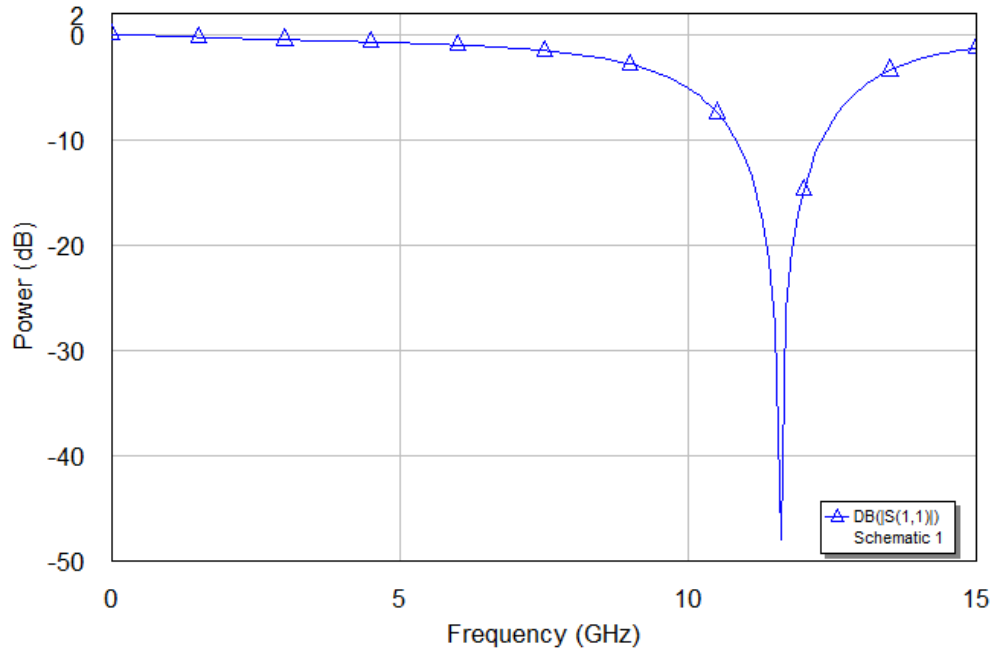


Figure 31. Swept frequency reflected power (S11) for a varactor shunt switch with a series inductor and capacitor at the middle resonant frequency point.

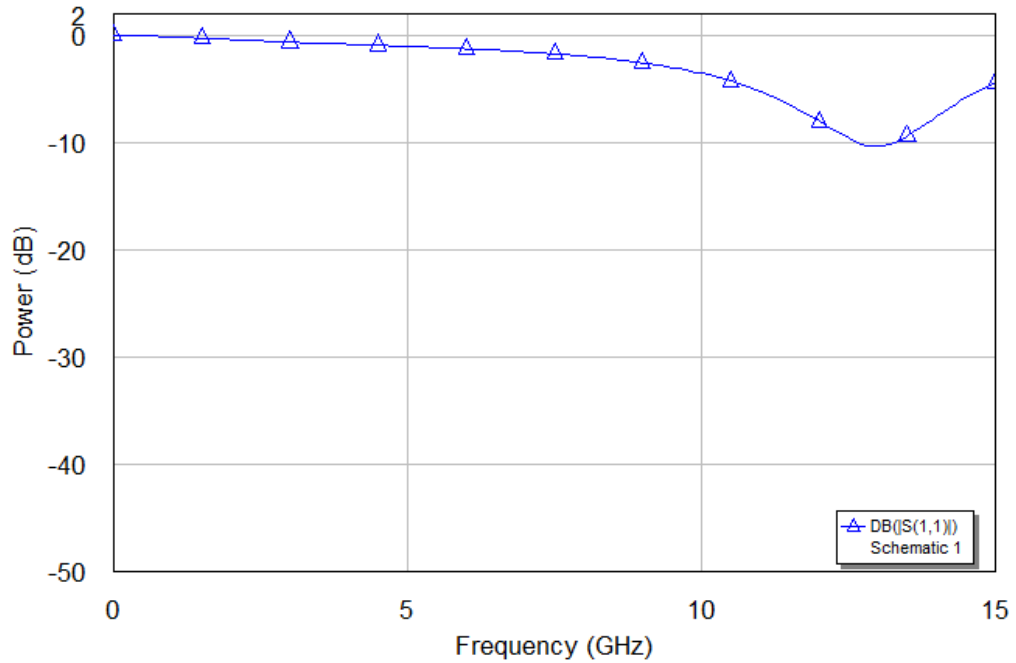


Figure 32. Swept frequency reflected power (S11) for a varactor shunt switch with a series inductor and capacitor at the high resonant frequency point.

A third concept involves a series transmission line between two varactor shunt switches. As capacitance changes, the resonance characteristics change as well.

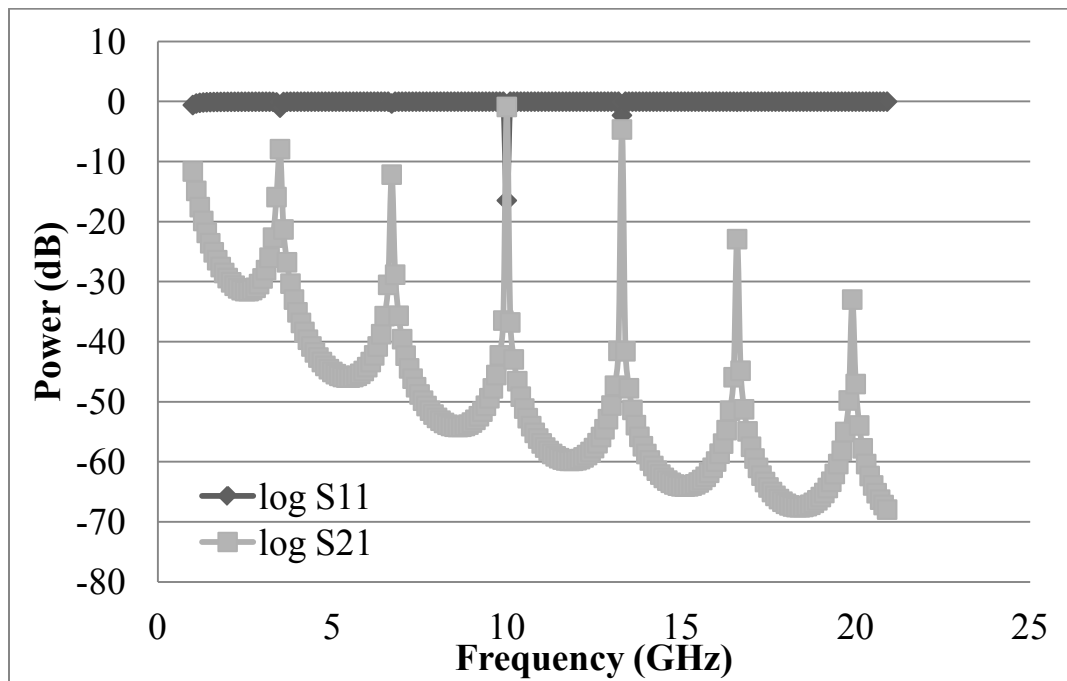
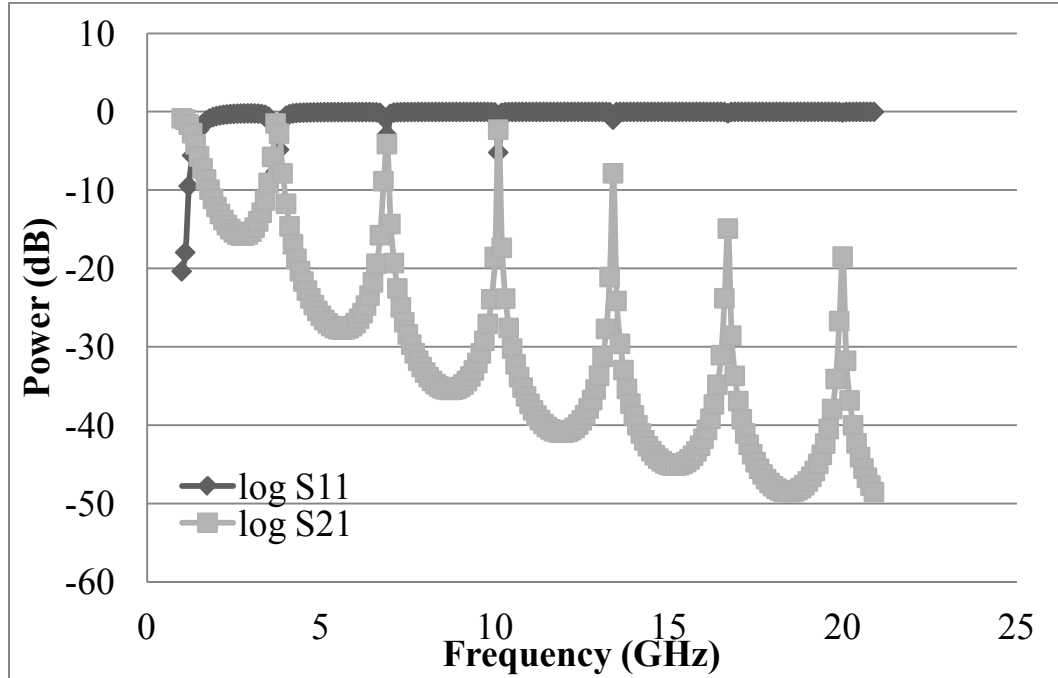


Figure 33. Twin varactor shunt switch with transmission line simulation at 0.2 pF and 0.6 pF respectively.

#### 4.4.1 RF Antenna Designs

Here are some of the antenna designs used in the RF designs. The loop antenna is the easiest to design by far. Loop antennas are insensitive to loop shape and depend primarily on the loop area. The one-wavelength square loop antenna is fairly common and consists of one quarter wavelength sides. The input impedance of this antenna is approximately  $102-100j$  ohms. This is good because the inductor and shunt switch has a resistance plus inductance to aid in conjugate impedance matching. In order to convert the balanced antenna to an unbalanced CPW line, a balun would be required. A microstrip sleeve balun would be easy to construct. The design of the balun can also accommodate for the impedance mismatch between the end switch and the antenna.

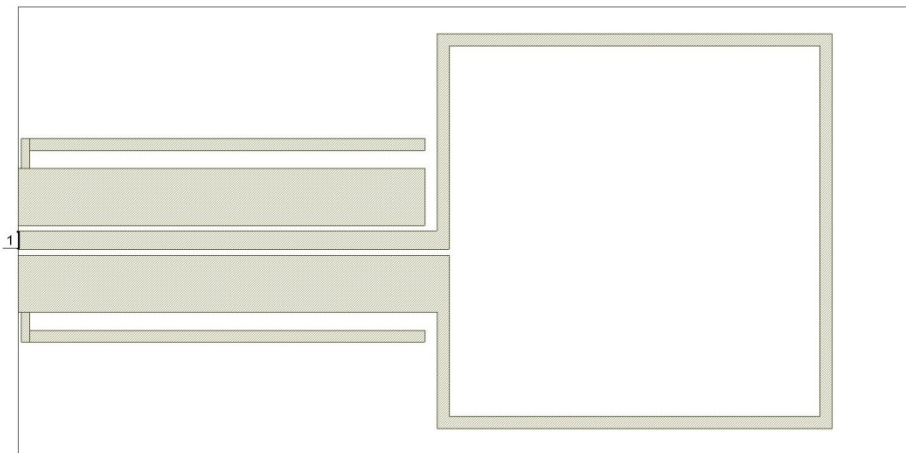


Figure 34. Coplanar waveguide loop antenna with balun.

The loopstick antenna is another version of the loop antenna. The loopstick antenna relies on the resonance of the coil. Loopstick antennas are very common in RFID's, cell phones, and other high frequency devices. The following picture shows a 900 MHz resonant RF inductive coil capable of being used as a transmit/receive antenna. It is in the standard 0805 package and can be hybridized easily with the other components on the substrate. Because this antenna is balanced, a balun would still be recommended. However in order to reduce the size of the sensor, the impedance mismatch will be tolerated (approximately half of the power is lost).



Figure 35. 900 MHz loopstick antenna.

#### 4.4.2 Complete Sensor Designs

Here is a design of a 900 MHz End Shunt Switch Sensor utilizing a series inductor in addition to a loopstick antenna. The final design measures 5 mm x 10 mm. This design will receive a signal in all directions except for the Y axis directly in line with the loopstick antenna. It will work with both vertically and horizontally polarized signals.

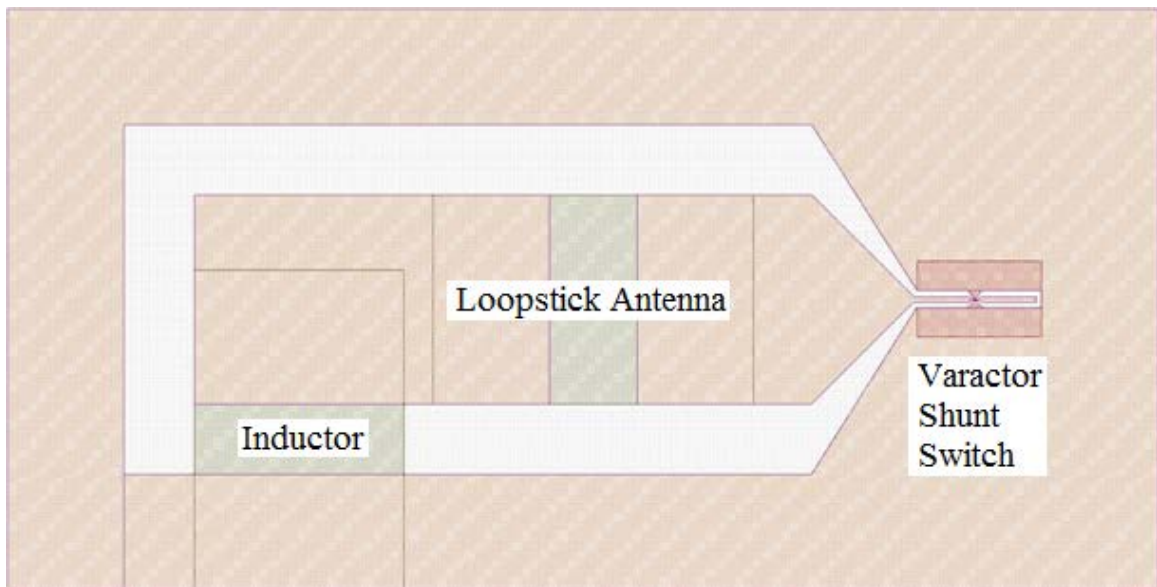


Figure 36. Complete sensor design 1.

Here is a design of a 10 GHz End Shunt Switch Sensor utilizing a series inductor and capacitor with space for a resistor to shunt the center conductor to ground in addition to a square large loop antenna and balun.

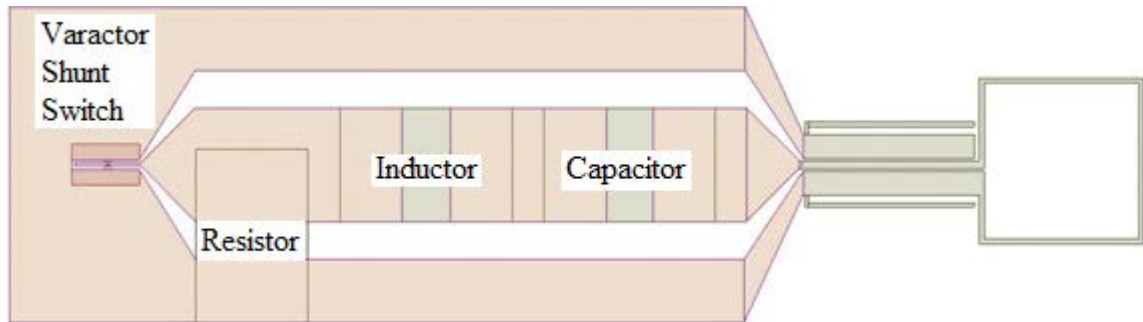


Figure 37. Complete sensor design 2.

In looking at the size of this structure, a microstrip stub for the inductor and capacitor of this design may shrink the design even more. This design is about 5 mm x 20 mm.

#### 4.4.3 IDC Based RF Designs

Another form of sensor uses just one CPW patch antenna and has an IDC that acts as a load. This design requires the interrogator to look at the reflected back signal and analyze the change in load impedance. The following figure shows the design that was built and tested. The IDC is coated with a functionalizing polymer similar to previous designs. There are no hybrid components to add and the design could be submerged in a liquid.

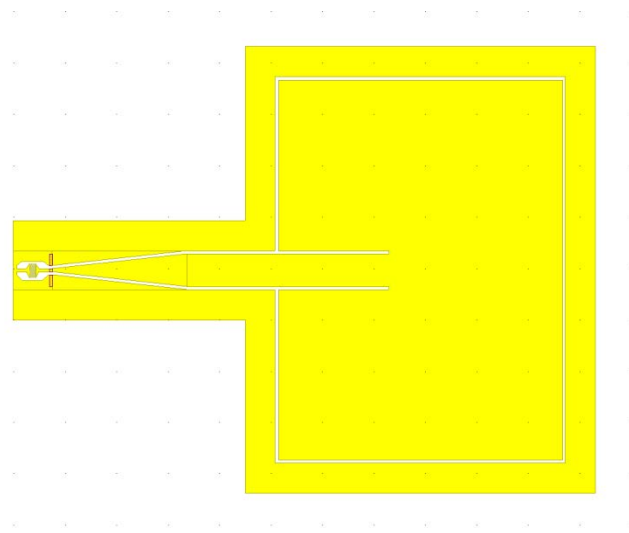


Figure 38. Single CPW antenna IDC based sensor.

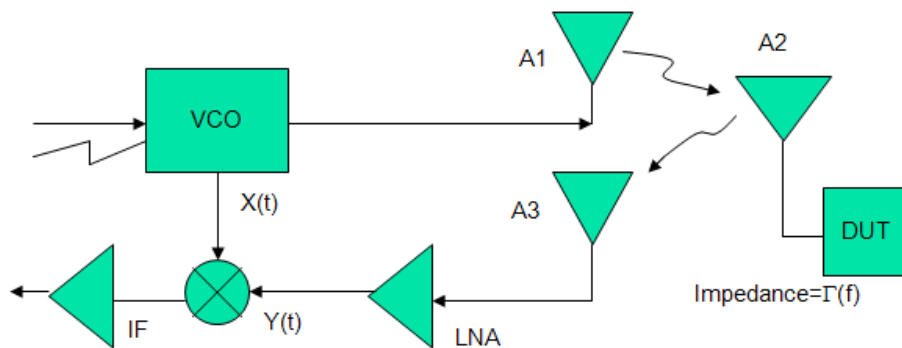


Figure 39. Interrogator for single CPW antenna IDC based sensor [111].

The  $S_{11}$  parameters of the passive wireless single CPW antenna sensor were tested. The antenna and IDC were deposited on top of Barium Strontium Titanate (BST) and DC voltage was used to try and tune the resonant frequency of the sensor. The DC voltage made a very small change in frequency. It is anticipated that a chemical on the IDC would make a much larger signature change.

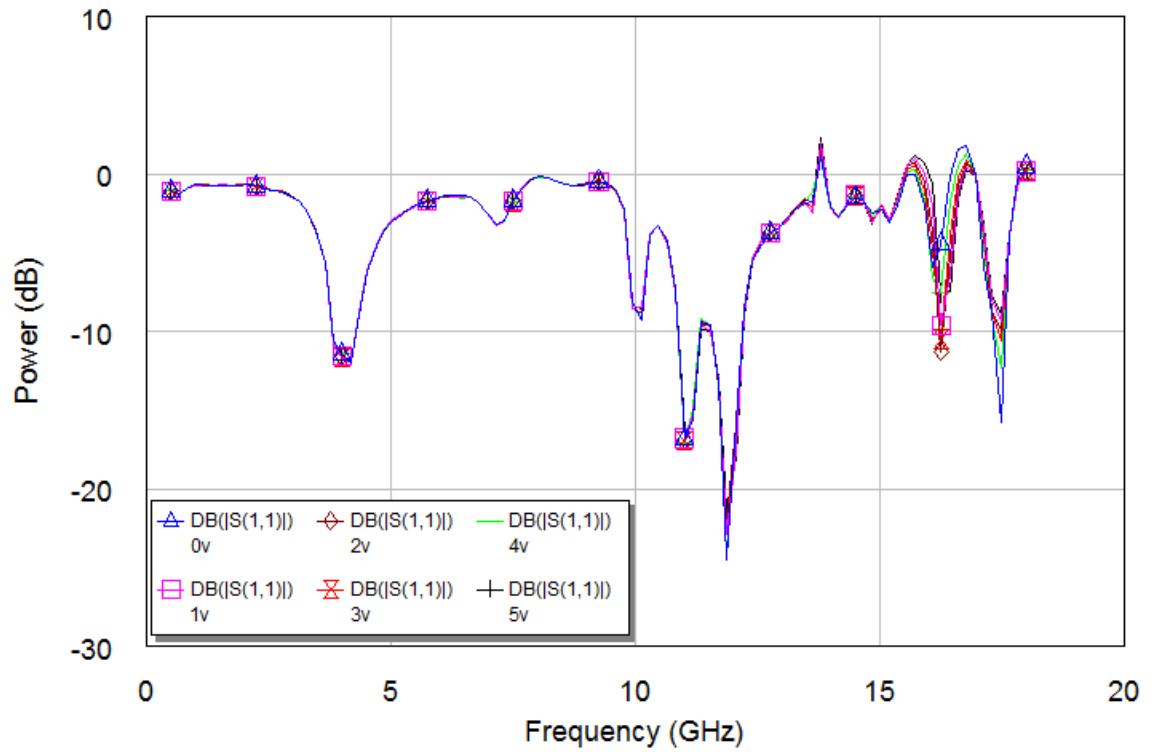


Figure 40. Swept frequency reflected power (S11) measurements of single CPW antenna IDC based sensor.

## CHAPTER V

### RESULTS

#### 5.1 IDSense Testing Results

The IDSense passive wireless platform was subjected to liquids, vapors, and other compounds in order to characterize its operation.

##### 5.1.1 IDSense Test Setup

The IDSense passive wireless platform was tested with a signal generator, an oscilloscope, and a specially made board that was matched to the antennas on the passive wireless sensor board. The oscilloscope leads were hooked to the receiving antenna and also across the charge capacitor on the passive wireless sensor board for correlation of the return signal.

##### 5.1.2 IDSense Platform Baseline Characterization

The characteristics of the IDSense passive wireless platform were tested to see what factors affect the operation of the platform. The factors included frequency, placement, and power. The interrogator was placed in a clear plastic box to insure there wasn't any electrical contact between the passive wireless board and the interrogator. The first test was performed by setting the board on the interrogator and adjusting the frequency output of the signal generator. This test was more to find a suitable frequency

for operation of the interrogator board with minimum carrier feedback and stable operation. Figure 41 shows the spectral response of the IDSense passive wireless platform. Voltage was induced in the power capacitor from low frequencies all the way to 30 MHz (limit of signal generator used). The best performance was achieved around 4-6 MHz.

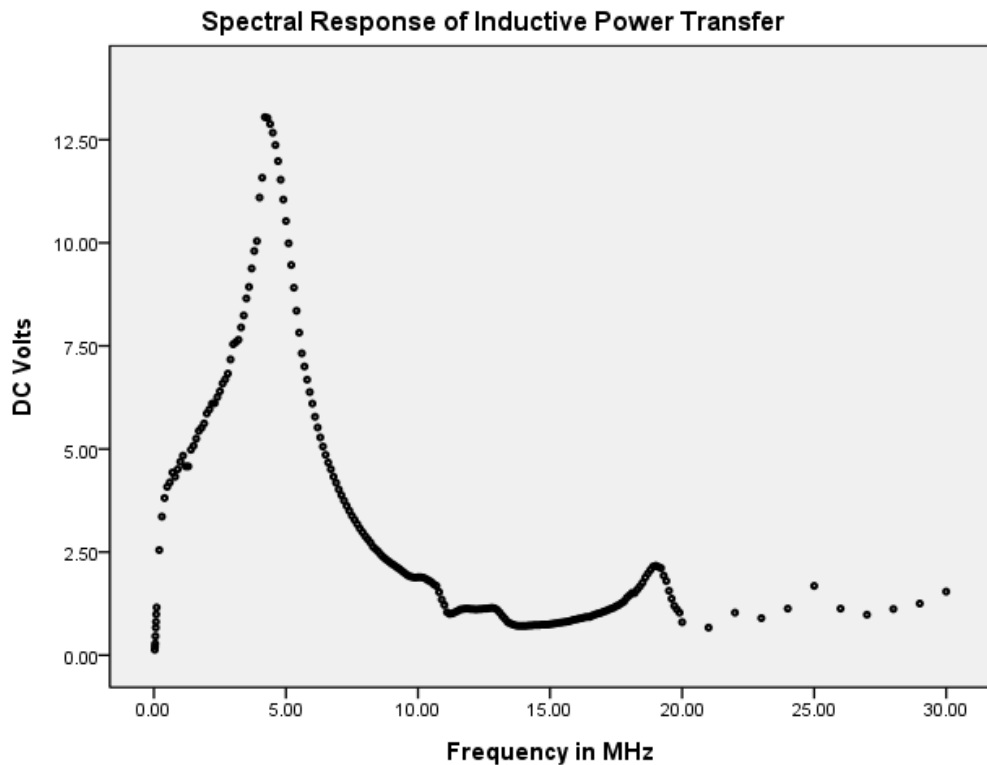


Figure 41. DC spectral response of IDSense passive wireless board.

While voltage was induced in the power capacitor, this didn't always mean that the device functioned properly. Figure 42 shows the AC Spectral Response received at the interrogator from the passive wireless board. Stable operation was achievable from 2 to 7 MHz with the most stable operation between 4 and 6 MHz.

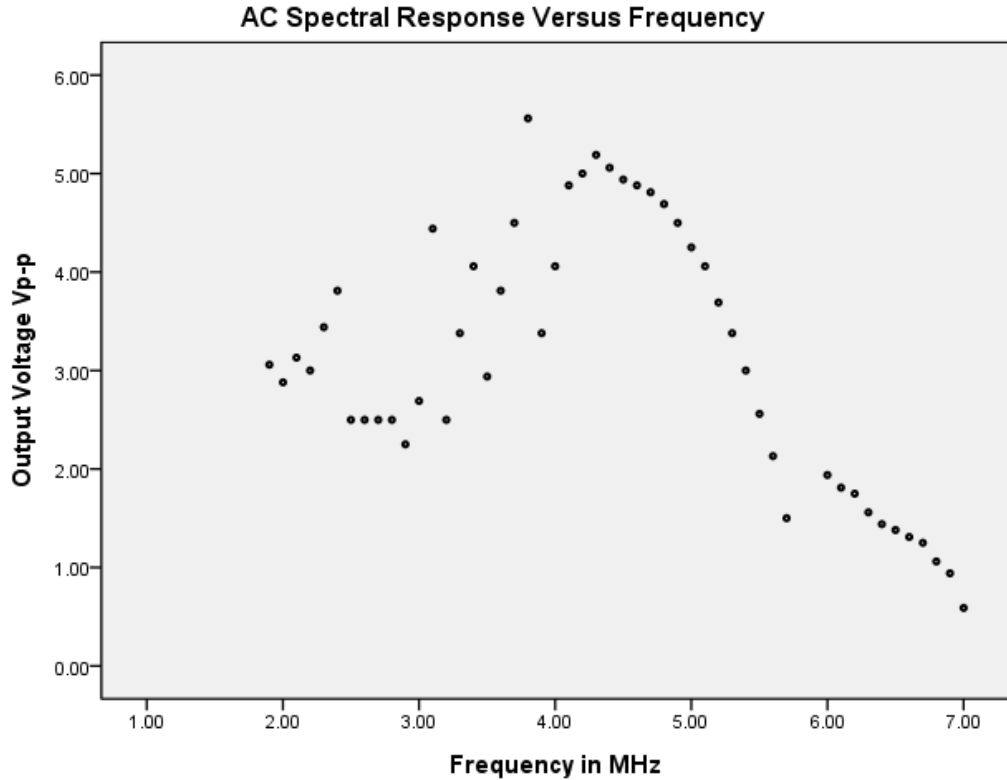


Figure 42. AC spectral response of IDSense passive wireless board.

The interrogator frequency also affected the output frequency of the passive wireless board as well. Figure 43 shows the shift in frequency that occurs when the interrogator frequency is between 2 and 7 MHz.

An analysis was performed between 2 and 5 MHz to determine the linearity and sensitivity of the interrogator frequency on the passive wireless board. Figure 44 shows the straight line fit between all of the points. The resulting linearity was 0.846. The output frequency curve fit yielded:

$$\text{Output Frequency} = 1.94 * \text{Input Frequency} + 29.525 \text{ KHz}$$

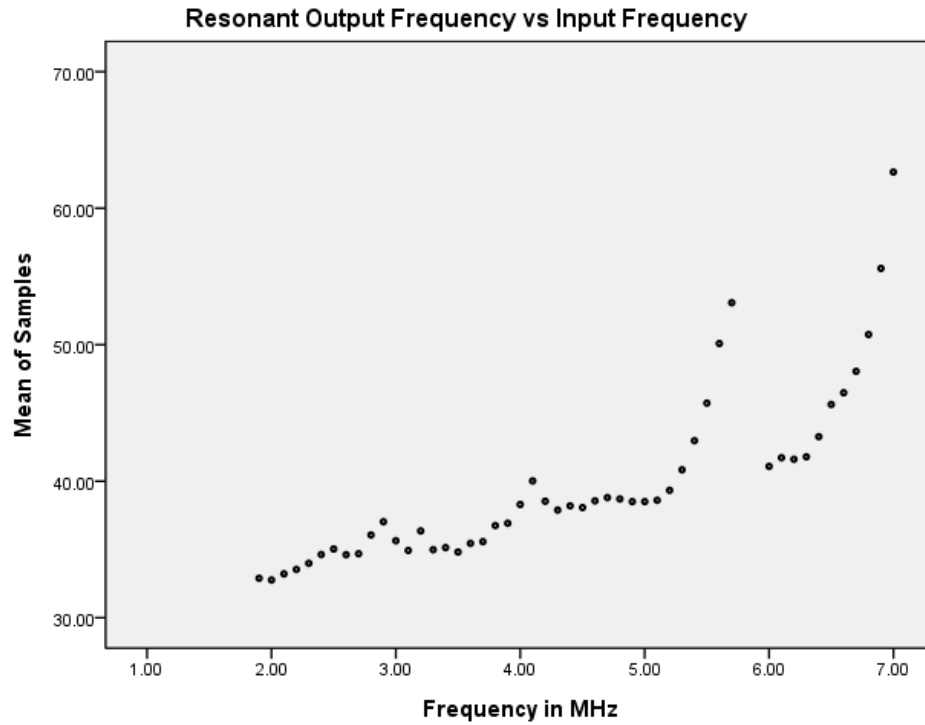


Figure 43. Output frequency spectral response of IDSense passive wireless board.

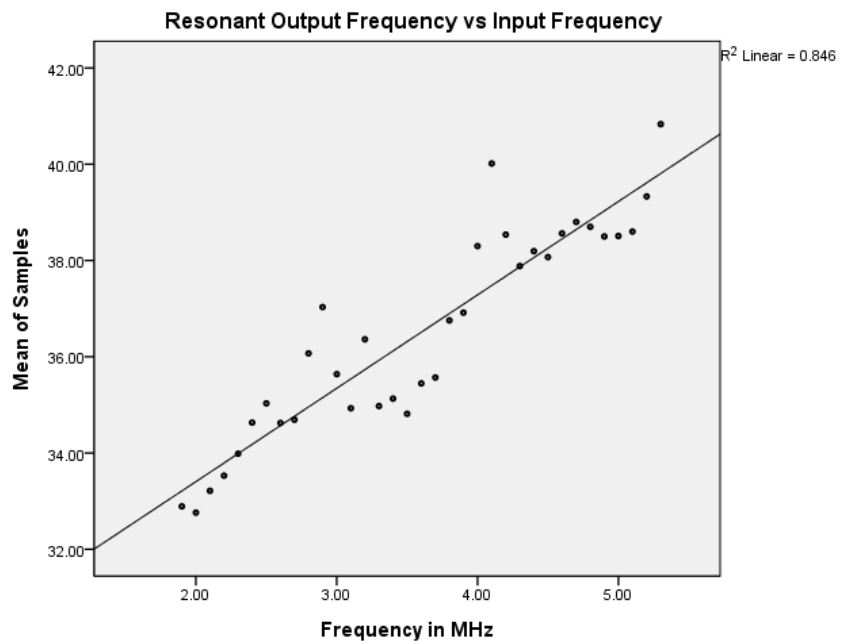


Figure 44. The curve fit of resonant output frequency vs. input frequency.

Table 2 shows the mean and the standard deviation of the samples taken at each frequency. The frequency range between 4.4 and 5.2 MHz produced very repeatable results.

Freq	Mean	SD									
1.9	32.89	0.36	3.2	36.36	2.4	4.5	38.07	0.08	5.7	53.08	3.02
2	32.76	0.35	3.3	34.98	1.07	4.6	38.56	0.07	6	41.09	0.14
2.1	33.22	0.43	3.4	35.13	1.32	4.7	38.8	0.01	6.1	41.72	0.18
2.2	33.53	0.44	3.5	34.82	0.79	4.8	38.7	0.04	6.2	41.61	0.28
2.3	33.98	0.25	3.6	35.45	0.82	4.9	38.5	0.04	6.3	41.79	0.13
2.4	34.63	0.59	3.7	35.57	0.52	5	38.51	0.03	6.4	43.27	0.15
2.5	35.03	0.71	3.8	36.75	0.76	5.1	38.6	0.06	6.5	45.62	0.28
2.6	34.62	0.76	3.9	36.92	1.37	5.2	39.33	0.06	6.6	46.48	0.2
2.7	34.69	0.53	4	38.3	2.19	5.3	40.83	0.15	6.7	48.05	0.3
2.8	36.07	1.01	4.1	40.02	0.21	5.4	42.97	0.26	6.8	50.75	0.5
2.9	37.03	1.72	4.2	38.54	0.05	5.5	45.72	0.33	6.9	55.59	0.65
3	35.64	1.83	4.3	37.88	0.24	5.6	50.08	0.35	7	62.65	0.97
3.1	34.93	1.81	4.4	38.19	0.05						

Table 2. Statistics of mean of samples.

The placement test was performed by taking a frequency reading from the received signal from the IDSense passive wireless board, picking the board up and then laying it down again. This was meant to test the accuracy of the system due to X & Y axis shifts and alignment issues. 52 trials were performed and a Pearson correlation coefficient of 0.993 was obtained. This means that the correlation is significant to the 0.01 level and that placement doesn't have an appreciable effect on the performance of the IDSense platform. Figure 45 shows the correlation results as a whole between samples.

**Pearson Correlations**

Sample	1	2	3	4	5	6	7	8	9	10	11	12	13
1	1	.957**	.979**	.993**	.984**	.987**	.987**	.977**	.989**	.982**	.987**	.976**	.985**
2	.957**	1	.950**	.953**	.967**	.948**	.952**	.959**	.958**	.949**	.954**	.959**	.963**
3	.979**	.950**	1	.978**	.981**	.992**	.979**	.974**	.977**	.992**	.992**	.978**	.982**
4	.993**	.953**	.978**	1	.982**	.985**	.985**	.972**	.987**	.973**	.982**	.976**	.980**
5	.984**	.967**	.981**	.982**	1	.981**	.987**	.991**	.993**	.984**	.985**	.986**	.992**
6	.987**	.948**	.992**	.985**	.981**	1	.986**	.973**	.976**	.988**	.992**	.977**	.980**
7	.987**	.952**	.979**	.985**	.987**	.986**	1	.979**	.990**	.979**	.984**	.978**	.984**
8	.977**	.959**	.974**	.972**	.991**	.973**	.979**	1	.986**	.980**	.983**	.993**	.991**
9	.989**	.958**	.977**	.987**	.993**	.976**	.990**	.986**	1	.979**	.981**	.984**	.989**
10	.982**	.949**	.992**	.973**	.984**	.988**	.979**	.980**	.979**	1	.994**	.977**	.986**
11	.987**	.954**	.992**	.982**	.985**	.992**	.984**	.983**	.981**	.994**	1	.982**	.988**
12	.976**	.959**	.978**	.976**	.986**	.977**	.978**	.993**	.984**	.977**	.982**	1	.990**
13	.985**	.963**	.982**	.980**	.992**	.980**	.984**	.991**	.989**	.986**	.988**	.990**	1

\*\* . Correlation is significant at the 0.01 level (2-tailed).

Figure 45. Placement correlation test results within a set.

Figure 46 shows the correlation results as a whole between two sets.

**Correlations**

		DC Voltage1	DC Voltage2
DC Voltage1	Pearson Correlation	1	.993**
	Sig. (2-tailed)		.000
	N	52	52
DC Voltage2	Pearson Correlation	.993**	1
	Sig. (2-tailed)	.000	
	N	52	52

\*\* . Correlation is significant at the 0.01 level (2-tailed).

Figure 46. Pearson set correlation between two placement sets.

The power test was performed by setting the board on the interrogator and adjusting the voltage output of the signal generator. This was meant to test the accuracy of the system due to Z axis shifts. Unfortunately, power affects the mean frequency of the IDSense board a little bit. This means that variances in the Z distance between the Interrogator and IDSense board will cause variances in the frequency received at the interrogator. This is a fairly common phenomenon and can be mitigated with fixtures or other mechanical methods to constrain depth. Figure 47 shows the fairly linear curve of mean frequency versus transmitter voltage. As the voltage increases (more power), the mean frequency also increases.

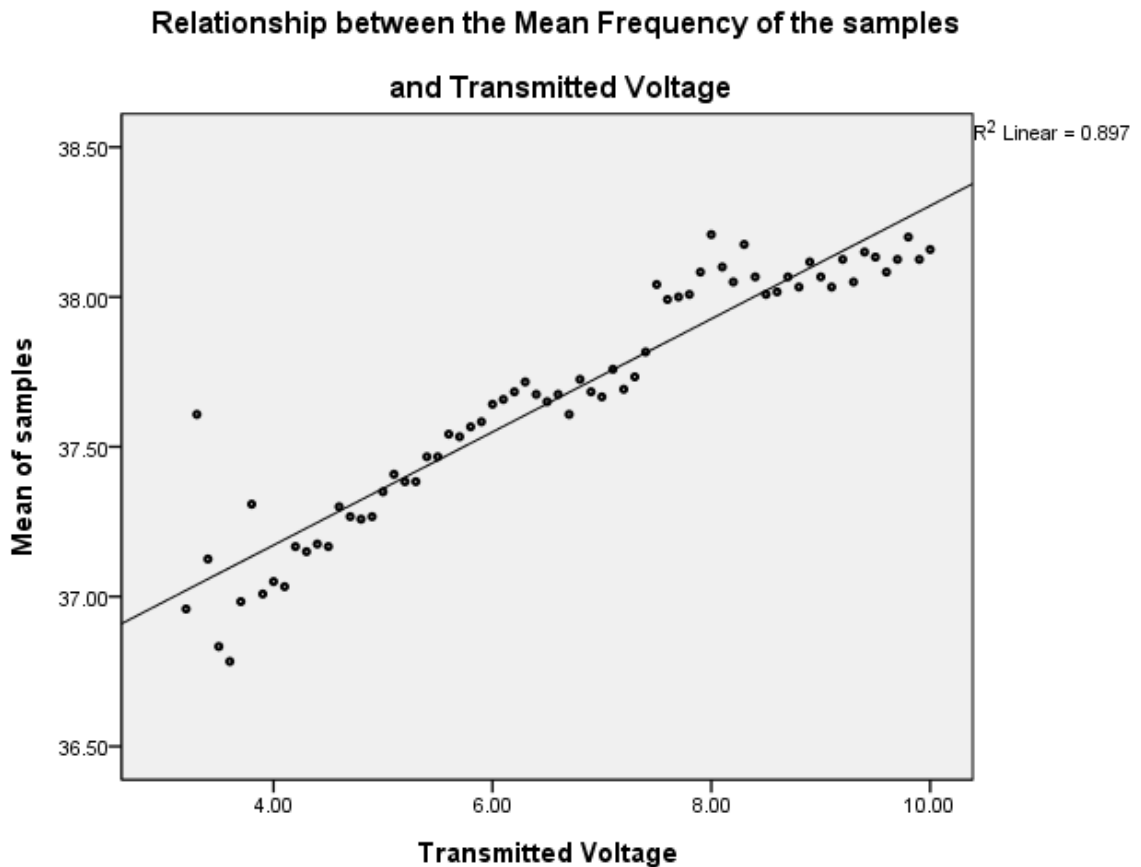


Figure 47. Relationship between the mean frequency of the samples and transmitted voltage.

**Model Summary**

Model	R	R Square	Adjusted R Square	Std. Error of the Estimate
1	.947 <sup>a</sup>	.897	.896	.12899

a. Predictors: (Constant), Transmitted Voltage

**Correlations**

		Transmitted Voltage	Mean of samples
Transmitted Voltage	Pearson Correlation	1	.947**
	Sig. (2-tailed)		.000
	N	69	69
Mean of samples	Pearson Correlation	.947**	1
	Sig. (2-tailed)	.000	
	N	69	69

\*\* . Correlation is significant at the 0.01 level (2-tailed).

**ANOVA<sup>b</sup>**

Model		Sum of Squares	df	Mean Square	F	Sig.
1	Regression	9.755	1	9.755	586.280	.000 <sup>a</sup>
	Residual	1.115	67	.017		
	Total	10.870	68			

a. Predictors: (Constant), Transmitted Voltage

b. Dependent Variable: Mean of samples

**Coefficients<sup>a</sup>**

Model		Unstandardized Coefficients		Standardized Coefficients	t	Sig.
		B	Std. Error	Beta		
1	(Constant)	36.417	.054		677.484	.000
	Transmitted Voltage	.189	.008	.947	24.213	.000

a. Dependent Variable: Mean of samples

Figure 48. IDSense statistical results comparing transmitted voltage and mean frequency.

The curve had a linearity of 0.897 which is acceptable but leads to reduced accuracy of the IDSense board. Figure 48 shows the model statistic results of the IDSense platform. The Pearson correlation between the transmitted voltage and frequency mean of all of the samples yielded 0.947. The standard error yielded 12.9%. The output frequency curve fit yielded:

$$\text{Output Frequency} = 0.189 * \text{Transmitted Voltage} + 36.417 \text{ KHz}$$

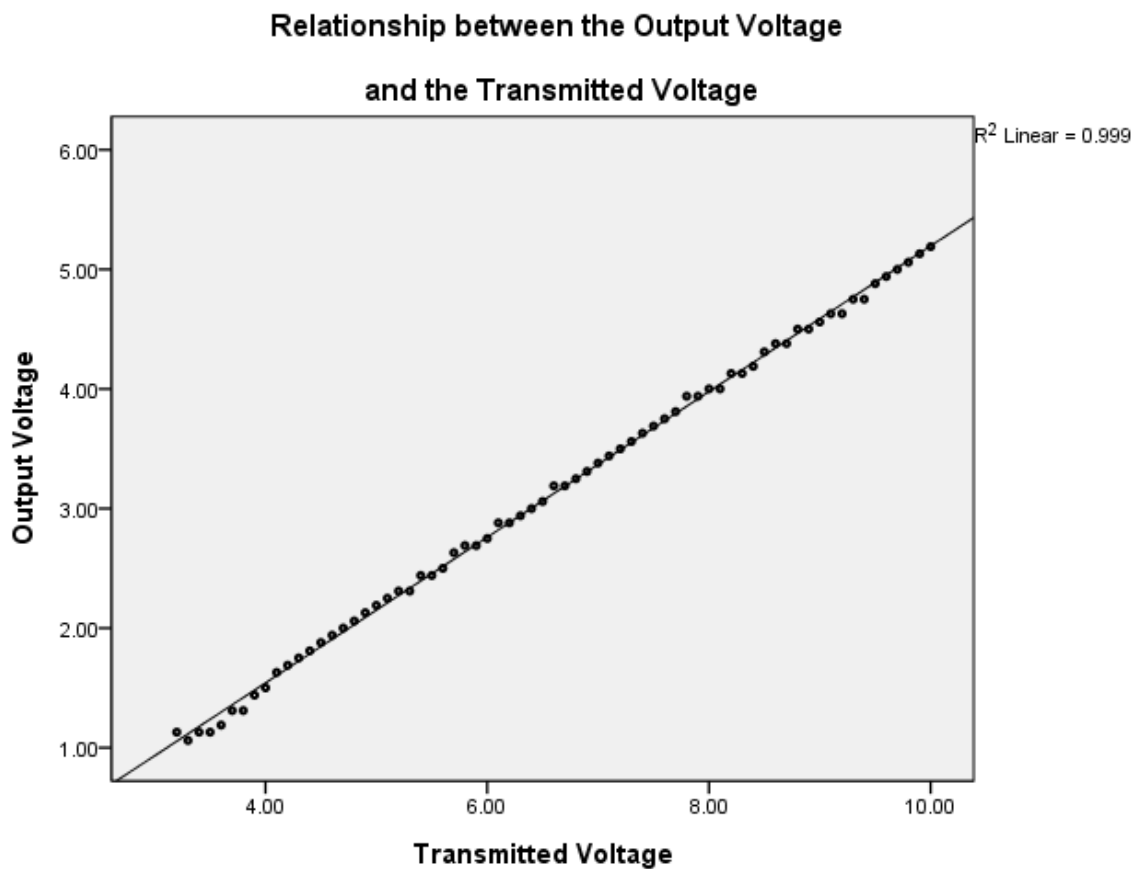


Figure 49. Relationship between the output voltage and the transmitted voltage.

The relationship between the output voltage received at the interrogator and the transmitted voltage was very linear as shown in Figure 49. The linearity result was 0.999. The Pearson correlation was also very high yielding a 0.999 value as well. Figure

50 shows the correlation data between transmitted voltage and capacitor voltage as well as output voltage. All correlations were very high.

**Correlations**

		Transmitted Voltage	Capacitor Voltage	Output Voltage
Transmitted Voltage	Pearson Correlation	1	1.000**	.999**
	Sig. (2-tailed)		.000	.000
	N	69	69	69
Capacitor Voltage	Pearson Correlation	1.000**	1	.999**
	Sig. (2-tailed)	.000		.000
	N	69	69	69
Output Voltage	Pearson Correlation	.999**	.999**	1
	Sig. (2-tailed)	.000	.000	
	N	69	69	69

\*\* . Correlation is significant at the 0.01 level (2-tailed).

Figure 50. Correlation relationship between the output voltage, capacitor voltage, and the transmitted voltage.

The model results for the statistical analysis of the relationship between the Transmitted voltage and the capacitor voltage is shown in Figure 51. The curve had a linearity of 1.000 which is technically perfect with likewise ANOVA results. The resulting capacitor voltage curve fit yielded:

$$\text{Capacitor Voltage} = -1.173 + 1.425 * \text{Transmitted Voltage.}$$

**Model Summary**

Model	R	R Square	Adjusted R Square	Std. Error of the Estimate
1	1.000 <sup>a</sup>	1.000	1.000	.04557

a. Predictors: (Constant), Transmitted Voltage

**ANOVA<sup>b</sup>**

Model		Sum of Squares	df	Mean Square	F	Sig.
1	Regression	555.547	1	555.547	267541.825	.000 <sup>a</sup>
	Residual	.139	67	.002		
	Total	555.686	68			

a. Predictors: (Constant), Transmitted Voltage

b. Dependent Variable: Capacitor Voltage

**Coefficients<sup>a</sup>**

Model		Unstandardized Coefficients		Standardized Coefficients	t	Sig.
		B	Std. Error	Beta		
1	(Constant)	-1.173	.019		-61.751	.000
	Transmitted Voltage	1.425	.003	1.000	517.244	.000

a. Dependent Variable: Capacitor Voltage

Figure 51. Model results between the capacitor voltage and the transmitted voltage.

The model results for the statistical analysis of the relationship between the Transmitted voltage and the output voltage is shown in Figure 52. The curve had a linearity of 0.999 which is close to perfect with likewise ANOVA results. The resulting output voltage curve fit yielded:

$$\text{Output Voltage} = -0.894 + 0.609 * \text{Transmitted Voltage.}$$

**Model Summary**

Model	R	R Square	Adjusted R Square	Std. Error of the Estimate
1	.999 <sup>a</sup>	.999	.999	.04139

a. Predictors: (Constant), Transmitted Voltage

**ANOVA<sup>b</sup>**

Model		Sum of Squares	df	Mean Square	F	Sig.
1	Regression	101.521	1	101.521	59265.866	.000 <sup>a</sup>
	Residual	.115	67	.002		
	Total	101.635	68			

a. Predictors: (Constant), Transmitted Voltage

b. Dependent Variable: Output Voltage

**Coefficients<sup>a</sup>**

Model		Unstandardized Coefficients		Standardized Coefficients	t	Sig.
		B	Std. Error	Beta		
1	(Constant)	-.894	.017		-51.834	.000
	Transmitted Voltage	.609	.003	.999	243.446	.000

a. Dependent Variable: Output Voltage

Figure 52. Model results between the output voltage and the transmitted voltage.

### 5.1.3 Wet Chemical Testing

The IDC was either left bare, coated with Nafion, or coated with a silk polymer for the chemical testing. The test was started with the IDC at room conditions. A drop of the chemical was then placed on the IDC and recording with an oscilloscope commenced. The period (frequency) of the waveform was what was measured over time and recorded. The following figures show the application and subsequent evaporation of the chemical on bare, silk, and Nafion boards. Both isopropanol and ethanol were used. The test was conducted by saturating the IDC with a drop of the chemical and then taking continuous samples with the oscilloscope until all of the chemical was evaporated. The first sample tested was isopropanol on a bare board.

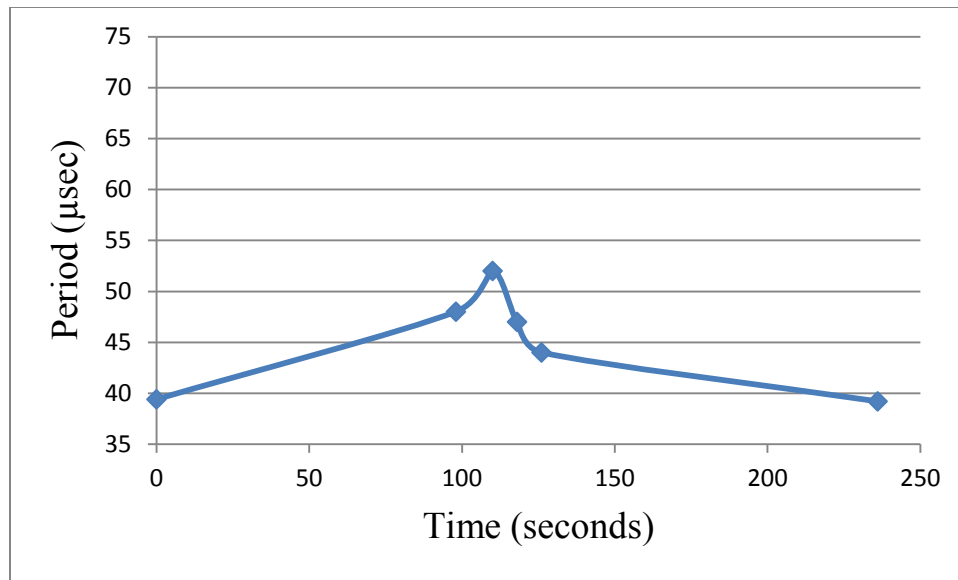


Figure 53. Evaporation testing of isopropanol on a bare board.

Figure 53 shows the initial period of the IDSense platform before the application of isopropanol (time 0). Previous figures had showed the frequency instead of the period of the waveform. When the IDC part of the sensor is flooded, the device fails to resonate.

The dielectric constant of isopropanol is 18.23 which is significantly different from air, but the sensor doesn't start to operate again until about after 100 seconds. At this point the isopropanol is mostly evaporated and is in a mixed vapor/liquid state. The isopropanol continues to evaporate until almost 250 seconds has elapsed in which the sensor period is back to its original value. Figure 54 shows the effect of isopropanol on a silk coated board.

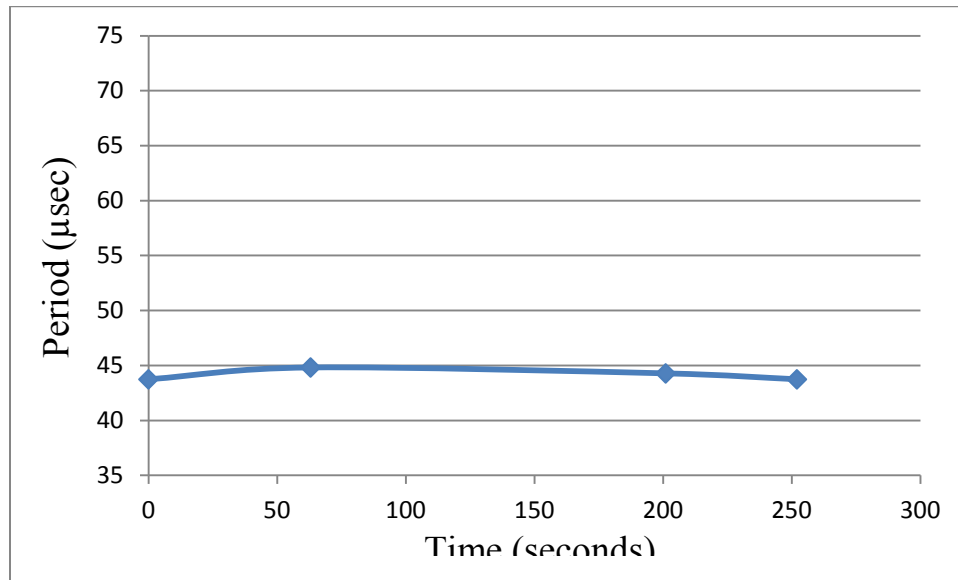


Figure 54. Evaporation testing of isopropanol on a silk coated board.

Silk is a biopolymer that can be made into a thick film and spread across a wafer. Isopropanol does not seem to have much effect on the silk coated IDC. The silk actually seems to repel the isopropanol and prevent it from contacting the sensing surface. Figure 55 shows the effect of isopropanol on a Nafion coated board.

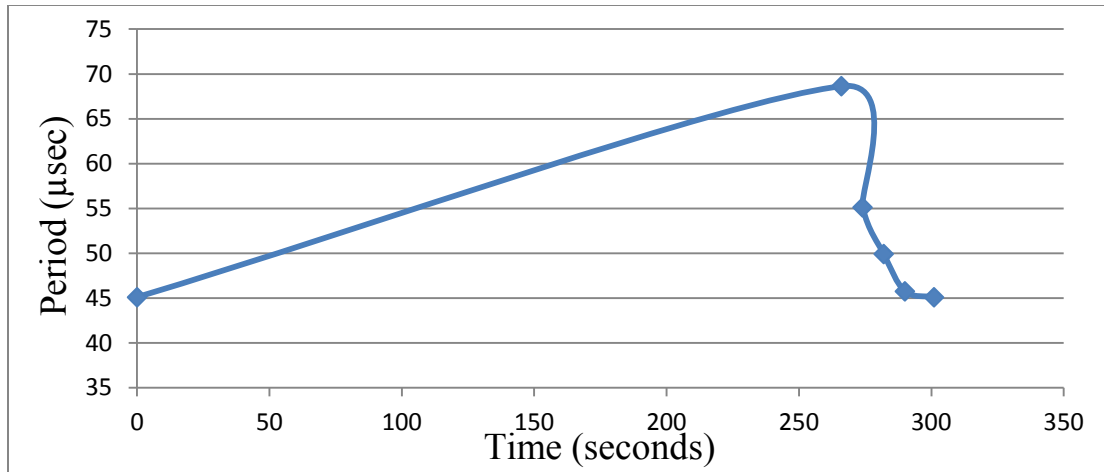


Figure 55. Evaporation testing of isopropanol on a Nafion coated board.

Nafion is polymer that can be made into a thin film and spread easily across a wafer. Isopropanol seems to have a huge effect on the Nafion coated IDC. The Nafion seems to hold the isopropanol and has a more marked effect on the sensor. The time before 250 seconds was when the sensor was flooded and not operating.

Ethanol has a different effect on the same types of boards than isopropanol.

Figure 56 shows the effect of ethanol on a bare board.

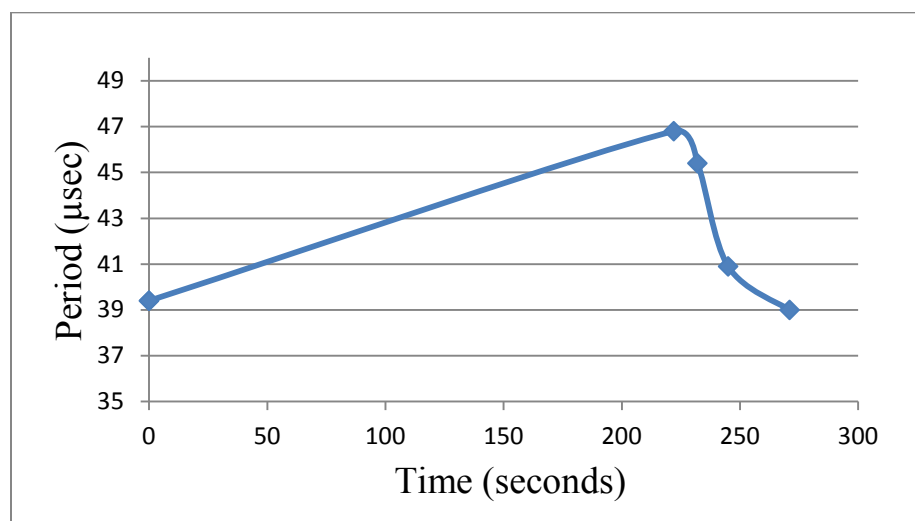


Figure 56. Evaporation testing of ethanol on a bare board.

Ethanol has a similar effect as isopropanol on the bare board. When the IDC part of the sensor is flooded, the device fails to resonate. The dielectric constant of Ethanol is 24.3 which is significantly different from air, but the sensor doesn't start to operate again until around 225 seconds. At this point the ethanol is mostly evaporated and is in a mixed vapor/liquid state. The ethanol continues to evaporate until 275 seconds in which the sensor period is back to its original value.

Ethanol has an effect on silk however unlike isopropanol. Figure 57 shows the effect of ethanol on a silk coated board. With isopropanol on the IDC, the period of the device barely changed. Here with ethanol, the period changed markedly until most of the ethanol had evaporated.

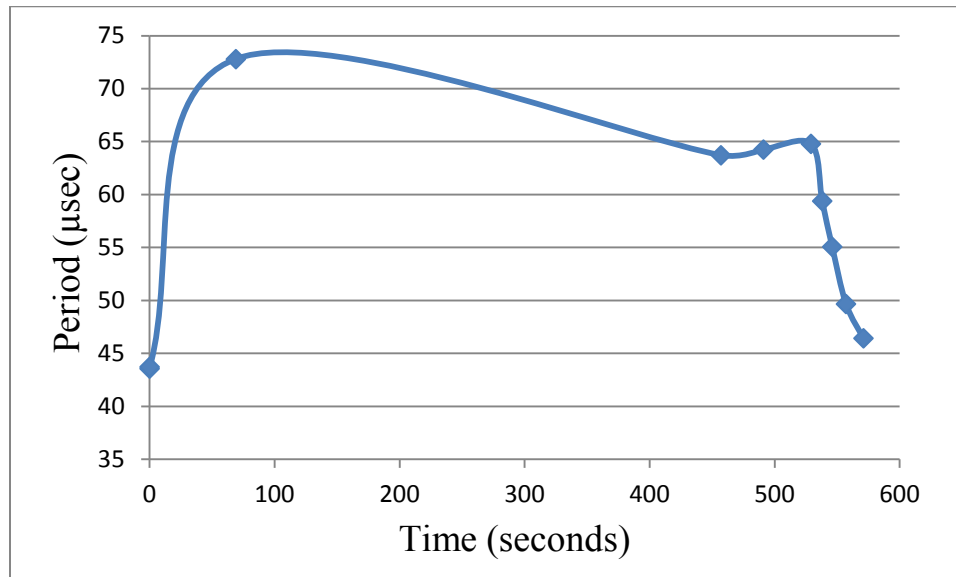


Figure 57. Evaporation testing of ethanol on a silk coated board.

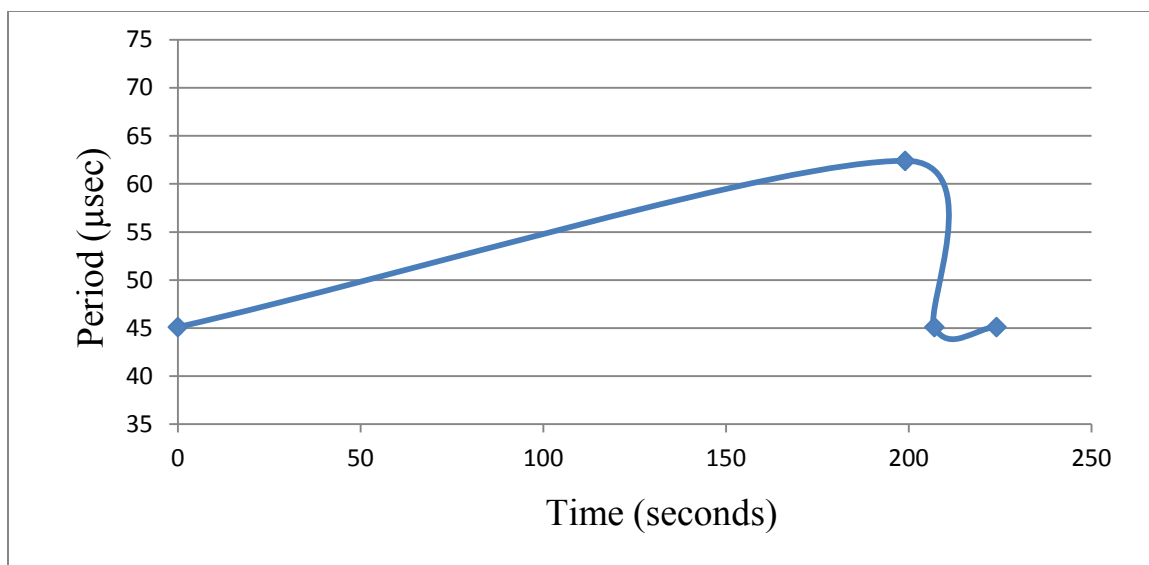


Figure 58. Evaporation testing of ethanol on a Nafion coated board.

Figure 58 shows the effect of ethanol on a Nafion coated board. Ethanol has a similar effect on the Nafion coated IDC as isopropanol did. The time before 200 seconds was when the sensor was flooded and not operating.

#### 5.1.4 Vapor Testing

Since the IDSense platform had a large change with liquids, the platform was also tested with vapors. However, the magnitude of the changes was greatly reduced. Table 3 shows the period of the IDSense board during different conditions.

Board Type	Room Conditions	N2 Purge	Ethanol	Humidity
Bare	52.4 µsec	52.0 µsec	52.8 µsec	
Nafion	52.0 µsec		52.4 µsec	
Silk	52.0 µsec		52.0 µsec	52.2 µsec

Table 3. Vapor testing with water and ethanol on various boards.

For testing, nitrogen was bubbled through water or ethanol at 50 sccm to create a vapor stream that was pointed at the IDC on the IDSense board. In general a dry board exhibited the lowest period compared to the other conditions. When subjected to humidity or a vapor, the period increased. Silk however did not show a change with an ethanol vapor, however it did with water vapor. Nafion changed with the ethanol vapor just like it did with the ethanol liquid, it just had a greatly reduced change. The resolution of the oscilloscope recording the measurements was only 0.2  $\mu\text{sec}$

#### 5.1.5 Compound Testing

Chemical testing was performed on boards that were coated with Nafion or silk polymers. There were five boards of each type. One board was left unaltered and the other four boards were exposed to a chemical of interest. Table 4 shows the result of silk chemical testing and Table 5 shows the result of Nafion chemical testing. Board #1 is the control board which was not exposed to chemicals. Boards 2-5 were exposed to hydraulic fluid, fuel, chlorine, and battery acid respectively. The control board for the silk testing showed good repeatability. Unfortunately the control board for the Nafion testing wasn't as repeatable.

The results for the different chemical tests are interesting. Some chemicals make the resonant frequency of the sensor go up while others make the resonant frequency go down. Even though the control for the Nafion testing goes down when re-tested, the Nafion boards tested with chlorine and battery acid cause the frequency to go significantly up. The effects of chlorine and battery acid are similar on the silk boards. The result that is the most interesting is fuel. The frequency goes up on the silk board and down on the Nafion board.

Board #	Freq Before	Freq After	T test
1	39.3533 KHz	39.2636 KHz	2.589
2	37.7933 KHz	36.5510 KHz	29.234
3	38.6867 KHz	41.6833 KHz	-7.748
4	37.0867 KHz	39.8417 KHz	-120.931
5	36.8400 KHz	41.8250 KHz	-13.130

Table 4. Results of silk chemical testing.

Board #	Freq Before	Freq After	T test
1	3.1773 Hz	2.5680 Hz	36.154
2	3.1780 Hz	3.0000 Hz	10.800
3	2.8633 Hz	2.2403 Hz	19.347
4	2.8553 Hz	3.7767 Hz	-85.751
5	2.4300 Hz	2.8550 Hz	-48.817

Table 5. Results of Nafion chemical testing.

The chemical testing for this dissertation is not to find the best polymer to apply to the IDC to detect a particular analyte of interest, but to show that the platform exhibits sensitivity to different analytes when exposed. All testing was performed wirelessly to show that the sensor platform does work. Figure 59 shows the statistics of the boards used prior to compound testing.

	N	Minimum	Maximum	Mean	Std. Deviation
Silk 1	15	39.20	39.40	39.3533	.06399
Silk 2	15	37.70	38.10	37.7933	.11629
Silk 3	15	35.80	39.50	38.6867	1.33356
Silk 4	15	36.90	37.10	37.0867	.05164
Silk 5	15	35.80	38.80	36.8400	1.30974
Nafion 1 (Hz)	15	3.09	3.23	3.1773	.03693
Nafion 2 (Hz)	15	3.10	3.25	3.1780	.05545
Nafion 3 (Hz)	15	2.74	2.94	2.8633	.06810
Nafion 4 (Hz)	15	2.79	2.89	2.8553	.03335
Nafion 5 (Hz)	15	2.41	2.45	2.4300	.01134

Figure 59. Statistical results of compound testing.

## 5.2 Passive RF Testing Results

The Passive RF wireless platform was constructed and analyzed. It was subjected to liquids and other compounds in order to characterize its operation.

### 5.2.1 Passive RF Test Setup

The Passive RF wireless platform was tested with a network analyzer and a specially made board that matched the antennas on the passive wireless sensor board.

### 5.2.2 Passive RF Platform Baseline Characterization

The antennas on the Passive RF wireless platform were tested with a network analyzer to make sure that they were all functional and identical. The antennas were designed for approximately 10 GHz and one of the resonant frequencies shows exactly this. Figure 60 shows the spectral response of the individual antennas.

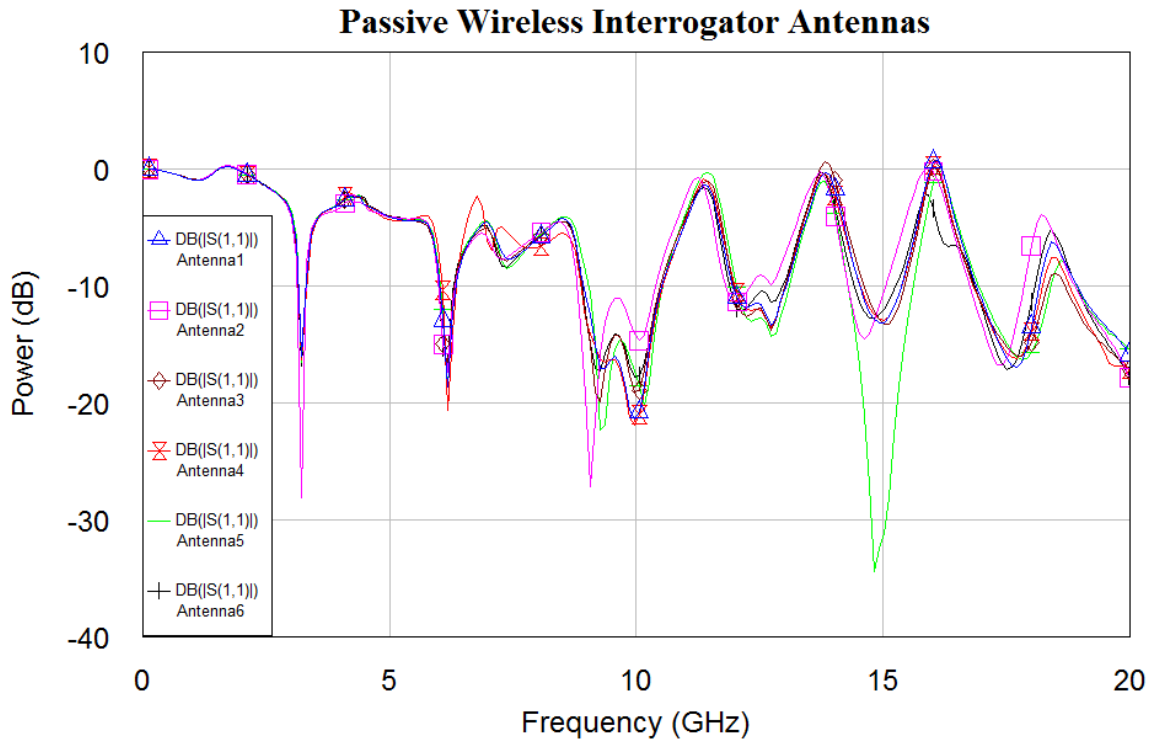


Figure 60. Swept frequency reflected power (S11) response for the passive wireless interrogator antennas.

The above figure shows that the manufacturing process showed excellent repeatability in constructing the antennas and soldering on their SMA-CPW connectors. There is a small anomaly on Antenna 5 around 15 GHz, but other than that the antennas line up on top of one another for the most part.

The interrogator was built in antenna sets so that one antenna could be the transmitter and the other antenna the receiver. Set 5-6 was used for all of the testing that follows. In order to make sure that the interrogator could see the Passive RF wireless sensor, a test was conducted on set 5-6 with and without the wireless sensor next to the antenna set. Figure 61 shows the difference between the open signal with no sensor and the loaded signal with the wireless sensor present. Both S21 and S11 showed a notable change around 10 GHz indicating that the wireless sensor was being detected.

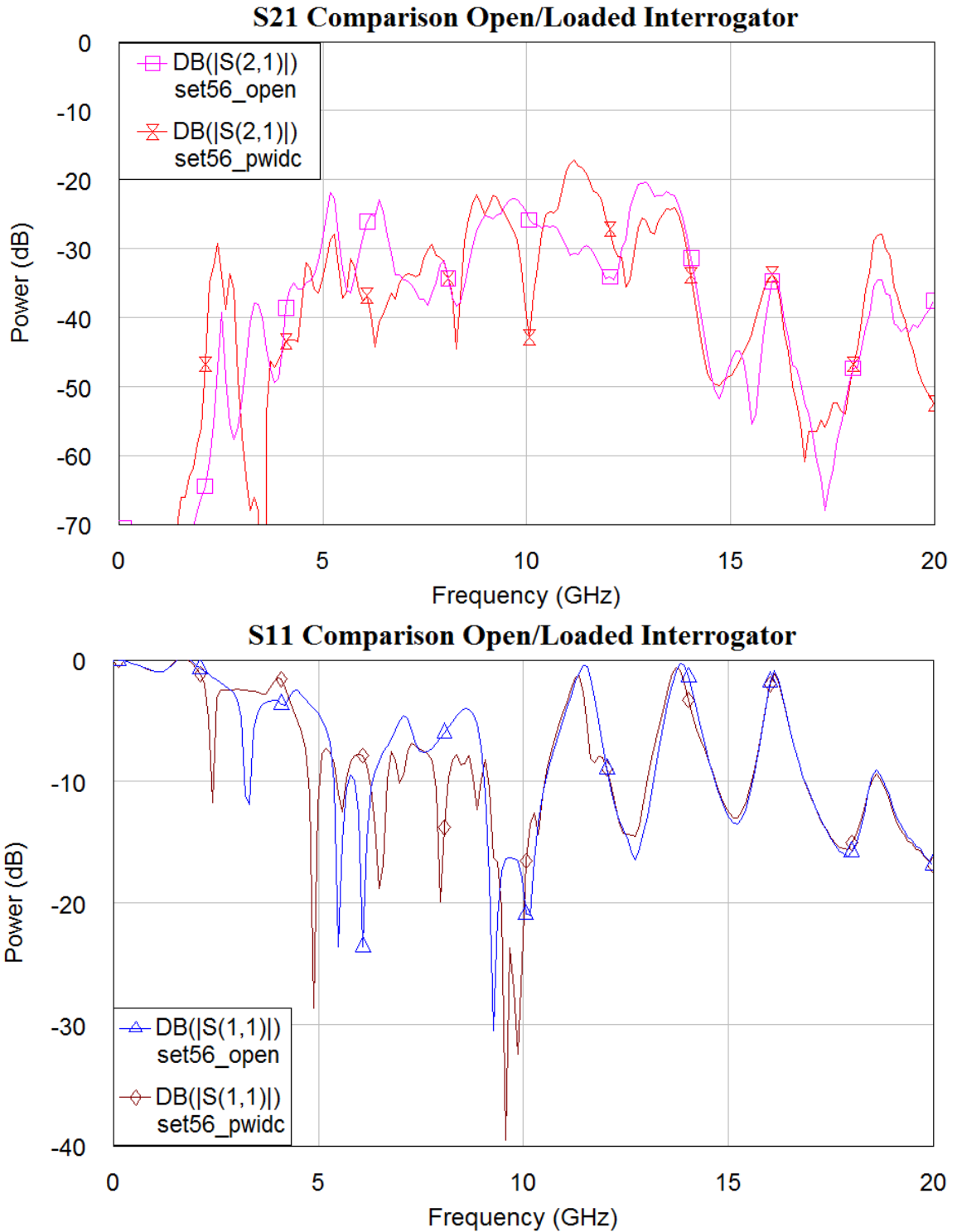


Figure 61. Swept frequency forward power (S21) and reflected power (S11) response with and without a wireless sensor on the interrogator antennas for the Passive RF wireless sensor.

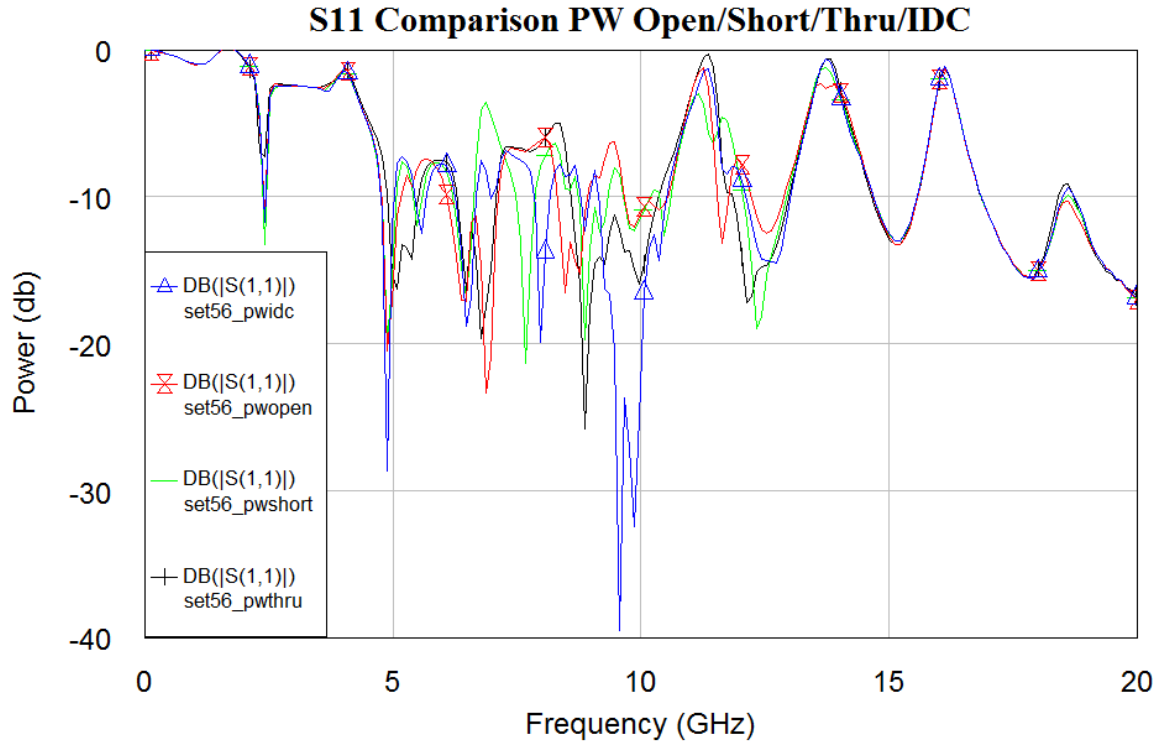


Figure 62. Swept frequency reflected power (S11) response with different calibration structures on the interrogator antennas for the Passive RF wireless sensor.

There were several structures built in addition to the Passive RF wireless IDC structures. The other structures were meant to be used for calibration and verification purposes. They were made in open, shorted, and through configurations. These structures help us to understand what is happening in the wireless sensor system with respect to impedance. In Figure 62 we will be analyzing the 10 GHz sample point for four different structures. The open and shorted configurations cause the maximum amount of reflection as expected. The through configuration causes less reflection indicating that power is going through one of the wireless sensor's antennas to the other. The IDC structure was expected to have a similar return signal as the through structure and it does right at 10 GHz, but not below 10 GHz. Monitoring the amplitude of S11 at 10 GHz is not the preferred method of monitoring this wireless sensor system. It is preferred to monitor the frequency dips and peaks of S21 because these signals won't be

affected by distance and the entire wireless sensor is utilized. Figure 63 shows the S21 parameters of the same structures shown in Figure 62.

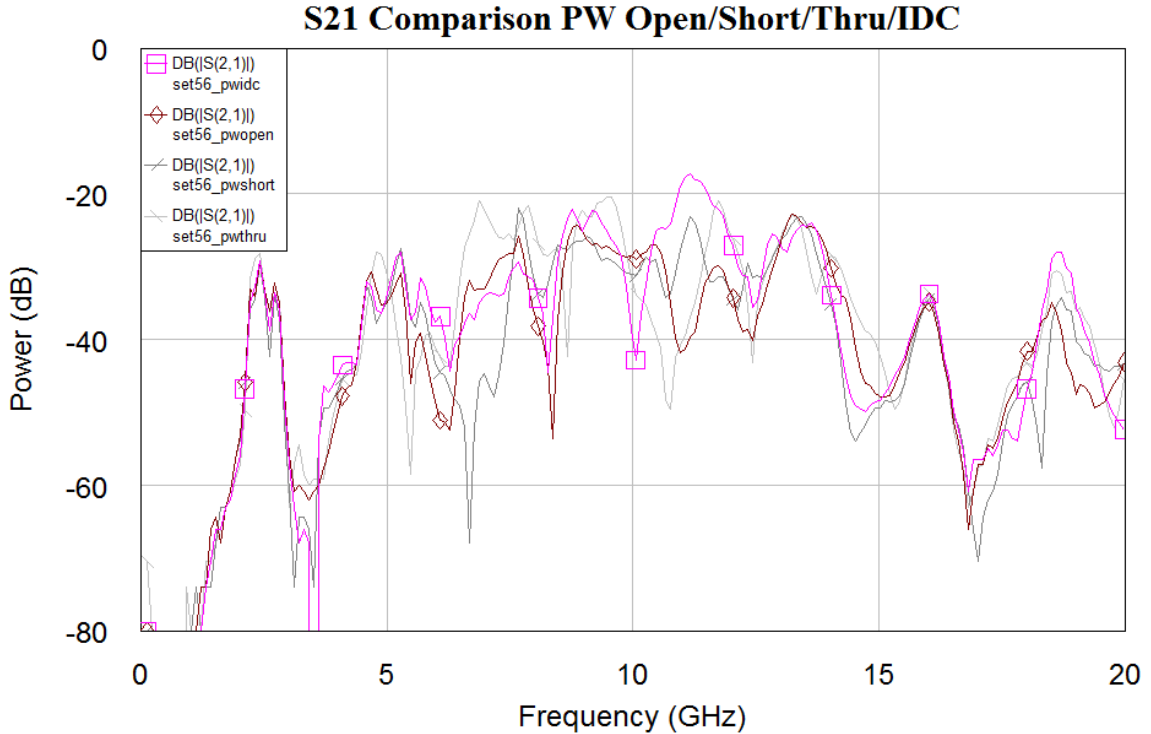


Figure 63. Swept frequency forward power (S21) response with different calibration structures on the interrogator antennas for the Passive RF wireless sensor.

The frequencies between 5 and 15 GHz look suitable for identifying a resonant frequency and observing its shift with impedance change of the sensor. There are several peaks and dips on either side of 10 GHz that move with impedance. It is important to notice that the IDC and through structures have the highest values indicating the power is transferring through the wireless sensor device. Likewise, the shorted and open configurations have the lowest values indicating the power is getting reflected back to the transmitting antenna. The clearest pattern observed in these measurements is the frequency range immediately below 10 GHz. The through structure has the highest frequency followed by the IDC and then the open and shorted structures have about the

same frequency. The magnitudes of these peaks also make sense and looking back at the antenna patterns, these signals are within the bandwidth of the antenna.

### 5.2.3 Passive RF Chemical Testing

The Passive RF boards were left bare and were not coated with Nafion or silk for the chemical testing. The IDC structure of the wireless sensor was used and subjected to either ethanol or isopropanol. Figure 64 shows the results of ethanol testing.

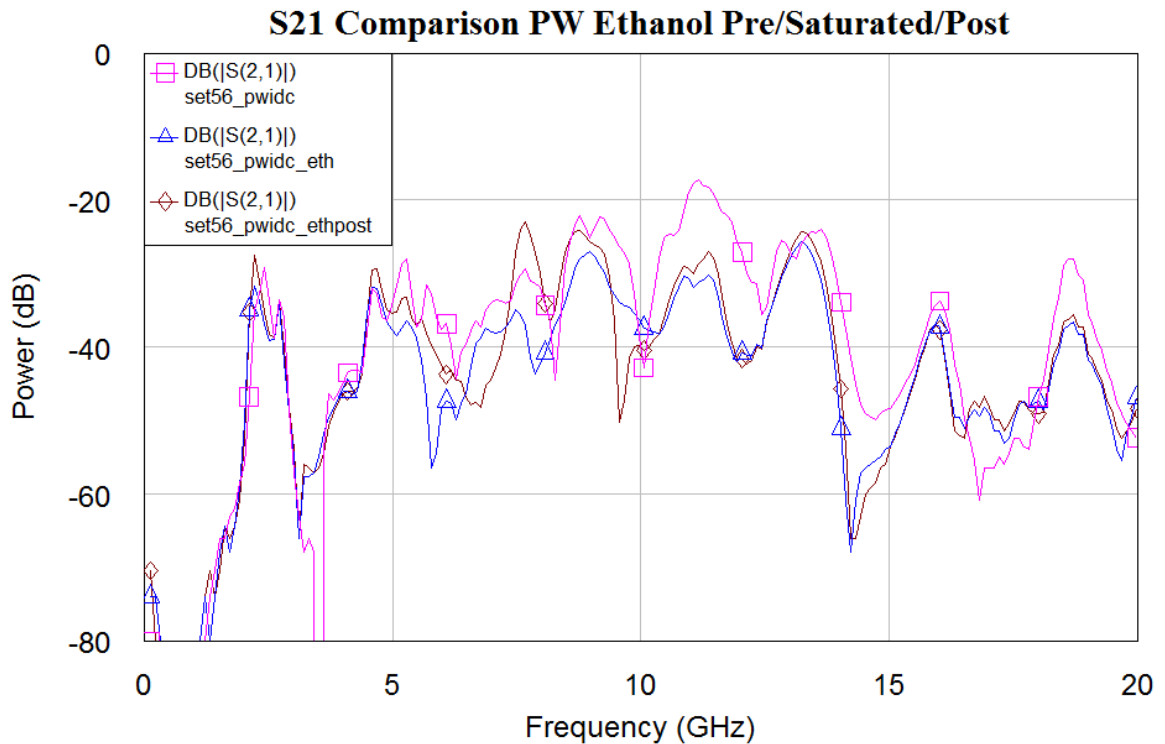


Figure 64. Swept frequency forward power (S21) measurements of the evaporation of ethanol on a bare Passive RF wireless IDC board.

The frequency range just below 10 GHz is used again to examine the effects of ethanol on the IDC structure. When a drop of ethanol saturates the IDC structure, the amplitude decreases and the frequency moves up. When the ethanol evaporates, the amplitude comes back up and frequency decreases. Unfortunately the post ethanol plot does not perfectly match the IDC plot of pre-test. This could possibly mean that a

residue was left over by the ethanol or there are other interfering factors that need to be considered or controlled. The S11 parameters showed a frequency shift in addition to amplitude; however the post ethanol plot still does not perfectly match the IDC plot of pre-test.

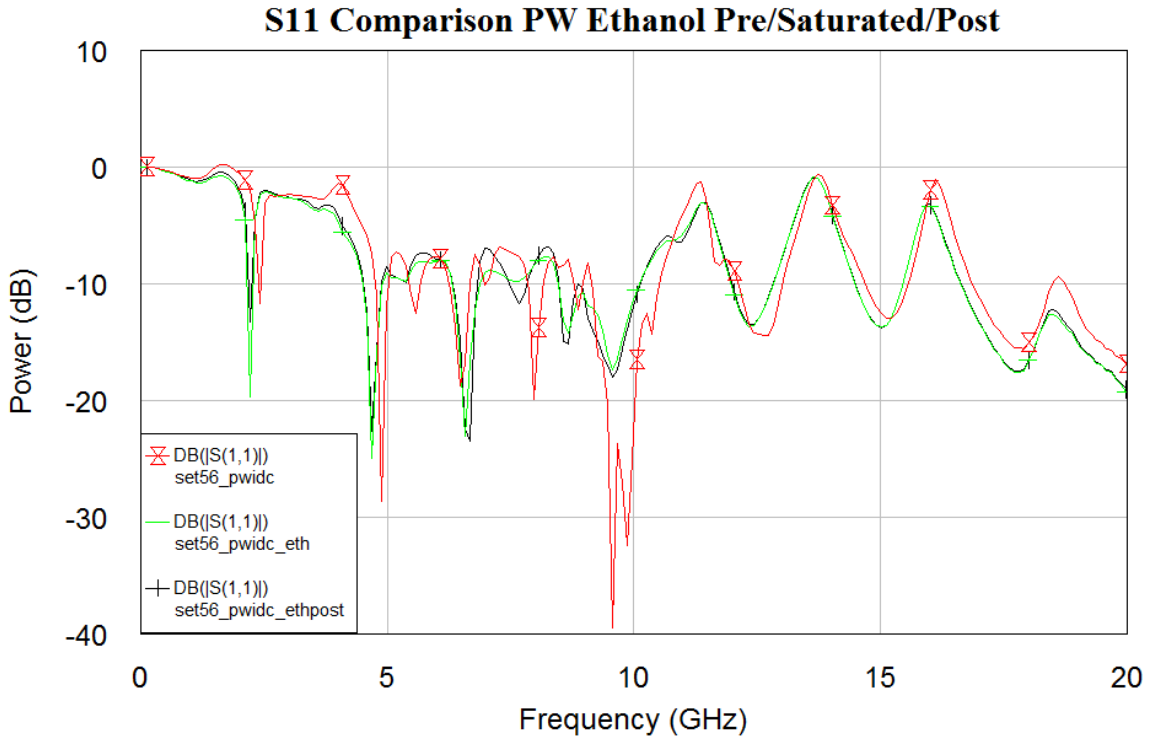


Figure 65. Swept frequency reflected power (S11) measurements of the evaporation of ethanol on a bare Passive RF wireless IDC board.

The frequency range just below 10 GHz is used again to examine the effects of isopropanol on the IDC structure. When a drop of isopropanol saturates the IDC structure, the amplitude decreases and the frequency also decreases. When the isopropanol evaporates, the amplitude comes back up a little and the frequency increases. Just like the post ethanol plot, the post isopropanol plot does not perfectly match the IDC plot of pre-test. This could possibly mean that a residue was left over by the isopropanol or there are other interfering factors that need to be considered or controlled.

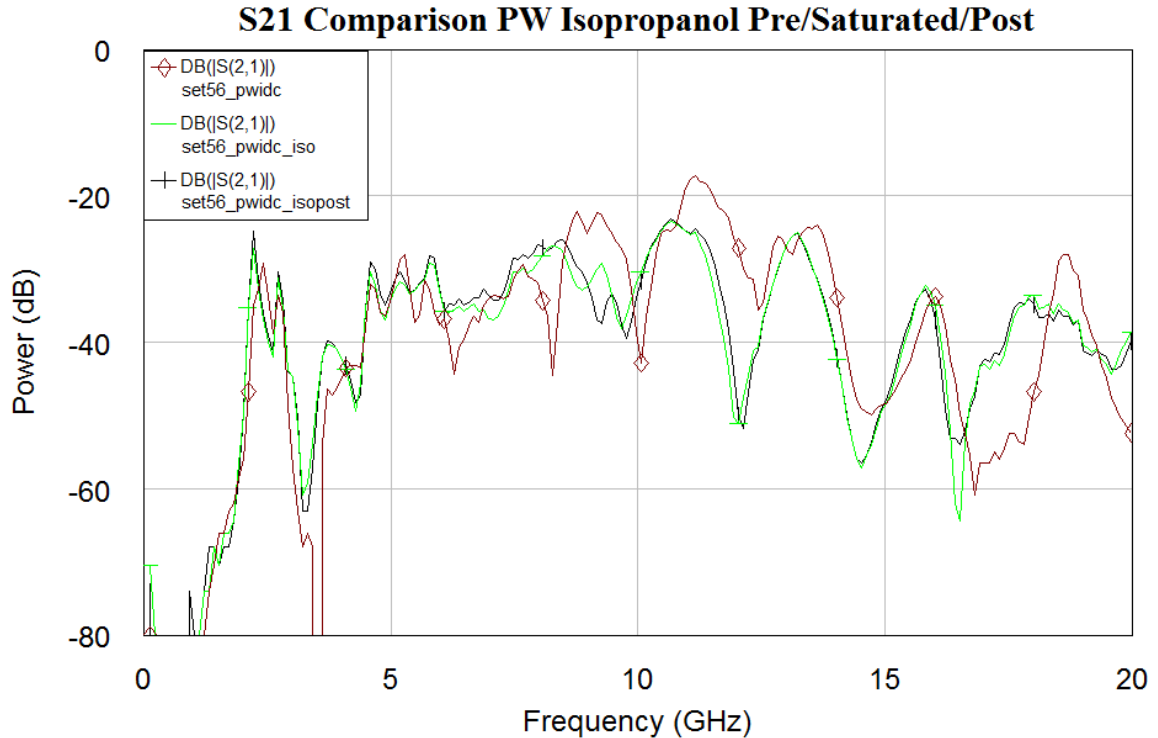


Figure 66. Swept frequency forward power (S21) measurements of the evaporation of isopropanol on a bare Passive RF wireless IDC board.

The S11 parameters also showed a similar frequency shift in addition to amplitude as expected. Figure 67 shows the S11 isopropanol testing results. There is very little difference between the saturated and post signals except for the frequencies immediately below 10 GHz. This was similar for the S21 test shown above. The amplitude shows a downward recovery towards the original IDC value. The amplitude on a S11 plot will be inverted when compared to a S21 plot. This is because when power is flowing through the device in the S21 case, less power is getting reflected. However the frequency will still move the same direction. The peak on a S21 plot will turn into a dip on a S11 plot. Isopropanol did not have as large of an effect on the wireless board as the ethanol did. This does not make sense because the permittivities of the two liquids are very similar.

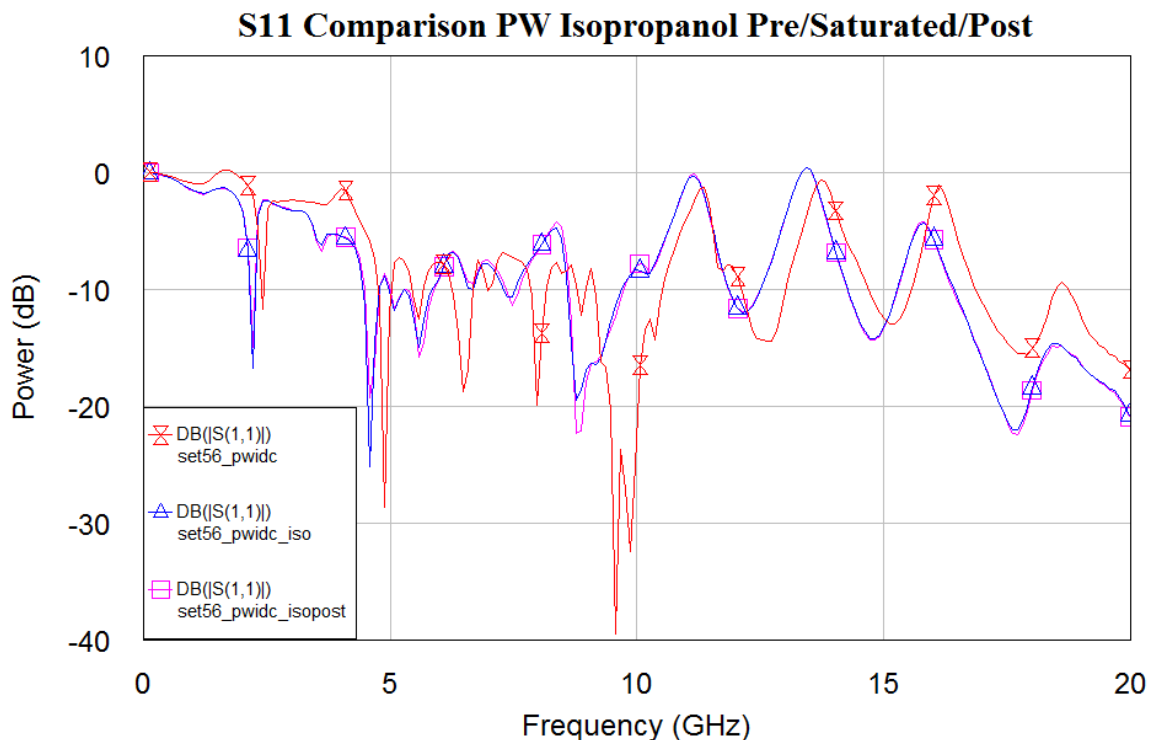


Figure 67. Swept frequency reflected power (S11) measurements of the evaporation of isopropanol on a bare Passive RF wireless IDC board.

### 5.3 Previous Chemical Testing Results

The results from the Passive RF testing are very similar to some previous testing of resonant test structures. Erica Jones as part of her Master’s thesis tested Nafion and silk films with ethanol, isopropanol, and water [112]. The silk films showed little to no effect due to ethanol or isopropanol. However they did show a substantial change when subjected to water as a liquid. This is one of the factors that led to the choice of silk as one of the primary polymers to use in the wireless sensor for characteristic testing. Figure 68 shows the swept frequency forward power measurements of the deposition and evaporation of water on the resonant test structure. The resonant frequency of the device changes from an initial value of 4.5 GHz all the way down to 3.25 GHz with the application of water. As the water evaporates, the resonant frequency returns towards the

original value. Water 1 is water in the liquid state while Water 2-5 is illustrating the evaporation of water and the water being in a mixed vapor/liquid state.

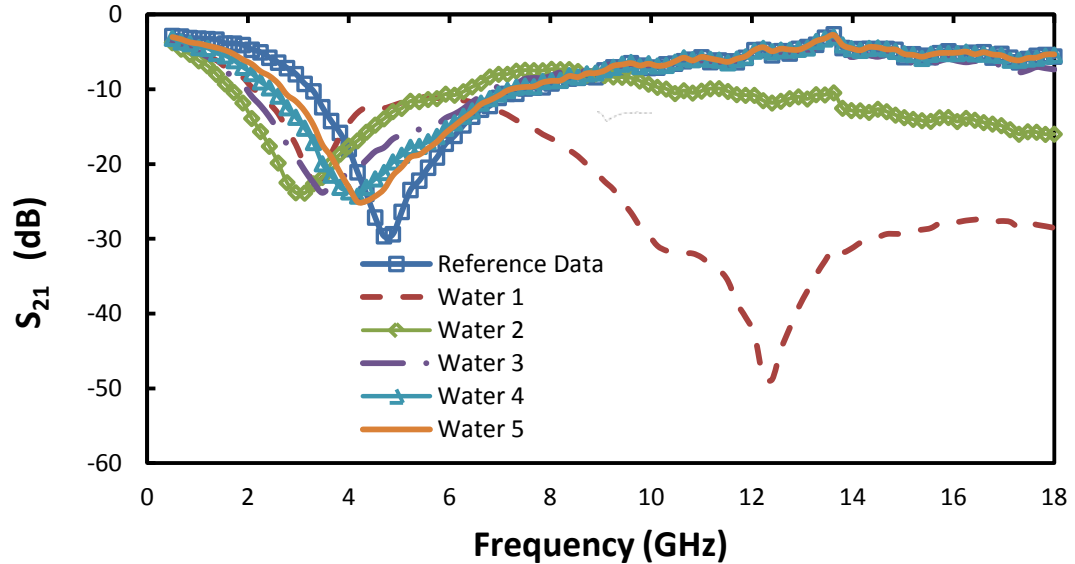


Figure 68. Swept frequency forward power ( $S_{21}$ ) measurements of the evaporation of water on the resonant test structure coated with silk [112].

The resonant frequency of the Nafion coated resonant test structure showed a substantial change due to humidity. Figure 69 shows the swept frequency forward power measurements of the deposition and evaporation of water vapor on the nafion coated resonant test structure. The humidity was changed by blowing on the device to simulate 100% humidity. The magnitude and frequency was very repeatable for the test sample. This is one of the factors that led to the choice of Nafion as the other primary polymer to use in the wireless sensor for characteristic testing. The resonant frequency of the device changes from an initial value of 7.25 GHz down to 6.9 GHz with the application of water vapor. This is equivalent to a change in capacitance of the sensor from 1.21 pF to 1.932 pF. When the water vapor evaporated, the resonant frequency returned to the original value.

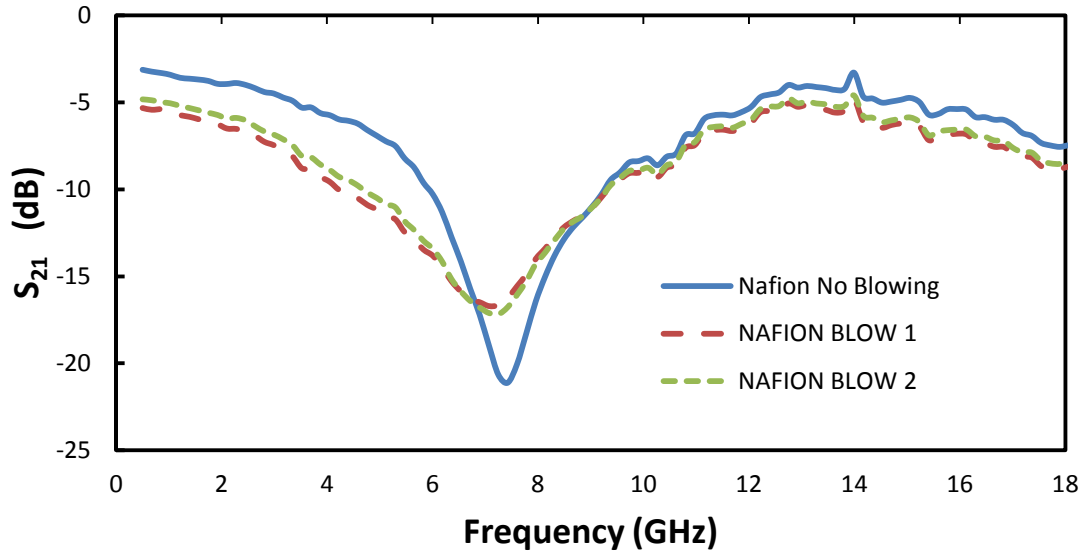


Figure 69. Swept frequency forward power ( $S_{21}$ ) measurements of the evaporation of water on the resonant test structure coated with Nafion [112].

The silk films showed little to no effect due to ethanol. This is evident in Figure 70. The application of ethanol to the silk film caused a loss in Q of the device evidenced by the rise in the transmitted power around 5.5 GHz.

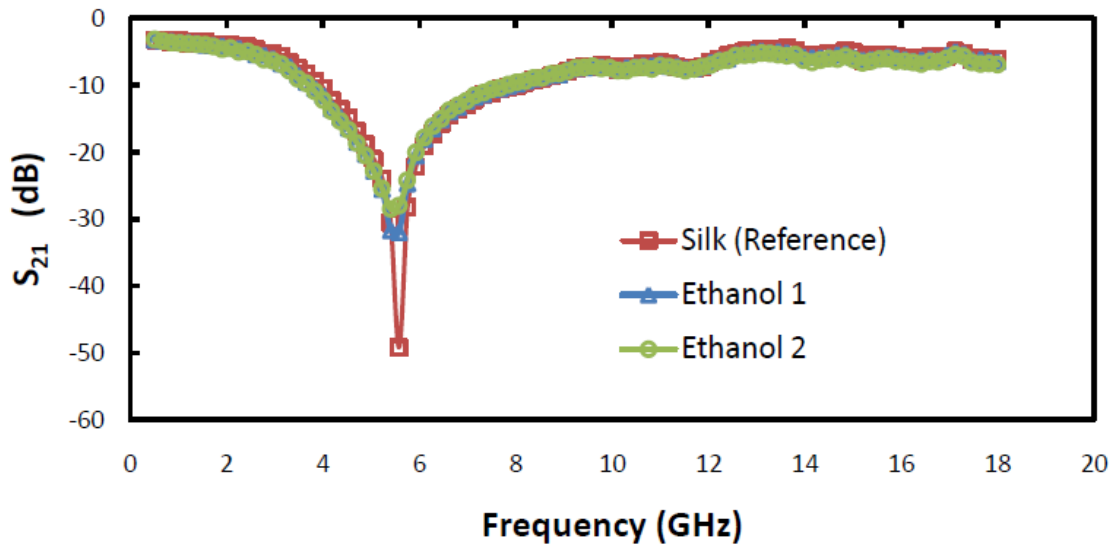


Figure 70. Swept frequency forward power ( $S_{21}$ ) measurements of the evaporation of ethanol on the resonant test structure coated with silk [112].

The silk films showed little to no effect due to isopropanol. This is evident in Figure 71 around 5.5 GHz. The application of isopropanol at first increased the Q of the device, but then decreased the Q of the device as it evaporated. Very little capacitance change was measured during this change. The capacitance of the sensor changed from 1.65 pF to 1.681 pF.

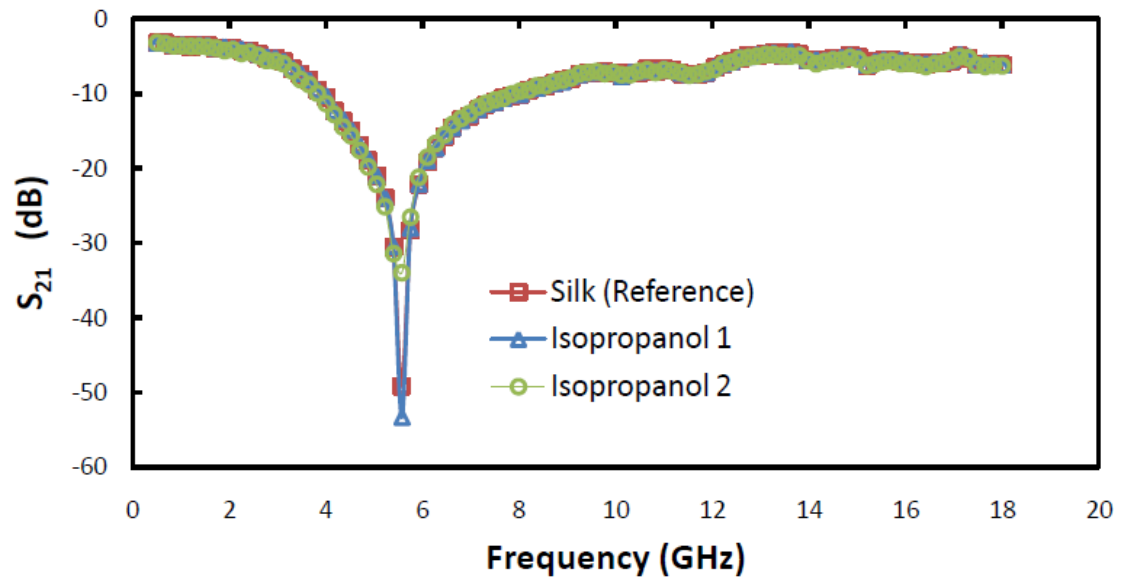


Figure 71. Swept frequency forward power ( $S_{21}$ ) measurements of the evaporation of isopropanol on the resonant test structure coated with silk [112].

## CHAPTER VI

### CONCLUSION

This research has looked at several different methods to obtain measurements wirelessly and has been used as the basis for three patent applications. Some of the devices are truly novel while others use technology that has existed for some time.

#### 6.1 Platform Comparisons

The different platforms are compared based on fifteen different parameters of interest listed in the introduction. They are also compared against legacy bio-chemical sensor platforms.

##### 6.1.1 Sensitivity

Sensitivity is one of the most important parameters in a sensor system. SAW sensors are passive and wireless but have very little sensitivity. Their resonant frequency only changes by a few Hertz when subjected to an analyte of interest. It is desired that a sensor platform be highly sensitive to the analyte of interest. The IDSense platform showed changes of almost 2:1 when subjected to liquids. However the sensitivity to vapors was almost as low as the resolution of the oscilloscope capturing the measurements. The IDSense platform showed changes of several kHz when subjected to the analyte of interest when used for compound testing. The Passive RF platform showed changes in the order of hundreds of MHz in its resonant frequency when subjected to a

liquid chemical. Current test equipment has the ability to measure frequency in very fine steps which makes a resonant frequency device a highly sensitive system.

### 6.1.2 Selectivity

Selectivity is one of the hardest parameters to obtain in a sensor. All of the platforms presented in this work rely on the functionalized surface to achieve selectivity. It is desired that the wireless sensor system exhibit a change only when subjected to the specific to the analyte of interest. Conventional chemical sensors also have this same problem. Most sensors use physical methods beforehand to limit the number of agents subjected to the sensor. The Nafion and silk coatings showed an affinity to certain compounds and not others. They could be used in the future to measure the selected analyte of interest. Multi-parameter testing can also be used to achieve selectivity. The goal of this work was to verify sensitivity of the different sensor platforms to analytes of interest, not to find functional surfaces that could achieve selectivity for those analytes.

### 6.1.3 Stability

Most sensor systems are stable under normal storage conditions for a good lifetime. Some systems achieve stability through packaging in controlled atmospheres. One of the biggest factors that needs controlled is humidity. All of the platforms presented have good stability. The only part of their system that could deteriorate is the functional surface. The IDSense system will have a lifetime limited by its programmable unijunction transistor. The rest of its components are passive and historically have an excellent lifetime. The functional surface on the IDSense platform may have a shorter life than the transistor. The Passive RF system will be limited only by its functional surface.

#### 6.1.4 Reproducibility

A quality manufactured sensor will show good reproducibility. The interrogator antennas for the Passive RF sensor system were checked to make sure they all had the same spectral signature. The placement for the IDSense platform was checked to make sure that placement didn't affect the accuracy of the measurements very much. The manufacturing quality of the IDSense platform was also verified. If a sensor system does not show good reproducibility over a large number of samples then it is not an accurate system and its readings could be construed as ambiguous.

#### 6.1.5 Dual Sensitivity

Dual sensitivity is very similar to selectivity. If the sensor system cannot be selective, then other agents will affect the operation of the device and make it dual sensitive or possibly even worse. Environmental factors very often cause dual sensitivity in sensor systems. Temperature, pH, flow, etc can all cause changes in the readouts. This is why most accurate sensor systems are only in a laboratory environment. Both the IDSense and the Passive RF sensor platforms showed sensitivity to other factors or agents. This was due to the functional surface not being particularly chosen for the analyte of interest.

#### 6.1.6 Minimal Volume

The smaller the sensor platform is the less chemical is required in order to cover the sensor surface to get the device to sense the agent. The IDSense platform needs milliliters of liquid in order to saturate the sensor. The Passive RF platform needs microliters of liquid to saturate its sensor. The Bio-Bridge platform is designed to work with only nanoliters of a chemical. Smaller amounts of a chemical will sometimes cause

a loss of sensitivity for the sensor. It is desired to have a minimal amount of chemical in which to achieve the interaction for sensing.

#### 6.1.7 Useful Range

A useful range is required of the sensor system so that it covers the needed detection levels of the analyte of interest. The IDSense platform suffered from a lack of range when doing liquid saturation testing. The IDSense platform had too much range for the vapor sensing application. The design of IDSense could be easily modified by adding a series capacitor to limit the sensitivity when subjected to a liquid. The Passive RF platform had plenty of range for liquid testing and did not show instabilities like the IDSense platform.

#### 6.1.8 Accuracy

Accuracy over the useable range of the device is one of the most important parameters for a sensor system. If a system has poor accuracy yet good resolution, the measurements are still useless. The only platform tested for accuracy, more so for repeatability, was the IDSense platform.

#### 6.1.9 Linearity

Linearity used to be a major parameter in sensor systems back when the amplifiers and signal conditioners were all analog. With the advent of digital systems, nonlinearities can be easily dealt with in look up tables or mathematical functions. The IDSense system was the only platform analyzed for linearity and it had excellent linearity for its useable range. It is desired for a sensor system to be linear over the useable range of the device.

#### 6.1.10 Noise

It is desired that sensor systems be free from noise effects. All of the platforms tested did not seem to be sensitive to noise. One of the antennas for the Passive RF system showed a dip that didn't match the other five antennas, but it didn't appear to be a noise phenomenon. The Bio-Bridge platform works with the lowest signal to noise ratio and could be susceptible to noise or interference.

#### 6.1.11 Size

Size and portability were two other important parameters in the consideration of a passive wireless sensor system. The military requires small handheld units that can be brought into the field and not weigh much. Normally, the smaller the device is, the less it costs to manufacture as well. The IDSense, Passive RF, and Bio-Bridge platforms are all about the size of a modern RFID system. It takes a fair amount of electronics to build an interrogator and to provide a readout. The current systems today are about the size of a free-standing copier.

#### 6.1.12 Bio-Compatibility

If the system is going to be used in a liquid stream, the sensor device needs to be biocompatible with its working environment. The electronics part of the IDSense, Passive RF, and Bio-Bridge platforms can be encapsulated so that it could be submerged in a liquid and kept separate from the environment with the exception of temperature. The sensing element would be the only part exposed to the environment and the functionalized surface could not be a biofouling type.

#### 6.1.13 Sterilizability

If the sensor device is going to be reused, the sensors will need to be sterilizable. This could either be through heat (autoclave) or a chemical process. The ability of the sensor device to make it through this process depends on the functionalized surface and the platform. The IDSense platform will be temperature limited to 150 degrees Celsius because of the programmable unijunction transistor which is hot enough to withstand the autoclave. The Passive RF and Bio-Bridge platforms can go much higher perhaps to 900 degrees Fahrenheit because they only contain wafer material and metallization. The Bio-Bridge platform will be limited to a much lower temperature if the DNA is required to stay intact and will not be reconstructed. The functionalized surface would be the main environmental limiter for all of these platforms. If the functionalized surface is going to be remade then the temperature and chemical limits go way up.

#### 6.1.14 Cost

The cost of the sensor system will dictate how far the usefulness of the system will expand. It is desired that the sensor system be inexpensive so that several sensor devices can be bought and a few number of interrogators. If the sensor devices are expensive, the application will be limited to those circumstances that can justify the increased cost because of the environment. The IDSense platform uses standard electronics manufacturing processes and is relatively small and inexpensive. In bulk, the sensor devices will cost approximately \$0.50 each to manufacture. The interrogator for the IDSense system will cost around \$25 each. The Passive RF sensor device would cost approximately \$5 each with the interrogator being roughly \$200 each. The Bio-Bridge sensor device may cost about \$1 each with the interrogator being roughly \$200 each.

### 6.1.15 Response Time

It is desired that a sensor system have a good response time. The IDSense, Passive RF, and Bio-Bridge platforms can all be interrogated in less than one second. The functionalized surface may take more time to react to the agent than one second, but the device itself can be read either several times a second to thousands of times a second. Some commercial sensors take minutes to hours to complete a measurement.

## 6.2 Summary

The purpose of this research was to design and build several types of sensor devices that could be used economically. The IDSense is the best example of a platform that fits most of the criteria. The reduction of components on the IDSense sensor board yields an accurate sensor platform that is very cheap to construct and is portable which is good for field testing. The characteristics of some of the sensor platforms were examined and the sensors were tested with several analytes of interest to show that they are capable of functioning. The platforms allow for many different types of analytes to be detected just by simply changing the functionalized surface for the analyte of interest. The platforms are very small and light. Depending on the resonant frequency of the sensor, the sensors can be read either several times per second or thousands of times per second for a quick reading. The sensor platforms exhibit excellent sensitivity and produces repeatable results.

## 6.3 Future Research

There remains a lot of development work and testing to get these systems fully developed and characterized for production sensors. The main purpose of this work was

to build a platform that could be easily modified for many different types of sensors. For example, just by changing the functional surface of the sensor device with a different polymer, the selectivity of the device will change to a different analyte. Luckily there is a wealth of information available which details the selectivity of different polymers to selected analytes. There are many possible uses for these sensor platforms limited only by creativity and the current need. The interrogator will have to be built eventually to get away from using common test equipment in the laboratory.

## BIBLIOGRAPHY

- [1] Retrieved from [www1.lsbu.ac.uk/enztech/biosensors.html](http://www1.lsbu.ac.uk/enztech/biosensors.html) on April 5<sup>th</sup>, 2010.
- [2] G. Subramanyam, M. Patterson, Wireless bio/chemical sensor development using a novel electrical resonant test structure. DARPA 2008 white paper, unpublished.
- [3] M. Gerard, A. Chaubey, B. Malhotra, Application of conducting polymers to biosensors. *Biosensors & Bioelectronics*, 17, pp 345-359 (2002).
- [4] C. Lowe, "Bioelectronics", in AccessScience@McGraw-Hill, <http://www.accessscience.com>, DOI 10.1036/1097-8542.082225.
- [5] A. Bhunia, A. Lathrop, "Pathogen detection, food-borne", in AccessScience@McGraw-Hill, <http://www.accessscience.com>, DOI 10.1036/1097-8542.YB031850.
- [6] M. Sakthivel, W. Weppner, Development of a hydrogen sensor based on solid polymer electrolyte membranes, *Sensors and Actuators B: Chemical*, Volume 113, Issue 2, Special Issue - In honour of Professor Karl Cammann, 27 February 2006, Pages 998-1004, ISSN 0925-4005, DOI: 10.1016/j.snb.2005.04.036.
- [7] H. Qiu, L. Xue, G. Ji, G. Zhou, X. Huang, Y. Qu, P. Gao, Enzyme-modified nanoporous gold-based electrochemical biosensors, *Biosensors and Bioelectronics*, Volume 24, Issue 10, 15 June 2009, Pages 3014-3018, ISSN 0956-5663, DOI: 10.1016/j.bios.2009.03.011.
- [8] O. Smutok, B. Ngounou, H. Pavlishko, G. Gayda, M. Gonchar, W. Schuhmann, A reagentless bienzyme amperometric biosensor based on alcohol oxidase/peroxidase and an Os-complex modified electrodeposition paint, *Sensors and Actuators B: Chemical*, Volume 113, Issue 2, Special Issue - In honour of Professor Karl Cammann, 27 February 2006, Pages 590-598, ISSN 0925-4005, DOI: 10.1016/j.snb.2005.07.055.
- [9] Y. Liu, H. Teng, H. Hou, T. You, Nonenzymatic glucose sensor based on renewable electrospun Ni nanoparticle-loaded carbon nanofiber paste electrode, *Biosensors and Bioelectronics*, Volume 24, Issue 11, 15 July 2009, Pages 3329-3334, ISSN 0956-5663, DOI: 10.1016/j.bios.2009.04.032.

- [10] Y. Bai, Y. Sun, C. Sun, Pt-Pb nanowire array electrode for enzyme-free glucose detection, *Biosensors and Bioelectronics*, Volume 24, Issue 4, 1 December 2008, Pages 579-585, ISSN 0956-5663, DOI: 10.1016/j.bios.2008.06.003.
- [11] M. Lacombe, V. Garcon, D. Thouron, N. Le Bris, M. Comtat, Silicate electrochemical measurements in seawater: chemical and analytical aspects towards a reagentless sensor, *Talanta*, Volume 77, Issue 2, 14th International Conference on Flow Injection Analysis and Related Techniques, 15 December 2008, Pages 744-750, ISSN 0039-9140, DOI: 10.1016/j.talanta.2008.07.023.
- [12] C. Batchelor-McAuley, Y. Du, G. Wildgoose, R. Compton, The use of copper(II) oxide nanorod bundles for the non-enzymatic voltammetric sensing of carbohydrates and hydrogen peroxide, *Sensors and Actuators B: Chemical*, Volume 135, Issue 1, 10 December 2008, Pages 230-235, ISSN 0925-4005, DOI: 10.1016/j.snb.2008.08.006.
- [13] V. Vamvakaki, N. Chaniotakis, Carbon nanostructures as transducers in biosensors, *Sensors and Actuators B: Chemical*, Volume 126, Issue 1, Functional Materials for Micro and Nanosystems - EMRS, Containing Selected papers from the European Materials research Society (E-MRS 2006) Symposium G., 20 September 2007, Pages 193-197, ISSN 0925-4005, DOI: 10.1016/j.snb.2006.11.042.
- [14] W. Liang, W. Yi, S. Li, R. Yuan, A. Chen, S. Chen, G. Xiang, C. Hu, A novel, label-free immunosensor for the detection of [ $\alpha$ ]-fetoprotein using functionalized gold nanoparticles, *Clinical Biochemistry*, Volume 42, Issue 15, October 2009, Pages 1524-1530, ISSN 0009-9120, DOI: 10.1016/j.clinbiochem.2009.07.009.
- [15] Y. Himuro, M. Takai, K. Ishihara, Poly(vinylferrocene-co-2-hydroxyethyl methacrylate) mediator as immobilized enzyme membrane for the fabrication of amperometric glucose sensor, *Sensors and Actuators B: Chemical*, Volume 136, Issue 1, 2 February 2009, Pages 122-127, ISSN 0925-4005, DOI: 10.1016/j.snb.2008.09.049.
- [16] J. Wan, H. Shu, S. Huang, B. Fiebor, V. Petrenko, B. Chin, Phage-based magnetoelastic wireless biosensors for detecting bacillus anthracis spores; *Sensors Journal*, IEEE Publication Date: March 2007 Volume: 7, Issue: 3 on page(s): 470 – 477.
- [17] T. Krishnakumar, R. Jayaprakash, N. Pinna, N. Donato, A. Bonavita, G. Micali, G. Neri, CO gas sensing of ZnO nanostructures synthesized by an assisted microwave wet chemical route, *Sensors and Actuators B: Chemical*, Volume 143,

Issue 1, 4 December 2009, Pages 198-204, ISSN 0925-4005, DOI:  
10.1016/j.snb.2009.09.039.

- [18] H. Xie, Q. Yang, X. Sun, J. Yang, Y. Huang, Gas sensor arrays based on polymer-carbon black to detect organic vapors at low concentration, *Sensors and Actuators B: Chemical*, Volume 113, Issue 2, Special Issue - In honour of Professor Karl Cammann, 27 February 2006, Pages 887-891, ISSN 0925-4005, DOI: 10.1016/j.snb.2005.03.116.
- [19] Q. Qi, T. Zhang, S. Wang, X. Zheng, Humidity sensing properties of KCl-doped ZnO nanofibers with super-rapid response and recovery, *Sensors and Actuators B: Chemical*, Volume 137, Issue 2, 2 April 2009, Pages 649-655, ISSN 0925-4005, DOI: 10.1016/j.snb.2009.01.042.
- [20] A. Mohd-Syaifudin, K. Jayasundera, S. Mukhopadhyay, A low cost novel sensing system for detection of dangerous marine biotoxins in seafood, *Sensors and Actuators B: Chemical*, Volume 137, Issue 1, 28 March 2009, Pages 67-75, ISSN 0925-4005, DOI: 10.1016/j.snb.2008.12.053.
- [21] S. Helali, A. Abdelghani, N. Jaffrezic-Renault, P. Trikalitis, C. Efstathiou, M. Prodromidis, On-site monitoring of fish spoilage using vanadium pentoxide xerogel modified interdigitated gold electrodes, *Electrochimica Acta*, In Press, Corrected Proof, Available online 19 January 2009, ISSN 0013-4686, DOI: 10.1016/j.electacta.2009.01.027.
- [22] M. Kitsara, D. Goustouridis, S. Chatzandroulis, M. Chatzichristidi, I. Raptis, T. Ganetsos, R. Igreja, C. Dias, Single chip interdigitated electrode capacitive chemical sensor arrays, *Sensors and Actuators B: Chemical*, Volume 127, Issue 1, Special Issue: Eurosenors XX The 20th European Conference on Solid-State Transducers, the 20th European conference on Solid-State Transducers, 20 October 2007, Pages 186-192, ISSN 0925-4005, DOI: 10.1016/j.snb.2007.07.021.
- [23] E. Valera, J. Ramon-Azcon, A. Rodriguez, L. Castaner, F. Sanchez, M. Marco, Impedimetric immunosensor for atrazine detection using interdigitated  $[\mu]$ -electrodes (ID $[\mu]$ E's), *Sensors and Actuators B: Chemical*, Volume 125, Issue 2, 8 August 2007, Pages 526-537, ISSN 0925-4005, DOI: 10.1016/j.snb.2007.02.048.
- [24] J. Ceriotti, J. Ponti, P. Colpo, E. Sabbioni, F. Rossi, Assessment of cytotoxicity by impedance spectroscopy, *Biosensors and Bioelectronics*, Volume 22, Issue 12, Chem and Biosensing Transistors: from materials to systems, 15 June 2007, Pages 3057-3063, ISSN 0956-5663, DOI: 10.1016/j.bios.2007.01.004.

- [25] S. Cho, S. Becker, H. von Briesen, H. Thielecke, Impedance monitoring of herpes simplex virus-induced cytopathic effect in vero cells, *Sensors and Actuators B: Chemical*, Volume 123, Issue 2, 21 May 2007, Pages 978-982, ISSN 0925-4005, DOI: 10.1016/j.snb.
- [26] E. Wongrat, P. Pimpang, S. Choopun, Comparative study of ethanol sensor based on gold nanoparticles: ZnO nanostructure and gold: ZnO nanostructure, *Applied Surface Science*, Volume 256, Issue 4, VASSCAA-4 - Proceedings of the Session on Surface Science of the 4th Vacuum and Surface Sciences Conference of Asia and Australia, 30 November 2009, Pages 968-971, ISSN 0169-4332, DOI: 10.1016/j.apsusc.2009.02.046.
- [27] J. Oikonomou, K. Manoli, D. Goustouridis, I. Raptis, M. Sanopoulou, Polymer/BaTiO<sub>3</sub> nanocomposites based chemocapacitive sensors, *Microelectronic Engineering*, Volume 86, Issues 4-6, MNE '08 - The 34th International Conference on Micro- and Nano-Engineering (MNE), April-June 2009, Pages 1286-1288, ISSN 0167-9317, DOI: 10.1016/j.mee.2008.11.081.
- [28] J. Robinson, E. Snow, F. Perkins, Improved chemical detection using single-walled carbon nanotube network capacitors, *Sensors and Actuators A: Physical*, Volume 135, Issue 2, 15 April 2007, Pages 309-314, ISSN 0924-4247, DOI: 10.1016/j.sna.2006.07.027.
- [29] R. Gelamo, F. Rouxinol, C. Verissimo, A. Vaz, M. Bica de Moraes, S. Moshkalev, Low-temperature gas and pressure sensor based on multi-wall carbon nanotubes decorated with Ti nanoparticles, *Chemical Physics Letters*, Volume 482, Issues 4-6, 12 November 2009, Pages 302-306, ISSN 0009-2614, DOI: 10.1016/j.cplett.2009.10.019.
- [30] M. Carotta, A. Cervi, A. Giberti, V. Guidi, C. Malagu, G. Martinelli, D. Puzzovio, Metal-oxide solid solutions for light alkane sensing, *Sensors and Actuators B: Chemical*, Volume 133, Issue 2, 12 August 2008, Pages 516-520, ISSN 0925-4005, DOI: 10.1016/j.snb.2008.03.012.
- [31] M. Abouzar, S. Ingebrandt, A. Poghossian, Y. Zhang, X. Vu, W. Moritz, M. Schoning, Nanoplate field-effect capacitive (bio-)chemical sensor array based on SOI structure, *Procedia Chemistry*, Volume 1, Issue 1, Proceedings of the Eurosensors XXIII conference, September 2009, Pages 670-673, ISSN 1876-6196, DOI: 10.1016/j.proche.2009.07.167.
- [32] B. Li, S. Santhanam, L. Schultz, M. Jeffries-EL, M. Iovu, G. Sauve, J. Cooper, R. Zhang, J. Revelli, A. Kusne, J. Snyder, T. Kowalewski, L. Weiss, R. McCullough, G. Fedder, D. Lambeth, Inkjet printed chemical sensor array based on

- polythiophene conductive polymers, *Sensors and Actuators B: Chemical*, Volume 123, Issue 2, 21 May 2007, Pages 651-660, ISSN 0925-4005, DOI: 10.1016/j.snb.2006.09.064.
- [33] F. Favier, Nanogaps for sensing, *Procedia Chemistry*, Volume 1, Issue 1, Proceedings of the Eurosensors XXIII conference, September 2009, Pages 746-749, ISSN 1876-6196, DOI: 10.1016/j.proche.2009.07.186.
- [34] A. Oki, K. Miyano, S. Hotta, D. Yano, K. Sano, K. Yamanaka, C. Kimura, T. Sugino, Amino acid sensing by impedance of porous monolith-type ion exchanger, *Electrochimica Acta*, Volume 53, Issue 22, 20 September 2008, Pages 6657-6661, ISSN 0013-4686, DOI: 10.1016/j.electacta.2008.04.037.
- [35] M. Knite, K. Ozols, G. Sakale, V. Teteris, Polyisoprene and high structure carbon nanoparticle composite for sensing organic solvent vapours, *Sensors and Actuators B: Chemical*, Volume 126, Issue 1, Functional Materials for Micro and Nanosystems - EMRS, Containing Selected papers from the European Materials research Society (E-MRS 2006) Symposium G., 20 September 2007, Pages 209-213, ISSN 0925-4005, DOI: 10.1016/j.snb.2006.11.049.
- [36] R. Morais, A. Valente, J. Almeida, A. Silva, S. Soares, M. Reis, R. Valentim, J. Azevedo, Concept study of an implantable microsystem for electrical resistance and temperature measurements in dairy cows, suitable for estrus detection, *Sensors and Actuators A: Physical*, Volume 132, Issue 1, The 19th European Conference on Solid-State Transducers, 8 November 2006, Pages 354-361, ISSN 0924-4247, DOI: 10.1016/j.sna.2006.04.011.
- [37] M. Hammond, K. Johnson, S. Rose-Pehrsson, J. Ziegler, H. Walker, K. Caudy, D. Gary, D. Tillett, A novel chemical detector using cermet sensors and pattern recognition methods for toxic industrial chemicals, *Sensors and Actuators B: Chemical*, Volume 116, Issues 1-2, ISOEN 2005 - Selected Papers from the 11th International Symposium on Olfaction and Electronic Noses - Barcelona, Spain, 13-15 April 2005., 28 July 2006, Pages 135-144, ISSN 0925-4005, DOI: 10.1016/j.snb.2005.12.065.
- [38] P. Sjoberg-Eerola, J. Bobacka, A. Lewenstam, A. Ivaska, All-solid-state chloride sensors based on electronically conducting, semiconducting and insulating polymer membranes, *Sensors and Actuators B: Chemical*, Volume 127, Issue 2, 15 November 2007, Pages 545-553, ISSN 0925-4005, DOI: 10.1016/j.snb.2007.05.004.
- [39] B. Jeon, M. Kim, J. Pyun, Application of parylene film as a linker layer of SPR biosensor, *Procedia Chemistry*, Volume 1, Issue 1, Proceedings of the

Euroensors XXIII conference, September 2009, Pages 1035-1038, ISSN 1876-6196, DOI: 10.1016/j.proche.2009.07.258.

- [40] X. Chen, M. Pan, K. Jiang, Sensitivity enhancement of SPR biosensor by improving surface quality of glass slides, *Microelectronic Engineering*, In Press, Corrected Proof, Available online 23 November 2009, ISSN 0167-9317, DOI: 10.1016/j.mee.2009.11.092.
- [41] Y. Mizuta, T. Onodera, P. Singh, K. Matsumoto, N. Miura, K. Toko, Development of an oligo(ethylene glycol)-based SPR immunosensor for TNT detection, *Biosensors and Bioelectronics*, Volume 24, Issue 2, 15 October 2008, Pages 191-197, ISSN 0956-5663, DOI: 10.1016/j.bios.2008.03.042.
- [42] G. Wilson, "Biosensor", in *AccessScience@McGraw-Hill*, <http://www.accessscience.com>, DOI 10.1036/1097-8542.757486.
- [43] A. Turner, "Biosensor", in *AccessScience@McGraw-Hill*, <http://www.accessscience.com>, DOI 10.1036/1097-8542.YB000170.
- [44] B. Cui, Y. Cortot, T. Veres, Polyimide nanostructures fabricated by nanoimprint lithography and its applications, *Microelectronic Engineering*, Volume 83, Issues 4-9, *Micro- and Nano-Engineering MNE 2005*, April-September 2006, Pages 906-909, ISSN 0167-9317, DOI: 10.1016/j.mee.2006.01.014.
- [45] Z. Zhao, M. Arrandale, O. Vassiltsova, M. Petrukhina, M. Carpenter, Sensing mechanism investigation on semiconductor quantum dot/polymer thin film based hydrocarbon sensor, *Sensors and Actuators B: Chemical*, Volume 141, Issue 1, 18 August 2009, Pages 26-33, ISSN 0925-4005, DOI: 10.1016/j.snb.2009.06.036.
- [46] S. Mosadegh Sedghi, Y. Mortazavi, A. Khodadadi, Low temperature CO and CH<sub>4</sub> dual selective gas sensor using SnO<sub>2</sub> quantum dots prepared by sonochemical method, *Sensors and Actuators B: Chemical*, In Press, Corrected Proof, Available online 12 November 2009, ISSN 0925-4005, DOI: 10.1016/j.snb.2009.11.002.
- [47] K. Liao, T. Hogen-Esch, F. Richmond, L. Marcu, W. Clifton, G. Loeb, Percutaneous fiber-optic sensor for chronic glucose monitoring in vivo, *Biosensors and Bioelectronics*, Volume 23, Issue 10, 15 May 2008, Pages 1458-1465, ISSN 0956-5663, DOI: 10.1016/j.bios.2008.01.012.
- [48] S. Topliss, S. James, F. Davis, S. Higson, R. Tatam, Optical fibre long period grating based selective vapour sensing of volatile organic compounds, *Sensors and Actuators B: Chemical*, In Press, Corrected Proof, Available online 29 October 2009, ISSN 0925-4005, DOI: 10.1016/j.snb.2009.10.008.

- [49] R. Chandrasekhar, J. Miecznikowski, D. Gaile, V. Govindaraju, F. Bright, K. Sellers, Xerogel package, *Chemometrics and Intelligent Laboratory Systems*, Volume 96, Issue 1, 15 March 2009, Pages 70-74, ISSN 0169-7439, DOI: 10.1016/j.chemolab.2008.12.002.
- [50] C. Lee, J. Yang, [alpha]-Cyclodextrin-modified infrared sensing system for rapidly determining the enantiomeric composition of chiral compounds, *Talanta*, Volume 74, Issue 5, 15 February 2008, Pages 1104-1112, ISSN 0039-9140, DOI: 10.1016/j.talanta.2007.08.010.
- [51] M. van der Werff, Y. Yuan, E. Hirst, W. Xu, H. Chen, J. Bronlund, Quartz Crystal Microbalance Induced Bond Rupture Sensing for Medical Diagnostics, *Sensors Journal*, IEEE Volume 7, Issue 5, May 2007 Page(s):762 - 769 Digital Object Identifier 10.1109/JSEN.2007.894131.
- [52] L. Carrascosa, M. Moreno, M. Alvarez, L. Lechuga, Nanomechanical biosensors: a new sensing tool, *TrAC Trends in Analytical Chemistry*, Volume 25, Issue 3, March 2006, Pages 196-206, ISSN 0165-9936, DOI: 10.1016/j.trac.2005.09.006.
- [53] J. Agusti, I. Pellejero, G. Abadal, G. Murillo, M. Urbiztondo, J. Sese, M. Villarroya-Gaudo, M. Pina, J. Santamaria, N. Barniol, Optical vibrometer for mechanical properties characterization of silicalite-only cantilever based sensors, *Microelectronic Engineering*, In Press, Uncorrected Proof, Available online 9 December 2009, ISSN 0167-9317, DOI: 10.1016/j.mee.2009.12.009.
- [54] V. Mortet, A. Soltani, A. Talbi, P. Pobedinskas, K. Haenen, J. De Jaeger, P. Pernod, P. Wagner, AlN on nanocrystalline diamond piezoelectric cantilevers for sensors/actuators, *Procedia Chemistry*, Volume 1, Issue 1, Proceedings of the Eurosensors XXIII conference, September 2009, Pages 40-43, ISSN 1876-6196, DOI: 10.1016/j.proche.2009.07.010.
- [55] S. Tetin, B. Caillard, F. Menil, H. Debeda, C. Lucat, C. Pellet, I. Dufour, Modeling and performance of uncoated microcantilever-based chemical sensors, *Sensors and Actuators B: Chemical*, In Press, Corrected Proof, Available online 14 October 2009, ISSN 0925-4005, DOI: 10.1016/j.snb.2009.09.062.
- [56] J. Leis, W. Zhao, L. Pinnaduwege, A. Gehl, S. Allman, A. Shepp, K. Mahmud, Estimating gas concentration using a microcantilever-based electronic nose, *Digital Signal Processing*, In Press, Corrected Proof, Available online 27 October 2009, ISSN 1051-2004, DOI: 10.1016/j.dsp.2009.10.026.
- [57] H. Lang, A. Filippi, A. Tonin, F. Huber, N. Backmann, J. Zhang, C. Gerber, Towards a modular, versatile and portable sensor system for measurements in

- gaseous environments based on microcantilevers, *Procedia Chemistry*, Volume 1, Issue 1, Proceedings of the Eurosensors XXIII conference, September 2009, Pages 208-211, ISSN 1876-6196, DOI: 10.1016/j.proche.2009.07.052.
- [58] R. Capuano, M. Santonico, D. Martinelli, A. D'Amico, R. Paolesse, D. Monti, C. Di Natale, Investigating the structure-sensitivity relationship of metalloporphyrins based chemical sensors, *Procedia Chemistry*, Volume 1, Issue 1, Proceedings of the Eurosensors XXIII conference, September 2009, Pages 228-231, ISSN 1876-6196, DOI: 10.1016/j.proche.2009.07.057.
- [59] M. Ayad, G. El-Hefnawey, N. Torad, A sensor of alcohol vapours based on thin polyaniline base film and quartz crystal microbalance, *Journal of Hazardous Materials*, Volume 168, Issue 1, 30 August 2009, Pages 85-88, ISSN 0304-3894, DOI: 10.1016/j.jhazmat.2009.02.003.
- [60] X. Xu, H. Cang, C. Li, Z. Zhao, H. Li, Quartz crystal microbalance sensor array for the detection of volatile organic compounds, *Talanta*, Volume 78, Issue 3, 15 May 2009, Pages 711-716, ISSN 0039-9140, DOI: 10.1016/j.talanta.2008.12.031.
- [61] M. Matsuguchi, Y. Kadowaki, K. Noda, R. Naganawa, HCl gas monitoring based on a QCM using morpholine-functional styrene-co-chloromethylstyrene copolymer coatings, *Sensors and Actuators B: Chemical*, Volume 120, Issue 2, 10 January 2007, Pages 462-466, ISSN 0925-4005, DOI: 10.1016/j.snb.2006.02.039.
- [62] F. Thery-Merland, C. Methivier, E. Pasquinet, L. Hairault, C. Pradier, Adsorption of functionalised thiols on gold surfaces: How to build a sensitive and selective sensor for a nitroaromatic compound?, *Sensors and Actuators B: Chemical*, Volume 114, Issue 1, 30 March 2006, Pages 223-228, ISSN 0925-4005, DOI: 10.1016/j.snb.2005.04.040.
- [63] M. Guillemot, F. Dayber, P. Montmeat, C. Barthet, P. Prene, Detection of explosives vapours on quartz crystal microbalances: generation of very low-concentrated vapours for sensors calibration, *Procedia Chemistry*, Volume 1, Issue 1, Proceedings of the Eurosensors XXIII conference, September 2009, Pages 967-970, ISSN 1876-6196, DOI: 10.1016/j.proche.2009.07.241.
- [64] H. Lobl, M. Klee, R. Milsom, R. Dekker, C. Metzmacher, W. Brand, P. Lok, Materials for bulk acoustic wave (BAW) resonators and filters, *Journal of the European Ceramic Society*. v 21, n 15. 2001, p 2633-2640.
- [65] A. Dickherber, C. Corso, W. Hunt, Lateral Field Excitation (LFE) of Thickness Shear Mode (TSM) Acoustic Waves in Thin Film Bulk Acoustic Resonators (FBAR) as a Potential Biosensor, *Engineering in Medicine and Biology Society*,

2006. EMBS '06. 28th Annual International Conference of the IEEE Aug. 2006  
Page(s):4590 – 4593.
- [66] G. Wingqvist, J. Bjurström, L. Liljeholm, I. Katardjiev, A. Spetz, Shear mode AlN thin film electroacoustic resonator for biosensor applications, *Sensors*, 2005 IEEE 30 Oct.- 3 Nov. 2005 Page(s):4.
- [67] I. Mannelli, M. Minunni, S. Tombelli, M. Mascini, Bulk acoustic wave affinity biosensor for genetically modified organisms detection, *Sensors Journal*, IEEE, Volume 3, Issue 4, Aug. 2003 Page(s):369-375.
- [68] R. Brederlow, S. Zauner, A. Scholtz, K. Aufinger, W. Simburger, C. Paulus, A. Martin, M. Fritz, H. Timme, H. Heiss, S. Marksteiner, L. Elbrecht, R. Aigner, R. Thewes, Biochemical sensors based on bulk acoustic wave resonators, *Electron Devices Meeting, 2003. IEDM '03 Technical Digest. IEEE International* 8-10 Dec. 2003 Page(s):32.7.1 - 32.7.3.
- [69] K. Lange, S. Grimm, M. Rapp, Chemical modification of parylene C coatings for SAW biosensors, *Sensors and Actuators B: Chemical*, Volume 125, Issue 2, 8 August 2007, Pages 441-446, ISSN 0925-4005, DOI: 10.1016/j.snb.2007.02.039.
- [70] K. Lange, A. Voigt, M. Rapp, Surface acoustic wave biosensors for biomolecular interaction analysis, *Sensors*, 2003. *Proceedings of IEEE* Volume 2, 22-24 Oct. 2003 Page(s):1174 - 1178 Vol.2.
- [71] J. Nosek, Extreme sensitive sensors using BAW and SAW, *International Conference on Road Vehicle Automation (2nd : 1995 : Bolton Institute) Road vehicle automation II : towards systems integration*. Chichester ; New York : Wiley, c1997. (OCOLC)36261552.
- [72] R. McGill, M. Anderson, D. Venezky, Fire detection by Surface Acoustic Wave chemical sensor systems, *Online*, 1993.
- [73] K. Kokkonen, M. Kaivola, S. Benchabane, A. Khelif, V. Laude, Scattering of surface acoustic waves by a phononic crystal revealed by heterodyne interferometry, *Applied Physics Letters*. v 91, n 8. 2007.
- [74] M. Assouar, O. Elmazria, P. Kirsch, P. Alnot, V. Mortet, C. Tiusan, High-frequency surface acoustic wave devices based on AlN/diamond layered structure realized using e-beam lithography, *Journal of Applied Physics*. v 101, n 11. 2007.
- [75] B. Paci, A. Generosi, V. Rossi Albertini, M. Benetti, D. Cannata, F. Di Pietrantonio, E. Verona, A study of highly c-axis oriented AlN films for diamond-

based surface acoustic wave devices: Bulk structure and surface morphology, *Sensors and Actuators, A: Physical*. v 137, n 2. Jul 4 2007 2007, p 279-286.

- [76] A. Nordin, M. Zaghoul, Modeling and fabrication of CMOS surface acoustic wave resonators, *IEEE Transactions on Microwave Theory and Techniques*. v 55, n 5. May 2007, p 992-1001.
- [77] A. Nordin, M. Zaghoul, C. Korman, S. Ahmadi, CMOS surface acoustic wave oscillators, 2005 IEEE International 48th Midwest Symposium on Circuits and Systems, v 2005, 2005, p 607-610.
- [78] W. Choy, B. Weiss, Interdiffusion induced modification of surface-acoustic-wave AlGaAs-GaAs quantum-well modulators, *Selected Topics in Quantum Electronics, IEEE Journal of Volume 4, Issue 4, July-Aug. 1998* Page(s):758 - 764 Digital Object Identifier 10.1109/2944.720489.
- [79] H. Hao, K. Tang, P. Ku, J. Chao, C. Li, C. Yang, D. Yao, Development of a portable electronic nose based on chemical Surface Acoustic Wave array with multiplexed oscillator and readout electronics, *Sensors and Actuators B: Chemical*, In Press, Accepted Manuscript, Available online 16 December 2009, ISSN 0925-4005, DOI: 10.1016/j.snb.2009.12.023.
- [80] E. Chevallier, E. Scorsone, P. Bergonzo, Modified diamond nanoparticles as sensitive coatings for chemical SAW sensors, *Procedia Chemistry, Volume 1, Issue 1, Proceedings of the Eurosensors XXIII conference, September 2009, Pages 943-946, ISSN 1876-6196, DOI: 10.1016/j.proche.2009.07.235.*
- [81] D. Fernandes, T. Rolo, J. Oliveira, M. Gomes, A new analytical system, based on an acoustic wave sensor, for halitosis evaluation, *Sensors and Actuators B: Chemical, Volume 136, Issue 1, 2 February 2009, Pages 73-79, ISSN 0925-4005, DOI: 10.1016/j.snb.2008.10.037.*
- [82] B. Joo, J. Huh, D. Lee, Fabrication of polymer SAW sensor array to classify chemical warfare agents, *Sensors and Actuators B: Chemical, Volume 121, Issue 1, Special Issue: 25th Anniversary of Sensors and Actuators B: Chemical, 30 January 2007, Pages 47-53, ISSN 0925-4005, DOI: 10.1016/j.snb.2006.09.013.*
- [83] N. Barie, M. Bucking, M. Rapp, A novel electronic nose based on miniaturized SAW sensor arrays coupled with SPME enhanced headspace-analysis and its use for rapid determination of volatile organic compounds in food quality monitoring, *Sensors and Actuators B: Chemical, Volume 114, Issue 1, 30 March 2006, Pages 482-488, ISSN 0925-4005, DOI: 10.1016/j.snb.2005.06.051.*

- [84] D. Matatagui, J. Marti, M. Fernandez, J. Fontecha, J. Gutierrez, I. Gracia, C. Cane, M. Horrillo, Optimized design of a SAW sensor array for chemical warfare agents simulants detection, *Procedia Chemistry*, Volume 1, Issue 1, Proceedings of the Eurosensors XXIII conference, September 2009, Pages 232-235, ISSN 1876-6196, DOI: 10.1016/j.proche.2009.07.058.
- [85] D. Fernandes, M. Gomes, Development of an electronic nose to identify and quantify volatile hazardous compounds, *Talanta*, Volume 77, Issue 1, 19 October 2008, Pages 77-83, ISSN 0039-9140, DOI: 10.1016/j.talanta.2008.05.042.
- [86] F. Chou, J. Shih, Electrochemical electrode/SAW system for metal ions and glucose in solutions, *Sensors and Actuators B: Chemical*, Volume 129, Issue 1, 29 January 2008, Pages 176-183, ISSN 0925-4005, DOI: 10.1016/j.snb.2007.07.101.
- [87] A. Nimal, U. Mittal, M. Singh, M. Khaneja, G. Kannan, J. Kapoor, V. Dubey, P. Gutch, G. Lal, K. Vyas, D. Gupta, Development of handheld SAW vapor sensors for explosives and CW agents, *Sensors and Actuators B: Chemical*, Volume 135, Issue 2, 15 January 2009, Pages 399-410, ISSN 0925-4005, DOI: 10.1016/j.snb.2008.08.040.
- [88] R. Wittstruck, X. Tong, N. Emanetoglu, P. Wu, Y. Chen, J. Zhu, S. Muthukumar, Y. Lu, A. Ballato, Characteristics of Mg/sub x/Zn/sub 1-x/O thin film bulk acoustic wave devices, *Ultrasonics, Ferroelectrics and Frequency Control*, IEEE Transactions on, Volume 50, Issue 10, Oct. 2003 Page(s):1272 - 1278 Digital Object Identifier 10.1109/TUFFC.2003.1244743.
- [89] G. Fischerauer, F. Dickert, An analytic model of the dynamic response of mass-sensitive chemical sensors, *Sensors and Actuators B: Chemical*, Volume 123, Issue 2, 21 May 2007, Pages 993-1001, ISSN 0925-4005, DOI: 10.1016/j.snb.2006.11.002.
- [90] M. Dubois, J. Carpentier, P. Vincent, C. Billard, G. Parat, C. Muller, P. Ancy, P. Conti, Monolithic above-IC resonator technology for integrated architectures in mobile and wireless communication; *Solid-State Circuits*, IEEE Journal of, Volume 41, Issue 1, Jan. 2006 Page(s):7 – 16, Digital Object Identifier 10.1109/JSSC.2005.858627.
- [91] J. Yook, Y. Kwon, Spiral inductors using polymer-core conductors, *IEEE Microwave and Wireless Components Letters*. v 17, n 7. July 2007 2007, p 495-497.
- [92] B. Lacroix, A. Pothier, A. Crunteanu, C. Cibert, F. Dumas-Bouchiat, C. Champeaux, A. Catherinot, P. Blondy, Sub-microsecond RF MEMS switched

capacitors, IEEE Transactions on Microwave Theory and Techniques. v 55, n 6. June 2007 2007, p 1314-1320.

- [93] P. Monajemi, P. Joseph, P. Kohl, F. Ayazi, Characterization of a polymer-based MEMS packaging technique, Proceedings of the International Symposium and Exhibition on Advanced Packaging Materials Processes, Properties.
- [94] W. Tonomura, R. Kitazawa, T. Ueyama, H. Okamura, S. Konishi, Electrophysiological Biosensor with Micro Channel Array for Sensing of Signals from Single Cells, Sensors, 2006. 5th IEEE Conference on Oct. 2007 Page(s):140 – 143.
- [95] S. Li, D. Fozdar, M. Ali, H. Li, D. Shao, D. Vykoukal, J. Vykoukal, P. Floriano, M. Olsen, A continuous-flow polymerase chain reaction (PCR) microchip with regional velocity control, Microelectromechanical Systems, Journal of Volume 15, Issue 1, Feb. 2006 Page(s):223 – 236.
- [96] A. Poghosian, S. Ingebrandt, M. Abouzar, M. Schoning, M. Schoening, Label-free detection of charged macromolecules by using a field-effect-based sensor platform: Experiments and possible mechanisms of signal generation. Applied Physics A, Material Science & Processing, 87, (3): 517-524 Jun. 2007.
- [97] A. Star, E. Tu, J. Niemann, J. Gabriel, C. Joiner, C. Valcke, Label-free detection of DNA hybridization using carbon nanotube network field-effect transistors. Proceedings of the National Academy of Sciences of the United States of America, 103, (4): 921-926 Jan. 24 2006.
- [98] E. Gui, L. Li, P. Lee, A. Lohani, S. Mhaisalkar, Q. Cao, S. Kang, J. Rogers, N. Tansil, Z. Gao, Electrical detection of hybridization and threading intercalation of deoxyribonucleic acid using carbon nanotube network field-effect transistors. Applied Physics Letters, 89 (23): Art. No. 232104 Dec. 4 2006.
- [99] A. Star, T. Han, J. Gabriel, K. Bradley, G. Gruner, Interaction of aromatic compounds with carbon nanotubes: Correlation to the Hammett parameter of the substituent and measured carbon nanotube FET response. Nano Letters 3, (10): 1421-1423 Oct. 2003.
- [100] A. Star, J. Gabriel, K. Bradley, G. Gruner, Electronic detection of specific protein binding using nanotube FET devices. Nano Letters 3, (4): 459-463 Apr. 2003.
- [101] A. Star, T. Han, V. Joshi, J. Gabriel, G. Gruner, Nanoelectronic carbon dioxide sensors. Advanced Materials 16, (22): 2049 Nov. 18 2004.

- [102] J. Bethoux, H. Happy, A. Siligaris, G. Dambrine, J. Borghetti, V. Derycke, J. Bourgoïn, Active properties of carbon nanotube field-effect transistors deduced from S parameters measurements, *Nanotechnology*, IEEE Transactions on, Volume 5, Issue 4, July 2006, Page(s):335 - 342 Digital Object Identifier 10.1109/TNANO.2006.876931.
- [103] A. Poghosian, A. Cherstvy, S. Ingebrandt, A. Offenhausser, M. Schoning, Possibilities and limitations of label-free detection of DNA hybridization with field-effect-based devices. *Sensors and Actuators B – Chemical* 111: 470-480 Sp. Iss. SI, Nov. 11 2005.
- [104] J. Wang, M. Patterson, G. Subramanyam, Design of 2.45 GHz rectifier antenna and frequency tunable antenna design. *IEEE National Aerospace Electronics Conference*, Dayton, OH. 2008.
- [105] Retrieved from [www.Powercastco.com](http://www.Powercastco.com) on 9/29/2012.
- [106] Y. Lu, B. Goldsmith, N. Kybert, A. Johnson, DNA-decorated graphene chemical sensors. *Applied Physics Letters* 97:083107. 2010.
- [107] J. White, L. Truesdell, M. Williams, M. Atkisson, J. Knauer, Solid-state, dyelabeled DNA detects volatile compounds in vapor phase. *PLoS Biology* 6:e9. 2008.
- [108] J. Genereux, J. Barton, Mechanisms for DNA charge transport. *Chemical Reviews* 110:1643-1662. 2010.
- [109] J. Slinker, N. Muren, S. Renfrew, J. Barton, DNA charge transport over 34 nm. *Nature Chemistry* 3:228-233. 2011.
- [110] Retrieved from [www.xamplified.com](http://www.xamplified.com) on 9/29/2012.
- [111] S. Mukherjee, Principle of wireless impedance by backscatter using a frequency modulated continuous wave (FMCW) radar. *Microwave Journal*, pp. 96-108, November 2004.
- [112] E. Jones, Development of biopolymer based resonant sensors. Master's Thesis, University of Dayton, 2011.